THE APPLICATION OF LC-ICP-MS TO STUDY METAL ION HOMEOSTASIS IN BIOLOGICAL SYSTEMS

A Dissertation

by

SEAN PATRICK MCCORMICK

Submitted to the Office of Graduate and Professional Studies of
Texas A&M University
in partial fulfillment of the requirements for the degree of

DOCTOR OF PHILOSOPHY

Chair of Committee,	Paul A. Lindahl
Committee Members,	Christian Hilty
	Jean-Philippe Pellois
	David Barondeau
Head of Department,	Francois Gabbai

December 2014

Major Subject: Chemistry

ABSTRACT

Eukaryotic cells contain low-molecular-mass metal complexes (LMMMCs), defined as having masses between 200 – 10,000 Da, but these so-called *labile* or *chelatable* metal pools are poorly defined in terms of structures and functions. LMMMCs are thought to participate in metal-ion regulation, trafficking, storage and/or signaling in cells. These cellular processes are often dysfunctional in metal-associated diseases. The objective of these studies was to detect and characterize LMMMCs in eukaryotic cells, organelles and tissues. A novel liquid chromatography system in a cold inert-atmosphere glove box was interfaced with an in-line inductively coupled plasma mass spectrometer, and this LC-ICP-MS system was used to detect LMMMCs in yeast cells, mitochondria, and vacuoles as well as in mouse brain and liver cells and mitochondria. In each biological system, this separations technique was applied to detect numerous LMMMCs. The molecular mass and concentration of such species were estimated.

In yeast, the previously reported mismetallation of MnSOD2 was examined in the mutant strain Δ*mtm1*. A combination of SEC and AEX chromatography revealed that the degree of mismetallation of the SOD2 protein, in which Fe replace Mn in the active site, was no greater in Δmtm1 cells than in WT cells. The mitochondria of such mutant cells did exhibit an intense chromatography peak of Mn corresponding to at mass of 2000 – 3000 Da. Mitochondria from WT cells exhibited a similar species, but at much

lower intensity. This was the only Mn species present, suggesting that it was the used to metallate apo-SOD2.

Mitochondria isolated from WT yeast cells contained 6 Co, 3 Cu, 2 Mn, 5 Fe and 3 Zn LMMMCs and approximately 6 P- and S- LLM species. Some of the P- and S-LMMCs probably arose from compounds like ATP, ADP, etc. Molecular masses of the LMM Cu peaks were higher (> 5 kDa) than for the LMM complexes of other transition metals. Zinc, Mn, and Fe had multiple species of interest which demonstrate the presence and labiality of the metals in pools.

The same separation system was utilized to examine mice brain LMM extracts were found to contain > 30 LMMMCs. Eleven Co, 2 Cu, 5 Mn, 4 Mo, 3 Fe and 2 Zn LLM complexes were detected. Most Cu and Zn complexes appeared to be protein-bound with masses ranging from 4–20 kDa. In these systems, Co was the only metal for which the aqueous complex was reproducibly observed.

A second mouse study used the LC-ICP-MS system to examine the forms of iron present in mouse plasma. Chromatograms exhibited ~6 Fe-associated peaks that were assigned to ferritin, transferrin, and hemopexin, respectively; the other 3 peaks could not be assigned. The LC-ICP-MS experiment demonstrates that numerous Fe-containing species coexist with transferrin in healthy WT mouse plasma.

DEDICATION

I dedicate this work to my mother and father for all their hard work in nurturing my creative and academic development as well as providing endless love.

ACKNOWLEDGEMENTS

I would like to extend my deepest gratitude to my advisor, Dr. Paul Lindahl. From our first conversation my first week of graduate school he has constantly poured excitement and energy into my project through its ups and downs. I would like to thank him for all his support in my research and graduate school as a whole. I would also like to thank my committee members, Dr. Barondeau, Dr. Vigh, Dr. Hilty, and Dr. Pellois, for their guidance and support throughout the course of this research, as well as teaching me a great deal in my academic course.

A great deal goes out to the past Lindahl Lab members Ren, Jessica, Marco, Ivan who all nurtured my early research in the lab and took me from a synthetic chemist to a biochemist. I am forever grateful for having a great friend, colleague, and mentor, Dr. Gregory Holmes-Hampton. I would like to thank Dr. Mrinmoy Chakrabarti for teaching me spectroscopy and commiserating with me on many issues during our four years together in lab. I would like to also thank Mike, Jinkyu, Nema, and Allison for all the great collaborations, conversations, and input. I would like to also thank Dr. Lora Lindahl for all she has done for the lab and I, from teaching us mouse anatomy to hosting a festive party.

I would like to thank the wonderful faculty and staff in the chemistry department for creating an excellent environment and providing the tools to be productive in both the learning and research process. I would like to thank two individuals personally for helping me with my graduate student journey. The first is Mr. William Seward in the

machine shop for teaching me a thing or two about machining, as well as patiently help me take some crazy ideas from the back of the napkin to a functional design and part. Secondly I'd like to thank Dr. James in the Center for Chemical Characterization for teaching me the basics of ICP-MS and having many useful conversations.

I could not have done graduate school without the support of an amazing group of friends from both Texas and Chicago. They provided the perfect mix of scientist and nonscientist individuals which allowed for different types of conversation. I love and cherish the years I've spent with them and wish them the best.

Finally, thanks to my mother and father for their encouragement throughout my life and to my brothers for their patience and love.

NOMENCLATURE

AD	Alzheimer's Disease
apo-Sod2p	Sod2 protein prior to metal installation
ASR	apo-Sod2p reactive
ATP	Adenosine Triphosphate
ADP	Adenosine Diphosphate
AMP	Adenosine Monophosphate
BBB	blood brain barrier
CD	central doublet
CIA	cytosolic iron sulfur cluster assembly
CVs	column-volumes
DNP	2,4-dinitrophenylhydrazine
DTPA	diethylenetriamine pentaacetate
ENDOR	electron nuclear double resonance
EPR	electron paramagnetic resonance
Fe_{ASR}	sought-after Fe species that misincorporates into apo-Sod2p
FeSod2p	inactive form of Sod2p, with Fe bound
FPLC	fast protein liquid chromatography
FRET	Forster Resonance Energy Transfer
FTS	flow-through solution
GSH	glutathione

GSSG	glutathione disulfide
HMM	high molecular mass
HPLC	high-performance liquid chromatography
HS	high spin
ICP-MS	inductively coupled plasma mass spectrometry
IMM	intermediate molecular mass
INT	iodonitrotetrazolium
IP_6	inositol hexaphosphate
ISC	iron sulfur cluster
LA	laser ablation
LC	liquid chromatography
LIP	labile iron pool
LMM	low molecular mass
LMMMC	low molecular mass metal complex
LS	low spin
MF	apo-Sod2p maturation factor
MM	molecular mass
MnASR	Mn species that incorporates into apo-Sod2p
MnSod2p	active form of Sod2p, with Mn bound
MRI	magnet resonance imaging
Mtm1p	manganese trafficking factor for mitochondrial SOD2, YGR257C; Mol. Wt 40,763 Da

NHHS	nonheme high spin
OD_{600}	optical density at 600 nm
PD	Parkinson's Disease
PMSF	phenylmethanesulfonylfluoride
ROS	reactive oxygen species
RT	room temperature.
SDH	succinate dehydrogenase
SOD2	superoxide dismutase 2
TMG	trace metal grade
V_e	elution volume
V_0	void volume
WT	wild type
XAS	X-ray absorption spectroscopy
XRF	X-ray fluorescence
YPAD	yeast extract, peptone, adenine hemisulfate, and dextrose

TABLE OF CONTENTS

CHAPTER

LIST OF FIGURES

Page

LIST OF TABLES

CHAPTER I

INTRODUCTION AND LITERATURE REVIEW

Transition Metal Ions in Biology

Transition metal ions are essential in biology due to their unique chemical properties.[1] They play important roles in catalysis[2], electron transfer processes[3], DNA replication and repair[4], gas storage and transport[5]. Metals are coordinated to various ligands affording prosthetic groups that impact protein structure and function. They also play important roles in the metabolism of multicellular organisms including humans.[6] Some diseases involve metal ion metabolism dysfunction. Genetic diseases involving mutations within the genome and proteome can affect metal ion utilization.[6]

Metals must be imported continuously from the environment as organisms grow. However, metals in the environment are not always present at sufficiently high concentration or in forms that are bioavailable.[7] For example, ferric oxides are present in high concentrations in the environment, but they are not bioavailable in that form. Numerous chemical properties of these compounds impact the ability of cells to uptake metals, including hydrolysis, solubility, redox state, ligand exchange rates of metal centers, and ligand competition. [7]

Metal ions become toxic to the cell when they accumulate beyond the concentration needed for normal functioning.[8] Different metals may compete for an enzyme active site, with occupancy by one metal activating the enzyme and occupancy by another causing inactivation.[9, 10] The hyper-accumulation of redox-active transition

metals such as copper and iron can generate reactive oxygen species (ROS) such as superoxide, hydrogen peroxide and hydroxyl radicals which damage proteins, lipids, and nucleic acids.[11, 12]

Cells have developed mechanisms for responding to the hyper-accumulation of metals, and for reducing their toxic effects. These mechanisms include the regulation of metal-ion uptake, the sequestration of metals into certain cellular compartments, the export of metals from the cell, and the transformation of dangerous metal ion complexes into more benign forms.[13]

Metal Related Diseases

Dysfunctions in metal homeostasis can cause different diseases in humans. All essential metals in the cell can be implicated in one or more disease states. Iron-related diseases fall under two categories, namely iron deficiency and iron overload. Anemia is the most prevalent iron-related condition, with one-in-six people affected worldwide.[14, 15] Anemia can be caused by either a dietary lack of iron or by genetic dysfunction. Iron overload diseases such as hemochromatosis occur in one of two hundred individuals.[16] Iron-overloaded patients accumulate iron in cells and tissues, leading to cirrhosis,[17] diabetes,[18] and heart failure[19]. At the cellular level, iron accumulation can come from genetic or metabolic disorders which create ROS. Other iron-related diseases include Sideroblastic anemia[20] and Friedreich's Ataxia[21]. Iron overload contributes to aging and neurological diseases such Alzheimer's and Parkinson's diseases.[22]

The two most prominent copper-specific genetic diseases are Menke's and Wilson's diseases. These are caused by the mutation of the copper transporters ATP7A and ATP7B, respectively.[23] Menke's disease affects a number of cuproproteins causing neurological and growth deficits along with "Kinky" hair.[24] Patients with Wilson's disease exhibit cirrhosis, chronic hepatitis, neurological, and psychiatric problems caused by the accumulation of copper in the liver as well as the brain.[24] Lou Gehrig's disease or Amyotrophic lateral sclerosis (ALS) is a fatal neuron disease which has been linked to mutation in the Cu/Zn superoxide dismutase gene.[25, 26] The effects of the disease are caused by the aggregation of immature protein which cannot reach full maturation because copper cannot be inserted by the chaperone CCS1.[27] Copper bound aggregates have been implicated in many neurological and neuromuscular diseases such as β-plaques aggregations in Alzheimer's patients and Lewy bodies in Parkinson's disease. Copper also catalyzes protein cleavage in Huntington's patients.[28]

Zinc deficiency can arise from inadequate uptake,[29] genetic disorders,[30] or environmental factors[31]. Zinc deficiency affects the immune system's T and B cells along with neutrophils and macrophages.[32] This results in a depressed immune response. Also seen in zinc-deficient patients are neurodeficiencies and thymus atrophy.[33] Zinc plays an important role in neurobiology. In contrast to metals like copper and iron, zinc prevents the oxidative damage associated with the binding of those metals with the amyloid β peptide. Zinc does this by binding the peptide and inducing a conformational change which inhibits the binding of these other metals.[34] At elevated Zn levels however, there is increased risk of plaques forming through aggregation.[35]

Individuals with manganese toxicity exhibit Parkinson-like symptoms which are referred to as "manganism".[36] Manganism patients exhibit lesions in the brain and do not respond to dopamine replacement therapy.[37] Prion proteins play a protective role in the brain when it is faced with metal misregulation. Prion proteins protect against apoptotic cell death and the formation of ROS by sequestering metal ions.[38] Individuals with prion diseases exhibit misfolding of the prion proteins which renders them unable to bind the potentially toxic metal ions. When manganese is present in patients with prion irregularities there is the possibility of cytotoxicity caused by the generation of ROS.

Cobalt also serves essential roles in human metabolism but can also be toxic when present in excess. Cobalt is essential to lipid biosynthesis,[39] and C_1 metabolism.[40] It is found in the B_{12} cofactor of the enzyme methionine synthase,[41] which is needed for methyl group transfer. Excess cobalt leads to the generation of ROS which can mutate DNA.

Molybdenum is the only metal in the second transitional series which is essential to mammals.[42] It plays a vital role as the metal cofactor in molybdenum hydrolases.[43] A deficiency of this cofactor in newborns renders them susceptible to seizures and death due to their inability to produce the cofactor.[44, 45] Molybdenum also is found in xanthine oxidase[46] and aldehyde oxidase[47] in the kidneys, liver, and milk.

Labile Metal Pools

Since metals are essential for metalloproteins, they need to be available to be inserted during the protein folding process for nascent proteins. Many proteins participate in metal homeostasis and in trafficking metals to recipient apo-proteins.[13] Metal homeostasis utilizes import proteins, storage proteins[48], metal chaperones[49], metal-sensing proteins,[50] and metal-inserting enzymes[13] to handle metal ions at different points in their cellular journey.

These proteins typically bind metals with high but varying affinities. Typically metal ions are passed from one protein to another that has a higher binding affinity for the metal. The final recipient metalloprotein typically has the highest binding affinity of all the metalloproteins participating in the trafficking process. This makes the pathway one directional.[51] The tight binding of metal to metalloenzymes requires that the cell contains a supply of metal ions which can be rapidly delivered to newly formed proteins, but how this occurs on the molecular level remains unknown. The cell has been hypothesized to contain pools of metal ions which are weakly bound to their ligands and participate in trafficking.[8] Such pools have been called the labile metal pool[52-54], exchangeable pool[55-57], bioavailable pool[58-60], or chelatable metal pool. The concentration of the metals in such pools is thought to be regulated by metal-sensing proteins which under states of metallic depletion or repletion cause a cellular response.[50]

Labile metal pools are poorly defined in terms of composition, function, and structure; there isn't even a consensus regarding their existence! Metal ions can

probably not roam “free” within the cell (coordinated only to water ligands) due to the toxicity of such complexes. “Free” metal ions in the cell would dangerous due to possibility of uncontrolled interactions with the proteins, enzymes, and small molecules that they encounter. Thus, metals in labile metal pools maybe composed of low molecular mass (LMM) complexes coordinated to non-proteinaceous ligands.

The first labile metal pool of interest was discussed by Greenburg and Wintrope [(61)], and subsequently by Jacob [(62)], as an intermediate or transitory pool between iron in the extracellular environment and cellular iron associated with proteins. The earliest experiments carried out by Greenburg and Wintrope used radiolabeled iron supplied to cells as a transferrin bound complexes. The radio labeled Fe allowed for pulse chase experiments and in combination with subfractionation of the cytosol into high and low molecular weight components provided insights by metal tracking. Radioactive Fe was taken up by the cell from the environment and trafficked in to the cell where it was detected. Over the course of a week radioactive Fe continued to be inserted into nascent proteins without the addition of iron to the media. Thus suggesting that the Radioactive iron was present in the cell as a form of iron which was waiting to be inserted into proteins. Labile metal pools may play a role in metal-associated diseases. Understanding these roles will require that the nature of these complexes and their location in the cell be identified.

Methods for Studying Metal Species in Brains and Cells

The first attempts to visualize metal species inside cells and in tissue samples were carried out using microscopic staining methods. In 1867, Max Perl used potassium ferrocynide to stain ferric ions in tissues.[63] Over the course of the next century new histochemical staining methods for other metals commonly (e.g. copper) found in biological samples were subsequently developed.[64] These methods are still used due to their simplicity." For example, Perl staining for iron was recently used utilized by Huang et al.[65] to show the effect of psychological stress on the LMM Fe pools present in different regions of the brain. However, the information obtained from these staining methods is limited. Samples must be fixed prior to staining such that time-dependent studies are not possible.

The ability to image metals in cells has progressed significantly in the past few decades due to advances in analytical instruments. The utilization of fluorescent microscopy and spectroscopy has yielded many insights into metal homeostasis. Three main platforms are used in fluorescent spectroscopy to image metals in living cells, including those based on small molecule, protein, and hybrid biosensors. Each type of biosensor varies in terms of dynamics, binding affinities, and specificity. In small-molecule biosensors, a fluorescent moiety is attached to a chelating agent. Fluorescence is quenched in the unbound state because energy is transferred between the moiety and chelating agent.

Chang and coworkers have developed multiple fluorescent sensors with different structures allowing for the detection of both Cu^{I} and Cu^{II} ions. The fluorescent sensor

RSC1 was used to selectively monitor the expansion of endogenous stores of exchangeable intracellular Cu^{I} triggered by ascorbate stimulation in kidney and brain cells.[58] Lippard and coworkers have used the fluorescent sensor ZP3 to monitor the synaptic zinc pool in neurons.[66, 67] Using ZP3, Zn was observed to load into vesicles of the cerebral cortex and to be subsequently released during synaptic activation.[67] Upon binding of the metal ion to the biosensor, fluorescent quenching declines and quantum yields increases. The increase in fluorescence is concentration-dependent and therefore provides local concentration information. Small molecule probes are highly tunable and modular in design, allowing for probe designs with various dynamic concentration ranges.

The disadvantages of small-molecules platforms become evident when attempts are made to introduce such molecules into an intracellular environment in a minimally invasive manner. The same membranes which hinder metal uptake block typically prevent small-molecule complexes from being imported. This is because the chelating agents and fluorescent component are generally charged. Importing such complexes often requires minimizing their charge by chemical modification. This will allow translocation of the complex across the membrane. Then, natural occurring enzymes will post-translationally modify the complex to an active form. Other methods of introducing the complex into the cell include microinjection, microencapsulation, DNA transfection, or tethering of the complex to cell-penetrating peptides.

Protein-based sensors are also used to image metals in cells. In these platforms fluorescent proteins are tethered to metal binding domains which are either naturally

occurring or custom engineered. The protein-based platforms can be singular or multi-protein in nature. In single protein platforms metal binding induces a conformational change which perturbs the fluorescent intensity or the wavelength. Multiprotein platforms rely heavily on Forster Resonance Energy Transfer (FRET) in which two fluorescent proteins are bridged by a metal binding domain. The metal ion binds in the domain and induces a change in the complex either in the orientation or distance between the proteins causing a change in the rate of energy transfer between the donor and acceptor proteins. Through monitoring the fluorescence of the donor and acceptor quantitative metal concentrations can be determined. Palmer and coworkers have developed organelle-specific protein based FRET sensors that detect zinc in Hela cells at low pM concentrations.[68, 69] Three genetically encoded FRET-based sensors have been developed for visualizing cellular Cu^{I} offering a range of affinities and the ability to quantify bioavailable copper in yeast at the range of 10^{-17} to 10^{-21} M.[70]

The use of protein-based platforms is inherently a dual-edge sword. Proteins can easily be genetically encoded in the cells or introduced using viruses. The expression of the sequence which encodes the protein-based sensor can be placed under an inducible promoter. One drawback is that expressing a nonnative protein might perturb the metal homeostasis in the cell.

Hybrid systems consist of a fluorescent protein fused to small-molecule sensors. Protein-based sensors allow for the genetic encoding needed to target a specific type of cell or a specific cellular organelle. Small-molecule sensors can be tuned to have specific properties like excitation wavelength for detection and a detectable

concentration range from pM to μM concentrations. These hybrid systems allow genetic specificity to be merged to spectral diversity and a large dynamic range.

Magnetic Resonance Imaging

MRI is a valuable technique for studying metal ions in samples that are opaque. MRI provides 3D imaging of metal ion distributions with high spatial resolution. Two types of MRI signals can be observed, each due to different phenomena. The first type of signal arises from the modulation of the relaxation properties of water associated protons. The second type of signal arises when contrast agents interact with metal ions.

Metals in the brain and other organs have been studied by MRI techniques without contrast agents. Chen and coworkers utilized MRI to look at changes in brain iron distribution after introventricular hemorrhage.[71] MRI has also been used to examine plaques present in the brains of Alzheimer's and Parkinson's patients. Second-generation contrast agents allow different metals to be selectively detected. Many examples of metal specific MRI contrast agents based on Gadolinium sensor have been developed. Meade and coworkers have designed Zn activated contrast agents which have high selectivity for Zn^{II}.[72] Other MRI sensors have been developed in the Chang Lab .[73-77] This group has designed sensors for both Cu^{II} and Cu^{III} labile metals whose binding affinities were measured to have K_d values spanning three orders of magnitude from 0.037 to 32 pM.[76] The sensors are highly specific for copper.[78] Their copper MRI contrast agents have been used to study cell lines which exhibit the Menke's disease phenotype.[79] Lippard's laboratory developed Mn^{III} based porphyrin contrast

agents which have a MRI relaxivity modulated by Zn^{II}.[80] When introduced into mammalian cell lines, the MRI probe exhibited a concentration-dependent response and a rather high degree of metal selectivity.

X-ray Fluorescence Spectroscopy

Another analytical imaging technique is x-ray fluorescence (XRF). For each element, XRF gives information on its concentration, oxidation state and average coordination environment. In XRF, samples are bombarded with X-rays, causing the excited core shell electrons of the atom to become excited. These electrons subsequently relax with the emission of photons. The emitted photon energy is specific for each element, allowing different elements within a sample to be distinguished. Nichol et al,[81-83] used fast-scanning XRF analysis to map the distribution of metals in various regions of the brain. Their results confirm that the *substania nigra* region of the brain contains a significant amount of iron.[84] They also suggest that regions containing pools of iron have low zinc concentrations. These researchers observed abnormalities in the metal distributions in brains from individuals with Parkinson's and Amyotrophic Lateral Sclerosis (ALS) diseases. Rabionet and Ide-ektessabi suggest that oxidative stress is a critical factor in neurodegenerative disease development or progression.[85] This is based on XRF data which shows an imbalance in Zn and Cu, as well as in the ferrous and ferric redox pair, within diseased brains.[85] These authors suspect that such imbalances are associated with an increase in oxidative stress. X-ray fluorescence is an extremely sensitive technique, with detection limits in the 10-100 μg/L range. By focusing the x-

ray beam and optimizing sample preparation, spatial resolution of 100 nm is possible. While XRF spectroscopy is a highly effective imaging tool, the limited availability of synchrotron sources and the need to chemically prepare a sample for analysis prevents it from becoming a mainstream technique.

Laser Ablation Inductively Coupled Plasma Mass Spectrometry

Another technique for imaging cells and tissues is Laser Ablation Inductively Coupled Plasma Mass Spectrometry (LA-ICP-MS). This technique is used to measure metal ion concentrations in solid samples. A laser beam is focused on the sample causing a micrometer diameter spot to ablate. The ablated sample enters the ICP using a stream of argon carrier gas. In the plasma, the sample is vaporized, atomized, and ionized. The ionized material is separated by mass-to-charge ratio and detected by the mass spectrometer. LA-ICP-MS has been used to study strokes and aging in mice brains. Becker et al.[86] induced thrombosis in mice similar to that expected in traumatic brain injury. Using LA-ICP-MS, they discovered a large concentration of iron at the site of the thrombosis. Becker et al. also found an increase in copper and zinc around the injury. They suggested that the copper and zinc became incorporated in Cu, Zn superoxide dismutase. This enzyme might be needed to scavenge ROS generated from the excess Fe which participated in Fenton chemistry. LA-ICP-MS has been utilized for a vast number of sample types including Alzheimer plaques,[87] brain stems and cerebellum samples,[88, 89] and spinal cords[90]. LA-ICP-MS has also been coupled to laser microdissection to better resolve brain regions.[91, 92]

LA-ICP-MS is a sensitive spectrometric technique useful in the bioimaging of trace metals sections of biological tissues. One disadvantage is its limited resolution. In current instruments the resolution is on the order of 5-150μm, nanometer resolution maybe possible in the near future. Another disadvantage is that the instrument must be calibrated using solid standards in matrixes similar to that of the sample, which is difficult to perform accurately. The biggest disadvantage in using LA-ICP-MS comes from its inability to reveal any speciation of compounds.

Problems with Metal Detection Methods in Cells

The methods discussed typically provide large amounts of spatially resolved data regarding the localization of metals and distributions of different metals as a whole within tissues and cells. The fluorescent-chelator approach has yielded critical information regarding the real-time trafficking of metals in cells. This approach affords high resolution images that are essentially selective for a given metal. The biggest question for scientist studying metal homeostasis is wither metals are trafficked solely by proteins or are there low molecular mass metal species which play a role in trafficking. Chelator based studies cannot directly answer the question due to their nondiscriminating nature. A chelator may be selective for a specific metal but not for a particular metal-bound species in the cell. This makes it extremely difficult to determine where the metal being detected comes from or how many different protein or LMM species are contributing to the fluorescent response. Pools of metals (either proteinaceous or non proteinaceous) used in trafficking should be composed of metals

with preferred redox states and coordination environments which would allow them to be useful but not toxic to the cell. However there have been no LMM complexes that have been isolated and characterized in the literature for eukaryotic systems. Knowledge of the structure and function of the proteins or LMM pools might eventually aid in treating metal related diseases by understanding ways to control metals species in cells.

Liquid Chromatography and Inductively Coupled Plasma Mass Spectrometry

The most direct method to separate and characterize metal containing complexes is to use liquid chromatography interfaced with inductively coupled mass spectrometry (LC-ICP-MS). The method draws on the strengths of two analytical techniques. LC is a very versatile technique with an extended range of possible separation mechanisms which utilize different combinations of stationary and mobile phases. This allows one to separate complexes with a high degree of resolution. The interfacing of LC to the ICP-MS allows for sensitive and selective detection of metals and nonmetals in a variety of sample matrices.

The use of traditional LC-ICP-MS methods comes with some complications. The mobile phase of the LC separation typically contains a buffer which stabilizes some biomolecules. However, such buffers often alter the equilibria of the target species, yield unnatural complexes, or contribute metal contaminates into the sample. The same types of issues arise with many stationary phases which suffer from chemical absorption, contamination, or alteration of the analyte during the course of the separation.

In 1989, prior to the interfacing of LC to ICP-MS, Pollack and Weaver utilized anion exchange chromatography to isolate Fe-AMP and Fe-ATP from guinea pig reticulocytes.[93] The separation was carried out under aerobic conditions using buffers with extreme pHs. Aerobic isolation is problematic because some labile metal complexes are susceptible to oxidation by molecular oxygen. In order to alleviate artifacts caused by the presence of molecular oxygen all sample preparation and manipulations, along with the separation, itself should be carried out in an anaerobic glovebox. The authors suggested that their results were potentially artifactual. The acid pH of the separation buffer used to prepare the sample causes the hemolytic release of a high concentration of iron from transferrin during lysis. This iron is free to react with ATP and ADP which is found at high concentrations in reticulocytes. The Fe-ATP, Fe-ADP, and Fe-AMP detected could be an artifact of the protocol.

The utilization of size exclusion chromatography (SEC) hyphenated to ICP-MS to detect metal containing protein separated by molecular weight is not a new technique for analytical chemists. SEC-ICP-MS has been used to study various trace metals in samples with a wide range of pathologies and disease states including but not limited to rat serum[94], cancerous thyroid tissues[95], mouse neurons[96], as well as various blood products[97].

While useful information has been obtained from the previous studies a majority of these studies were focused on metal-containing proteins such as transferrin, copper zinc superoxide dismutase, or ferritin. Experiments which focused on small metal complexes required the addition of nonphysiological concentrations of metals to

measure detectible signals. The experiments were also carried out aerobically and at ambient temperature. From an inorganic chemistry prospective this could be problematic. The aerobic handling of metal complexes (iron in particular) offers the possibility of oxidation and thus most likely changes in the coordination environment of the complexes. Executing the experiment at ambient temperature increases the possibility of ligand exchange. Thus that complexes detected could be the result of unnatural ligand exchange over the time course of the experiment.

A final concern is the lack of documented reproducibility in published chromatograms. Biochemical research is in itself susceptible to variations of varying degrees, therefore reproducibility must be demonstrated. Previous publications do not typically show data or chromatograms from more than one experimental run. The reader is expected to accept the results with little to no demonstrated reproducibility.

Objectives

The lindahl lab is focused on iron trafficking in cell biology. The literature has made cases for metal trafficking involving solely protein bound iron chaperones, as well as cases for iron trafficking using labile metal pools. Previous studies of iron pools have not yielded precise chemical information on these pools, such that the composition and functions of such pools remains uncertain. The objective of my research was to detect and isolate the iron isolated which constitute the labile pools in different biological systems. One major problem in isolating these iron species is that Fe^{2+} readily oxidizes in air to form Fe^{3+}. We suspect that in previous studies of labile iron pools using LC, the

iron in the sample became oxidized and precipitated on the column or was eluted as a non-native species. In order to detect and isolate the iron containing species LC-ICP-MS was selected. The LC was placed inside an anaerobic glovebox to avoid oxidation. To decrease the rate of ligand exchange the system has been refrigerated to 5^{o}C. These two approaches in combination with LC-ICP-MS have not been previously reported in the literature.

In 2009, Culotta hypothesized the existence of a large "bioavailable" pool of iron in the mitochondria of *Δmtm1* yeast.[98] She proposed that this "bioavailable" iron pool would interact with SOD2 protein causing mismetallation and inactivation of the enzyme. We suspected that this "bioavailable" iron would be in the high spin Fe^{II} form and could be the long sought-after mitochondrial labile iron pool. In chapter 3 of this dissertation we sought to characterize the "bioavailable" iron in the mitochondria of *Δmtm1* using a combination of biophysical and bioanalytical approaches.

After studying iron and manganese in the previous chapter we moved on to study all LMM species in yeast mitochondria while addressing all biologically interesting transition metals along with sulfur and phosphorus. Little is known about these pools and in chapter 4 we discuss the knowledge gained through our studies.

The brain is thought to be susceptible to metal misregulation.[99] Previous research has shown elevated levels of ROS in many neurological disease states. The misregulation of metals and its subsequent generation of ROS make it an important area to study. Numerous groups have studied the localized concentrations of metals in the brain and the spectroscopic properties of metals in the brain.[89, 100-103] The problem is

still the lack of knowledge about the structure of these LMM metal complexes which make up the pools. In Chapter 5, we will utilized LC-ICP-MS to determine the presence of LMM metal species in the brain and provided the groundwork for their future in depth studies.

A second mouse experiment is carried out in chapter 6. We use LC-ICP-MS to examine the forms of iron present in the plasma of mice. Along with determining the forms of iron we investigated the iron uptake variety of organs and in the plasma using stable isotope analysis. Overall, the results presented in this dissertation include the detection of over 50 previously unreported LMM metals complexes in biological systems, the detection of 6 different iron compounds in mouse plasma, and insight into what happens to iron in the brain during aging. These advances constitute a solid foundation for future LMM metal studies in the Lindahl Lab.

.

CHAPTER II

MATERIALS AND METHODS*

The primary methods used in these studies are liquid chromatography (LC) and inductively coupled plasma – mass spectrometry (ICP-MS). The LC served as a method of biochemical separation and the ICP-MS served a dual role as an element specific detector for the LC, as well as a highly sensitive method for determining metal concentrations in the various systems.

Inductively Coupled Plasma –Mass Spectroscopy (ICP-MS)

ICP-MS is an analytical technique developed in mid-1980's by Alan Gray and Sam Houk as a means of detecting and measuring all metallic elements from lithium to uranium with detection limits around 100ppb with modest level of error. The capability that separates ICP-MS from its predecessors, atomic absorption based techniques, is the ability to gain isotopic information about the samples, which is why it's a mass spectrometry based instrument.

While ICP-MS instrument designs have advanced over the past half a century all ICP-MS follow a basic design with four main components: sample introduction, argon plasma torch, ion extraction/focusing, mass separation and detection. All four components will be briefly discussed.

Solution based samples are introduced into the plasma using a combination of Micromist nebulizer, Peltier cooled spray chamber and a quartz torch. The Micromist

nebulizer aerosolizes the solution in a argon gas stream creating droplets of the solution of various sizes which are sprayed into the spray chamber. The spray chamber is cooled to 2o C using a Peltier cooler. The spray chamber removes the larger droplets though a complex cooled flow path and allows only the smallest uniform droplets to pass reducing the amount of solvent vapor entering the torch and the plasma. The droplets then pass through to the torch. The torch is a piece of quartz consisting of three concentric tubes which are positioned inside a copper coil which is connects to a radiofrequency (RF) generator.

A tesla spark ignites the plasma at the end of the torch and the plasma is maintained using oscillating magnetic fields created from the RF flow in the copper coils. The tesla spark causes electrons to be stripped off the argon atoms, resulting in argon ions. The argon ions interact with the oscillating magnetic and electric fields causing intermolecular collisions to occur amongst argon atoms, thus resulting in an argon discharge, or more commonly caused plasma formation. When a sample is introduced in to the plasma it is rapidly desolvated and atomized into the gas phase. Once in the gas phase the atoms are ionized to single charged ions. It is these ions which will be analyzed by the mass spectrometer.

Ions entering the mass spectrometer do so through an interface region of the ICP-MS consisting of interface cones under pressure of 1-2 torr. The interface cones are referred to as the sampling and skimmer cones. The sampling cone contains a 1mm ID orifice in a platinum cone, while the skimmer cone contains a 0.4mm ID orifice. The decrease in pressure from atmospheric to 1-2 torr causes the ion beam to undergo

supersonic expansion resulting in a ion beam with a steady composition. This allows for a representative sampling of the plasma at the skimmer cone region.

The ions focused through the skimmer cones then enter the low pressure region of the instrument, less than 1x 10^{-5} torr, where they are focused through a series of electrostatic plates, known as ion lenses. The ion lenses guide and focus the ion beam, while also separating the ions from photons and neutrals created within the plasma. This decreases the background signals created through random collisions with the detector. The focused ion beam is introduced into the collision/reaction cell, where gases such as Hydrogen or Helium can be added to remove spectral interferences. The gases in the reaction cell can remove polyatomic interferences using one of two methods. The first is reaction mode (Hydrogen Mode). In reaction mode polyatomic interferences are removed or minimized through chemical reaction with the gas. The second mode is collision mode (Helium Mode). In collision mode, the gas (helium) collides with the larger polyatomic interfering ion resulting in the loss of kinetic energy. The increased size of polyatomics ions over analytes results in an increase number of collisions for the polyatomic ions. The increased number of collisions causes a greater loss in kinetic energy allowing for energy discrimination to be used to separate analyte from polyatomic interferences. In both cases these polyatomic interferences are then removed by an octopole.

Upon passing through the ion lens as well as the collision/reaction cell the ions finally make it to the mass analyzer. In the case of the Agilent system a quadruple is used to separate ions based on their mass to charge ratio (m/z). A quadropole is a mass

filter composed of two pairs of parallel cylindrical rods positioned on the axis of the ion beam. A dynamic hyperbolic electric field (DHEF) is created using a combination of AC and DC voltages. The 2 pairs of rods have the same AC voltage applied out phase between the two pairs. The DC voltage is made positive for one pair and negative on the other. The DHEF filters ion out which are above or below the mass desired by causing the ion to have an unstable trajectory and be lost for the ion beam. Different masses can be selected for by varying the AC and DC fields but keeping the ratio on one to another constant. The ability to rapidly change voltages allows for the nearly simultaneous detection of multiple elements. The ions of interest which make it through the quadropole are then ready for detection. ICP-MS utilizes an electron multiplier to generate detectable signal pulse from the impact of a single ion. The positive ion reaches the detector and is deflected by the first dynode. The impact causes the release of several free electrons which bounce from dynode to dynode creating a cascade of electrons repelled from the previous dynodes to an ECD which measures the ion count.

The use of ICP-MS comes with both advantages and limitiations. ICP-MS is a "hard" ionization technique which allows for the complete dissociation of molecule to atoms and atomic ions allowing for elemental detection even in complex matrices. ICP-MS has detection limits 100x better than that of optical based emission techniques and can measure the full range of metals within a 2-3 min window. It has a large linear dynamic range over a concentration range of 10^9 provides elemental isotope information which can be used to correct for polyatomic interferences in the plasma or carry out experiments using single isotope incorporation or spiking. The robustness and advances

in ICP-MS systems allow for customization of techniques for sample introduction. ICP-MS does suffer from some limitations including high instrument cost both initially and operationally. The sensitivity of ICP-MS requires those who operate and prepare samples to be trained in trace metal techniques and to operate in a clean environment or risk misleading data.

Liquid Chromatography (LC)

LC is widely used analytical technique used to separate components from a mixture. In liquid chromatography the separation is carried out by applying the sample to a column containing a solid stationary phase while a liquid mobile phase is pumped through the column continuously. A physical or chemical interaction of the analytes with the stationary phases causes them to separate. The two chromatographic methods used in the following work are size exclusion and ion exchange chromatography.

Size exclusion chromatography (SEC) is a separation technique which utilizes the molecular sieve effect to separate molecules based mostly on their size but also partially on the molecular shape. The theory is a small analyte will be retained longer in a pore on the stationary phase due to its ability to penetrated deeper into pore and explore a greater amount of the interparticular volume. Larger analytes lack the ability to penetrate the well-defined pores and thus take less time to be eluted from the column.

Ion exchange Chromatography (IEC) is separation technique which involves the interaction of a negatively charged analyte with a cationic stationary phase or a positively charged analyte on an anionic stationary phase. The stationary phase is either

a polymeric or silica bead which is functionalized with typically a quaternary amine or a sulfonate type group. The analyte is retained by the stationary phase if the charge of the complex is opposite that of the stationary phase and the relative strength of the retention is dependent on the electrostatic interactions present. The analyte is eluted off the column using an aqueous solution and a gradient of increasing salt concentration. The salt in the elution buffer displaces the analyte from the stationary phase as long as it has higher ionic strength.

Hyphenation of LC- ICP- MS

HPLC-ICP-MS is the most popular of all hyphenation techniques used in elemental speciation because it offers unparallel opportunities. HPLC-ICP-MS offers scientist the variety of separation mechanisms afforded by HPLC, a highly sensitive and robust element specific detection methods, and a straightforward interface between the LC and ICP.

As mentioned earlier the application of LC with ICP affords the users a variety of separation methods to applies to their sample. These separation methods each have different mobile phases most containing a gradient of either salt or organic solvent. The main issue with using linear gradients of salts for the elution of small metal complexes comes when the mobile phase often exceeds 0.1M salt concentration. This results in instability and decreased sensitivity of the ICP-MS because of the clogging of the nebulizer and sampler and skimmer cones with crystallized salt. When organic solvent gradients are utilized the same plasma instability and loss of sensitivity can be observed.

This is due to the large amount of carbon which can be deposited in the sample path and on the ion optics in the system from the burning of the organic phase. The advances in capillary and nano flow LC systems have made LC-ICP-MS even more attractive because the decreased amount of matrix sprayed into the ICP-MS affects the plasma less.

The interface allows for the connection of the post column eluent flow to be directed directly in to the ICP-MS with simple connections. The flow rate of current LC systems can be accommodating by the ICP-MS using the standard spray chambers and nebulizers. The online coupling of Liquid chromatography methods and ICP-MS has successfully utilized ICP-MS as an element specific detector to monitor the chromatographic separation. ICP-MS are preferred to other atomic spectroscopy techniques due to its high sensitivity (pg mL^{-1}), wide dynamic range, multielement capabilities and its ability to monitor multiple isotopes. In order to minimize contamination, obtain better analytical repetition, and decrease analysis time the online hyphenation of the LC to the ICP is preferred relative to the offline system.

Chemicals and Standards

The water used was house-distilled, deionized using ion-exchange columns (Thermo Scientific 09-034-3), and then distilled again using a sub-boiling still (Savillex

DST-1000). Cytochrome *c* (*Saccharomyces cerevisiae*), aprotinin (bovine lung), ATP, ADP, AMP, and cyanocobalamin were from Fisher Scientific (Pittsburgh, PA, USA). Inositol hexaphosphate (IP_6), oxidized and reduced glutathione, sodium molybdate, and sodium phosphate were from Sigma Aldrich (St. Louis, Mo, USA). The molybdopterin cofactor was isolated as described[43] from xanthine oxidase. The sample buffer was 20 mM Tris (Fisher) pH 7.4.

Yeast Strains and Media

The *Δmtm1* mutant strain used in Chapter 3 was derived from WT strain W303 (*MATα, ura3-1, ade2-1, trp1-1, his3-11,15, leu2-3,112*). Gal-YAH1 is a derivative of W303 containing a galactose-inducible *YAH1* promoter.[104] W303 and *Δmtm1* cells were grown on standard rich medium with 2% (w/v) glucose and 40 mg L^{-1} adenine hemisulfate dihydrate (YPAD) agar plates for 3–4 days. Gal-YAH1 cells were grown on standard rich medium with 2% (w/v) galactose and 40 mg L^{-1} adenine sulfate agar plates for 3–4 days. Generally a colony taken from the agar plate was inoculated in Fe-deficient minimal medium containing 2% (w/v) glucose, supplemented with 100 mg L^{-1} leucine, 40 mg L^{-1} adenine hemisulfate dihydrate, 20 mg L^{-1} uracil, 20 mg L^{-1} histidine, 50 mg L^{-1} tryptophan, and 1 μM copper sulfate. Either natural-abundance Fe-citrate or ^{57}Fe-citrate was added to minimal medium at 20 μM final concentration. For manganese supplementation, 200 μM $MnCl_2$ was added to minimal medium (the [Mn] in unsupplemented minimal medium was ~2 μM).

Yeast defined as wild type in chapter 4 is of the BY4741 (*MATα*, *ura3Δ0, leu2Δ0, met15Δ0, his3Δ1*) strain. BY4741 cells were grown on standard yeast peptone medium with 2% glucose (YPD) agar plates for 3-4 days. Colonies were selected from agar plates and inoculated in to iron free minimal media containing 2% (w/v) glucose, supplemented with 100 mg/L Leucine, 40 mg/L adenine hemisulfate dihydrate, 20mg/L uracil, 20mg/L histidine, 20 mg/L methionine, and 50 mg/L tryptophan. Metals were added to the media in the form of copper sulfate and ^{57}Fe citrate to achieve final concentrations of 1μM and 10μM, respectively. For metal supplementation experiments, Zn acetate or $MnCl_2$ were added in addition to the copper sulfate and iron citrate.

Cell Growth and Mitochondria Isolation

Cell stocks were prepared in 15% glycerol and frozen at −80 °C. As needed, frozen cells were scraped with a sterile wooded stick, and spread onto an agar plate. Single colonies were used to inoculate 50 mL of medium. Once grown, the cultures were used to inoculate 1 L of minimal medium (YPAD medium for *Δmtm1* cells). When OD_{600} reached ~1, cultures were transferred into 24 L of minimal medium at 30 °C in a stirred glass fermenter. Solutions were purged with O_2 or Ar (~1 L min^{-1}) to achieve aerobic and anaerobic growth conditions, respectively. Cells were harvested at OD_{600} = 1.0 ± 0.1.

Mitochondria were isolated in a refrigerated Ar-atmosphere glovebox as described.[105] Solutions used under anaerobic conditions were degassed on a Schlenk line and then brought into the box. Isolated mitochondria were packed into EPR tubes or

Mössbauer cups by spinning either at 10 000 × g for 1 hr or at 18 000 × g for 30 min in an ultracentrifuge with a swinging-bucket rotor. Samples were frozen in liquid N_2 for further analysis.

SOD Activity Assays

Six batches each of WT and *Δmtm1* cells were grown on 200 mL of minimal medium and harvested at OD_{600} between 0.6–1.8, matched to within 0.2 absorbance units for each pair of batches. Cells were harvested and lysed by glass-bead agitation. For anaerobic growth, the medium was purged with Ar, and cells were harvested in the glovebox and processed under an Ar atmosphere. Cells were resuspended in lysis buffer containing 10 mM sodium phosphate (pH 7.8), 0.1% (v/v) Triton X-100, 5 mM EDTA, 5 mM EGTA, and 50 mM NaCl. An equivalent volume of 0.5 mm glass beads (Biospec Inc.), 1 mM PMSF and 1% (v/v) protease inhibitor cocktail (P8340, Sigma) were added to cell suspensions. Cells were agitated by vortex action for 1 min and cooled on ice for ≥1 min; this procedure was repeated 6 more times. Lysate was clarified by centrifugation at 16 000 × g for 10 min at 4 °C. The supernatant was passed through a 0.45 μm centrifuge tube filter (Millipore), and the filtrate was stored at 4 °C or in the glovebox.

The SOD activity gel assay was performed using 60 μg of whole-cell protein was loaded onto 12% Tris-HCl gels (Bio-Rad). Native gel electrophoresis was performed at 4 °C. The gel was soaked in a stain containing 50 mM potassium phosphate (pH 8.2), 0.16 mM nitro blue tetrazolium (NBT), 0.27 mM riboflavin, 1mM sodium cyanide, 6.7mM TEMED (N,N,N′,N′-tetramethylethylenediamine), and was incubated in the dark for 1 h

at 4 °C. The yellowish gel was exposed to light from a 40 W white bulb for 10-15 min to develop a blue background with colorless SOD bands. Gels were imaged by a Fujifilm LAS-4000 mini imaging system. The density of each band corresponding to SOD2 activity was quantified by using NIH ImageJ software and normalized to aerobically grown W303 activity.

Sod2p solution activity was measured by monitoring the reduction of NBT by a photochemical flux of O_2^-. The reaction mixture was prepared in 330 μL of 50 mM potassium phosphate buffer at pH 7.8 containing 0.1 mM EDTA, by adding 10 μL of 90 mM NaCN, 33 μL of 1 mM NBT, 50 μL of 0.1 M methionine, and 10 μL of 0.16 mM riboflavin. Enzyme and water were added to a final volume of 1.0 mL. In the absence of enzyme, background formation of blue formazan was monitored at 550 nm after every 10 s exposure to a 40 W white light bulb at the intensity required for the absorbance to increase at a rate of 0.05 min^{-1}. One unit of SOD activity was defined by the amount of protein required to inhibit formazan formation by 50%.

Western Blots

Whole cell lysates and purified mitochondria were analyzed by Western blot. Lysate (60 μg) and mitochondrial (20 μg) proteins were resolved by 12% SDS-PAGE and transferred onto polyvinylidene fluoride membranes (Bio-Rad). Membranes were blocked with 1% casein and incubated with an antibody against Sod2p. Blot densities on membranes were quantified as above.

Yeast Protein and Iron Content Analysis

Whole cell lysate and mitochondrial protein concentrations were measured by the BCA protein assay kit (Pierce). Mitochondrial and whole cell metal concentrations were measured by ICP-MS (Agilent, Inc., Tokyo, Japan; model 7700×). Packed mitochondria and whole cells were diluted 2-fold with water. Then 50, 75 and 100 μL of the resulting suspensions were dissolved overnight in 200 μL of 30% trace-metal grade HNO3 and 100 μL of 35% trace-metal grade HCl (Fisher Scientific). Reported protein concentrations in mitochondria and whole cells were acquired from packed mitochondria and cells, and adjusted using previously reported packing efficiencies of 0.70 for whole cells and 0.77 for mitochondria.

Chapter 3 Separation Experiments

In the first group of experiments, isolated mitochondria were resuspended in 10 mM HEPES (pH 7.2) containing 1 mM PMSF, and sonicated 3 times for 30 s each with a Branson 450 sonifier at a 60% duty load using a two-step microtip. The suspension was pelleted at 18 000 × *g* for 30 min and the soluble mitochondrial layer was collected. For the first LC-ICP-MS experiment of this group, the pellet was resuspended in buffer, and the second soluble fraction was collected after centrifugation and combined with the first soluble fraction. For the second and third experiments of this group, the second soluble fraction was not combined. Extracts (2 mL injections) were passed through a Superdex 200 pg 16 × 600 mm column (GE Life Science) equilibrated in 25 mM Tris-HCl pH 7.7. Buffer was prepared in double-distilled deionized trace-metal-free water.

The elution flow rate was 0.75 mL min^{-1}, controlled by an ÄKTA (GE Healthcare Life Science, New Jersey, USA) FPLC. The entire system was housed in a refrigerated (7 °C) Ar-atmosphere glovebox (Mbraun USA Inc., Stratham, NH) with O_2 < 3 ppm as monitored by a Teledyne Model 310 analyzer.

The second group of LC studies involved size-exclusion chromatography of LMM species. Isolated mitochondria were solubilized with 1% (w/v, final concentration) sodium deoxycholate in 100 mM Tris at pH 7.4, and the supernatants were filtered through a 10 kDa cut-off membrane using an Amicon stirred concentrator. The filtrates were applied (0.5 mL injections) to two Superdex Peptide 10 × 300 mm columns (GE Life Science) connected in series and equilibrated with 25 mM Tris-HCl pH 7.7, driven by a Bio-Inert HPLC (Agilent, Tokyo, Japan). The elution flow rate was 0.375 mL min^{-1}. The entire system was located within a refrigerated glovebox.

The third group of LC studies involved anion-exchange chromatography (Mono Q 4.6/100 PE GE Healthcare; 1.7 mL column volume, CV) of mitochondrial extracts. Extracts were prepared as described above for HMM size-exclusion studies involving sonication, except that the sonication buffer was 20 mM Tris pH 7.2. Buffer A (20 mM Tris pH 7.2) and Buffer B (same as A but with 1 M NaCl) were used to generate the elution buffer gradient. The column was washed with 8 CVs of Buffer A. Proteins were eluted using 25 CVs of a 0 → 1 M NaCl linear gradient, followed by 8 CVs of Buffer B. For the second study, 5 CVs of Buffer A were passed through the loaded column followed by 3 CVs of 71% Buffer A mixed with 29% Buffer C (20 mM Tris pH 7.2 plus 0.35 M NaCl). This was followed by 25 CVs of a linear gradient (29% → 100% Buffer

C) and finally by 5 CVs of Buffer C. The elution flow rate was 1 mL min^{-1}. The Bio-inert HPLC was used for these studies.

Aqueous Fe^{III} and many other Fe^{III} complexes are insoluble at neutral pH and tend to adhere to column media. Fe^{II} is easily oxidized to Fe^{III} in air, and even under essentially anaerobic conditions, Fe accumulated on our LC columns. Thus, after each use, the size-exclusion columns were cleaned by passing 5 CVs of a chelator cocktail containing 10 μM each of EGTA, EDTA, diethylenetriamine pentaacetate, and 2,2-bipyridine followed by 10 CVs of elution buffer. (WARNING: Early attempts to use 10 mM of the same chelator cocktail seemed to damage the column media.) This was followed by 15 CVs of elution buffer. The Mono Q column was cleaned by passing 15 CVs of 20 mM Tris plus 1 M NaCl, then 15 CVs of 10 μM EGTA and EDTA, followed by 10 CVs of 20 mM Tris (without NaCl).

The ICP-MS was used in collision cell mode (He: 4.3 mL min^{-1}) with platinum cones. The instrument was optimized daily using manufacturer's tuning solution. The sample was introduced through a standard Micromist nebulizer (Glass Expansion, Australia). For size-exclusion chromatography, the eluent was split using a micro splitter valve (Upchurch Scientific, USA) with ~30% directed to ICP-MS and the remainder to the ÄKTA 950 fraction collector where 500 μL fractions were collected in Deep Well 96 well plates (Greiner, Germany). For anion exchange chromatography using the on-line ICP-MS, ~80% of the eluent was collected in 680 μL fractions using an 1260 Infinity Analytical-Scale Fraction Collector (Agilent, Tokyo, Japan). The remaining ~20% of

the eluent flowed to the ICP-MS. ^{56}Fe, ^{57}Fe, ^{55}Mn, ^{31}P, and ^{34}S were monitored with a dwell time of 100 ms.

Chapter 4 LMM Mitochondria Methods

Mitochondrial Isolation and LMM Fraction Preparation

Mitochondrial purification and manipulations were carried out anaerobically in refrigerated Ar-Atmosphere gloveboxes to maintain native redox states. Yeast mitochondria were isolated from large scale (24L) liquid culture containing minimal media and glucose using a combination of enzymatic lysis and density ultracentrifugation described in Methods in Enzymology. Mitochondria from human Jurkat cells were also isolated from a large scale suspension culture and isolated using nitrogen cavitation and subsequent density ultracentrifugation as described previously.[106] Dissected mouse tissues from the brain and liver were separately homogenized, subjected to nitrogen cavitation, and mitochondria were purified using density ultracentrifugation as described previously.[107] All Purified mitochondria batches were washed 2-3x in 50mM Tris Buffer (pH 7.4) and then resuspended 1:1 (v/v) in 50mM Tris Buffer (pH 7.4) containing 2% Triton 100x. The sample was mixed for 15 minutes. An aliquot of the mixture was removed and saved to determine total mitochondrial metal concentrations. The remaining mixture was then centrifuged at 12,000xg for 15 minutes. The supernatant was transferred to an Amicon stirred cell concentrator containing a 10kDa cutoff membrane and the flow through was collected. A

sample of the flow through was collected for each preparation to determine LMM metal concentration in the mitochondria.

Chromatographical Separation of LMM Mitochondria Metal Species

Samples (500µL) were in to the system previously described LC-ICP-MS system using two in series Superdex peptide 10 x 300 mm columns as the stationary phase and 50mM Tris buffer (pH 7.4) as the mobile phase. Elution was carried out at 0.350 mL min^{-1} for a total of 2CV (50mL). Columns were regenerated with 10CV of a chelator cocktail described previously.[(107)]

Elemental Analysis of "Complete" and LMM Mitochondrial Fraction

Aliquots (75µL) of complete and LMM fractions from each run were placed in individual 15mL Polypropylene nitric acid cleaned screw cap tubes along with 100 µL of concentrated TMG nitric acid and sealed. After samples were digested for 12hrs at 90^{o}C, samples were diluted to a total volume of 10mL for analysis by ICP-MS. ICP-MS analysis was carried out in Helium collision mode on an Agilent 7700x ICP-MS. Concentrations were determined using calibration curves prepared from standards containing P, S, Mn, ^{56}Fe, ^{57}Fe, Co, Cu, and Zn. Absolute mitochondrial concentrations were calculated using measured dilution factors and known packing efficiencies.

Chapter 5/6 Mice Studies

Animal Care and Dissections

C57BL/6 mice were raised and manipulated in accordance with the TAMU Animal Care and Use committee (AUP 2010-226) for experiments involving organ development. ICR (Imprinting Control Region) outbred mice were raised and manipulated with the same AUP were utilized for LMM brain experiments. Mice were housed in disposable plastic cages (Innovive Innocage Static Short) with all-plastic water bottles and plastic feeders with zinc electroplated reinforcements. Mice were fed Fe-deficient chow (Harlan Laboratories, Inc. Teklad ID TD.80396.PWD) supplemented as follows. For experiments involving ^{56}Fe or ^{57}Fe, the chow was supplemented with 50 μg/g of either natural abundance Fe citrate or ^{57}Fe citrate (IsoFlex USA) prepared as described. For each kg of chow, 22 mL of a 40 mM stock solution of Fe citrate (adjusted to pH 7) was added. The chow was further moistened with ca. 45 mL of double-distilled water containing 0.6 ng Fe/g water. The chow was compressed into pellets, heated at 100 °C for 20 min, and then stored at −20 °C in zip-locked plastic bags. Samples of the 7 batches of this chow examined contained an average of 33 ± 2 μg Fe/g chow as determined by ICP-MS.

Fe-deficient pups were born to a mother that was fed the Fe-sufficient diet until ~3 days prior to birth when her diet was switched to Fe-deficient (1.2 μg Fe/g chow). Fe-

deficient animals received water that was house-distilled, deionized using ion-exchange columns (Thermo Scientific 09-034-3), and distilled again using a sub-boiling still (Savillex DST-1000). The resulting sub-boiling distilled water contained 0.02 ng Fe/g water.

Each cage contained ca. 200 g of synthetic bedding (Ketchum Omega Dry) with 1.5 μg ^{56}Fe/g. Nestlets (Ancare) that were included in the cages of pregnant females weighed ~10 g and contained 20 μg ^{56}Fe/g. Nitrile gloves were worn when mice, chow, water, bedding, etc. were handled. So-called "^{56}Fe-enriched" mice were treated equivalently but were raised on chow supplemented with natural-abundance Fe citrate.

Mice were euthanized by an IP injection of a solution that provided 3 mg ketamine and 0.5 mg xylazine per 20 g body wt. Immediately after breathing ceased and the heart stopped beating, animals were imported into a refrigerated (5–10 °C) argon-atmosphere glove box (MBraun Labmaster) containing between 2–20 ppm O_2, where all dissections and tissue manipulations were performed. The "hands" of a pair of standard butyl rubber gloves on the box were cut off and replaced with tight-fitting surgical gloves using custom-designed plastic cuffs. The open end of each surgical glove was stretched over one end of a cuff and secured with two O-rings that fit into grooves on the cuff. The other end of the cuff was attached similarly to a butyl rubber glove, the other end of which was secured on the box glove port in standard fashion.

Unless noted otherwise, animals were perfused with Ringer's buffer (155 mM NaCl, 5 mM KCl, 2 mM $CaCl_2$, 1 mM $MgCl_2$, 2 mM NaH_2PO_4, 10 mM HEPES, 10 mM glucose, and ~10 U heparin/mL). A 27 gauge 1/2" long stainless-steel needle was

inserted into the left ventricle of the heart, and buffer was pumped at ca. 0.7 mL min^{-1}. After ensuring proper placement of the needle, the caudal vena cava was severed, and pumping continued for an additional 1–2 min until blanching of the liver appeared complete. For some dissections, blood diluted with Ringer's buffer was collected.

Immediately after perfusion, brains and other organs were isolated by dissection using stainless steel and/or titanium instruments. The Fe concentration of a 50 mL solution of Ringer's buffer into which the stainless steel instruments were immersed for 30 min increased by 190 nM. This is far longer than animals contacted the instruments. Thus, an insignificant amount of Fe was leached from these instruments during dissections and none of the Fe-associated features observed in the spectra originated from them.

Preparation of LMM Brain Extract

Animals were perfused with degassed heparinized Ringer's buffer at 1.0 mL min^{-1} for 0.5 min g^{-1} mouse, and then dissected as described.[6] Immediately after isolation, 3–4 brains were added to a known volume (2–3 mL) of degassed 20 mM Tris buffer (pH 7.4). The solution was homogenized for 1 min using a plastic rotary knife inserted into a tissue grinder (Omni TH). The resulting homogenate was disrupted by nitrogen cavitation (model 4639, Parr Instruments) at 800 psi for 10 min. The resulting extract was treated with Triton X-100 and Sodium deoxycholate (final concentrations of 1% (v/v) and 1% (w/v), respectively) for 10 min. The sample was removed from the box in an air-tight centrifuge bottle and spun at 110 000× g for 30 min. The bottle was

returned to the box and the resulting supernatant fraction (~3 mL) was transferred to a stirred cell concentrator (Amicon Model 8003, Millipore) fitted with a 10 kDa cutoff membrane (YM-10, Millipore). The supernatant was passed through the membrane with a head pressure of 90 psi Ar, and ~2 mL of the flow-through solution (FTS) was collected in a plastic screw-top tube. The tube was sealed with electrical tape, placed inside of a second container that was then sealed, removed from the box, and immediately imported into a second glovebox that contained the LC. In one experiment, the FTS was split into two aliquots, one of which was spiked with 100 μL of 180 nM stock solutions (prepared in 20 mM Tris pH 7.4) of $FeSO_4$, $CuCl_2$, $MnCl_2$, $CoCl_2$, $ZnCl_2$ and Na_2MoO_4. After 3 h, aliquots were injected, one after the other, into the LC-ICP-MS system.

Elemental Concentrations in Flow-Through Solutions

Aliquots (150 μL) of the FTS for each run were placed into 15 mL plastic screw-top tubes (BD Falcon) containing 100 μL of concentrated trace-metal-grade (TMG) nitric acid (6.4 M final concentration). After ~12 hr at 90 °C, samples were diluted with 9.75 mL of distilled-and-deionized water, affording a final acid concentration of 0.14 M. Calibration curves were prepared from standard solutions containing P, S, Co, Cu, Zn, Fe, Mn, and Mo (Inorganic Ventures, Christiansburg Virginia, USA) at known concentrations, prepared in trace-metal-grade nitric acid and diluted using distilled-and-deionized water. Data were collected in He collision mode using an inductively coupled plasma mass spectrometer (ICP-MS, model 7700x, Agilent Technologies, Tokyo,

Japan). Elemental concentrations were determined using the calibration curve. Values obtained were adjusted for dilution factors.

Chromatography Instrumentation

HPLC separations were carried out in a refrigerated Ar-atmosphere glove box (Labmaster, Mbraun, USA) using an Agilent 1200 Bioinert LC composed of a metal-free Infinity 1260 Quaternary Pump equipped with a manual injection valve fitted with a 500 µL PEEK injection loop. Two size-exclusion Superdex Peptide GL 10/300 columns (300 × 10 mm, GE Life Science, USA) were combined in series using a male-to-male union connector. The mobile phase was 20 mM Tris buffer (pH 7.4). Post-column eluent flow (0.35 mL min^{-1}) was mixed in real-time with a solution of 4% trace-metal-grade nitric acid plus 100 µg L^{-1} ^{116}In, diluting the eluent 2-fold. The resulting solution flowed into the ICP-MS in an on-line configuration, and ^{31}P, ^{34}S, ^{55}Mn, ^{63}Cu, ^{59}Co, ^{65}Zn, ^{95}Mo, $^{56/57}Fe$, and ^{116}In were detected. Indium was used as an internal standard to monitor plasma suppression. Other ICP-MS conditions: RF power, 1500 W; Ar flow rate, 15 L min^{-1}; collision cell He flow rate, 4.3 mL min^{-1}; sampling/skimmer cones, Pt, Pt; dwell time, 0.2 s; internal standard pump rate, 0.35 mL min^{-1}.

The column was cleaned after each run using 10 column volumes (CVs) of a chelator cocktail at a flow rate of 150 µL min^{-1} and then regenerated with the elution buffer (20 mM Tris, pH 7.4). The chelator cocktail was composed of 20 mM Tris pH 8.0 plus 10 µM each of ethylenediaminetetraacetic acid (EDTA), ethylene glycol tetraacetic acid, tetrakis-(2-pyridylmethyl)ethylenediamine (TPEN), Phen and 2,2′-bipyridine.

Molecular Mass (MM) Calibration

The MM associated with each chromatographic peak was calculated using a standard curve constructed from 14 known species. Standard stock solutions were prepared in 20 mM Tris pH 7.4, affording concentrations ranging from 1–200 μM. Each solution was injected individually onto the column. Elution volumes V_e were determined using either the ICP-MS or UV-vis detector response. In cases where multiple forms were evident (GSH, GSSG, ATP, ADP, and AMP), the peak with the MM nearest to the known mass of the species was assigned to that species. Void volume V_0 was determined using Blue Dextran (MM 2000 kDa). The logarithm of the MM was plotted *vs.* the ratio V_e/V_0 . The best-fit linear regression curve was constructed through the data points.

CHAPTER III

INSIGHTS INTO THE IRON-OME AND MANGANESE-OME OF *ΔMTM1 SACCHAROMYCES CEREVISIAE* MITOCHONDRIA*

Introduction

The Mtm1p protein found in the budding yeast *Saccharomyces cerevisiae* is a member of the mitochondrial carrier family.[108, 109] Located in the mitochondrial inner membrane (IM), members of this family transport low-molecular-mass (LMM) species between the cytosol and the matrix of the organelle. The substrate transported by Mtm1p has not been identified and so the exact cellular function of the protein is unknown. Carriers can be organized according to whether their substrates are nucleotides, carboxylates, or amino acids, with Mtm1p in the last group.[110] Substrates tend to be negatively charged and carriers often catalyze an exchange in which protons move in opposition to substrates.

Deleting the *MTM1* gene partially inactivates Mn superoxide dismutase (MnSod2p),[108, 111] suggesting that Mtm1p might be involved in Mn metabolism. During maturation, apo-Sod2p is sent to the mitochondrial matrix where Mn is installed during folding, suggesting that Mtm1p either imports Mn or is a chaperone for that installation.

---

* This chapter is reproduced in part with permission from "Insights into the iron-ome and manganese-ome of *Δmtm1 Saccharomyces cerevisiae* mitochondria" by Jinkyu Park, Sean P. McCormick, Myrinmoy Chakrabarti, Paul A. Lindahl, 2013, Metallomics, 5, 656-672, copyright 2013 Royal Chemical Society

However, the Mn concentration within *Δmtm1* mitochondria is elevated relative to that of WT mitochondria,[108] discounting the possibility that Mtm1p imports Mn.

Attention shifted to Fe metabolism when Sod2p was found to be inactivated in association with an elevation of Fe in *Δmtm1* cells.[108, 111] Genetic and chromatographic results suggest that an *Apo-Sod2p-Reactive* (ASR) pool of Fe in the matrix (referred to as Fe_{ASR}) competes with Mn ions for installation into the active-site of apo-Sod2p. Indeed, Fe misincorporates into superoxide dismutases, a process that prevents the apo-enzyme from being activated by Mn.[112] The size of the Mn pool in yeast mitochondria varies with the concentration of Mn in the growth medium.[108] The mitochondrial Fe concentration increases under Mtm1p-deficient conditions.

The extent of Fe misincorporation appears related to the Fe concentration in the growth medium, in that Fe-deficient conditions (created by adding the chelator bathophenanthroline disulfonate) prevent both Fe accumulation and loss of SOD2 activity in *Δmtm1* mitochondria.[111] Misincorporation is also prevented by additionally deleting *MRS3/4*, the genes encoding high-affinity Fe transporters on the mitochondrial IM.[111] This suggests that the Fe_{ASR} pool enters the mitochondria through Mrs3p/4p.

A single Mn species, associated with MnSod2p, was identified in fractions obtained by passing WT mitochondrial extracts through an anion-exchange column; no such species was observed with *Δmtm1* extracts. Replacing this peak in chromatograms of *Δmtm1* mitochondrial extracts was a dominating Fe peak that co-eluted with Sod2p. This peak, attributed to FeSod2p, was absent in extracts of a *Δmtm1* Δ*sod2* double-deletion mutant. This was the only Fe-containing peak evident in soluble *Δmtm1*

extracts, and the peak was absent in WT extracts. This suggested that the majority of the soluble Fe in *Δmtm1* mitochondrial extracts that eluted through the column was misincorporated into apo-Sod2p.

The situation is actually more complicated in that a deficiency of Mtm1p is not unique in causing Fe to accumulate or misincorporate.[(111)] Depleting the cell of Ssq1p, Grx5p, and Atm1p also causes Fe to accumulate in mitochondria and Sod2p to partially inactivate. These proteins are involved in mitochondrial Fe metabolism, but they have distinct functions. Ssq1p is a soluble Hsp70-family chaperone that helps install nascent Fe/S clusters into recipient apo-Fe/S proteins.[(113)] Atm1p is a mitochondrial IM ABC transporter that exports an unknown sulfur-containing species required for cytosolic Fe/S cluster assembly.[(114)] Grx5p is a monothiol glutaredoxin that binds the scaffold proteins Isa1p/Isa2p.[(115)] Based on these diverse functions, it would appear that neither apo-Sod2p-misincorporation nor Fe accumulation in mitochondria are *primary* effects of Mtm1p deficiency. Rather, they appear to be *secondary* effects arising in mitochondria lacking Mtm1p, Grx5p, Ssq1p, or Atm1p.

Another complexity is that Fe accumulation and misincorporation appear to be independent of each other. The absence of certain mitochondrial proteins, *e.g.* yeast frataxin homolog Yfh1p[(116)] and the scaffold protein Isu1p, cause Fe accumulation but not misincorporation. Interestingly, the proteins which, when depleted in cells, cause Fe to accumulate but NOT misincorporate (*e.g.* Yfh1p and Isu1p) help *build* Fe/S clusters. In contrast, proteins which, when lacking, cause both Fe accumulation AND misincorporation (*i.e.* Atm1p, Grx5p, and Ssq1p) may help *transfer* assembled clusters

into recipient apo-proteins.[98] This correlation implies that Mtm1p functions in cluster transfer, not assembly. The misincorporated Fe has been proposed to originate from the Fe/S cluster donated by Isu1p. This is consistent with the increased level of Isu1p in *Δmtm1* cells relative to in WT cells[98, 117] in that the cell may compensate for a deficiency of Fe/S clusters by increasing Isu1p levels.

Another complexity in understanding the *Δmtm1* phenotype is that the *type* of Fe that accumulates in Atm1p-depleted mitochondria (and in Δ*yfh1* and Yah1p-depleted mitochondria) is ferric oxyhydroxide (phosphate or polyphosphate) nanoparticles.[118-120] This insoluble form of Fe seems unlikely to insert into apo-Sod2p; we would expect that soluble Fe^{II} ions insert. Also, the size of the Fe_{ASR} pool is unknown. It should enlarge in strains lacking Mtm1p, Atm1p, Grx5p, and Ssq1p, relative to in WT cells, but there is no certainty that the majority of the Fe that accumulates in the mitochondria of these strains is that particular pool of Fe.

To address this question, X-ray absorption spectroscopy (XAS) was performed on *Δmtm1* mitochondria as well as on mitochondria from a control mutant (*rho*$^{-}$) that also accumulates Fe but exhibits normal SOD2 activity when the growth medium is supplemented with 2 mM Fe.[98] No difference in the properties of the accumulated Fe, including oxidation state, geometry, or ligand environment, could be discerned. This suggests that the Fe_{ASR} pool that misincorporates into apo-Sod2p must be quite *small* – so small that it is undetectable by XAS.

Mtm1p has also been suggested to function in heme biosynthesis. One of the five mitochondrial proteins that coexpresses with other proteins involved in heme

biosynthesis in zebrafish is an ortholog of yeast Mtm1p.[117] Silencing this gene prevented Fe incorporation into protoporphyrin IX. This suggests that this Mtm1p-like protein is involved *early* in heme biosynthesis, *i.e.* prior to insertion by ferrochelatase, perhaps by regulating *d*-aminolevulinate synthase, the committed step in heme biosynthesis.

Previously, we studied the iron-ome of mitochondria from WT and mutant strains related with mitochondrial Fe/S and heme biosynthesis.[119-121] The iron-ome of fermenting WT mitochondria is mainly composed of Fe/S clusters, heme centers, HS $Fe^{II/III}$, and Fe^{III} nanoparticles. However, mutant mitochondria commonly exhibit a dominant Fe^{III} nanoparticle feature, and are largely devoid of intact Fe/S clusters and heme centers. In this paper, we describe the iron-ome of mitochondria from *Δmtm1* yeast using biophysics and liquid chromatography (LC) in conjunction with an on-line inductively coupled plasma mass spectrometer (ICP-MS). Similarly to the previous studies, most of the accumulated Fe is present as Fe^{III} oxyhydroxide nanoparticles, which is unlikely to misincorporate into apo-Sod2p. LMM Mn and Fe species were observed in mitochondrial extracts that could potentially represent the sought-after pools. An Fe-containing protein comigrated approximately with MnSOD-containing fractions, but the relative level of this protein was similar in both WT and *Δmtm1* mitochondria. We conclude that deleting *MTM1* diminishes SOD2 activity in a manner that does not involve Fe misincorporation, and suggest alternative cellular functions for this protein.

This chapter summarizes the LC-ICP-MS experiments used to investigate the role of the *MTM1* protein on both Fe and Mn metallomes. Dr. Jinkyu Park, who was a

graduate student in the lab, was primarily responsible for the studies involving the Mtm1 strain. My role on this study was to setup, operate, and maintain the LC-ICP-MS system, help run the separations and collect the data, and analyze the results we obtained. I also participated in the broader discussions on this project.

Results

Initial experiments conducted by Dr. Park, were unable to located the speculated pool of "bioavailable" iron Fe_{ARS} or the misincorporation of iron into the SOD protein. It was at this point in which it was decided LC-ICP-MS may be able to assist in addressing these hypothesis. Soluble WT and *Δmtm1* fractions were subjected to liquid chromatography, and the eluent was monitored for metal ions using ICP-MS. In most experiments, the ICP-MS was configured on-line, such that the eluent was split, with a portion flowing into fractions and the remainder to the ICP-MS in real time during the chromatography run. In off-line experiments, the entire eluent was fractionated, and fractions were individually analyzed by ICP-MS.

The A_{280} trace of the eluent off the Superdex column (not shown) indicated that >90% of the protein in the soluble samples eluted in the void volume. This volume was ca. 46 mL and corresponded to molecular masses >600 kDa. Also eluting in the void volume was a small proportion of the Mn in the injected sample (Figure 3.1.a and b, upper traces). Two major Mn peaks were observed in later fractions, called Mn_{100} and $Mn_{2\text{-}3}$, with molecular masses of ca. 100 kDa and <10 kDa respectively (Figure 3.1.a and

b). Mn_{100} co-eluted with active tetrameric Sod2p while $Mn_{2\text{-}3}$ corresponded to the LMM species.

We have sufficient information to roughly estimate the speciation of Mn in mitochondria. In WT mitos grown on normal medium, ca. 64% of the soluble Mn was SOD2-associated. Thus, ~24% (0.64 × 38%) of total Mn ions in the original mitochondrial sample was associated with 28% of the total SOD2 activity. The similarity of these two numbers suggests that the remaining 72% of MnSod2p in the pellet represented another 62% of the Mn in WT mitochondria. Thus, the majority of the Mn in these organelles (28% + 62% = 90%) appears to be associated with MnSod2p. $Mn_{2\text{-}3}$ represented 32 ± 3% of the soluble Mn in our WT samples, corresponding to 12% (0.32 × 38%) of total WT mitochondrial Mn. These results indicate that the Mn in WT mitochondria is distributed into two species – ca. 90% is associated with MnSod2p and ca. 10% is present as soluble LMM species.

In *Δmtm1* mitochondria, about 45% of total Mn was soluble. Of this, 89% was LMM and 9% was associated with MnSod2p. Only ca. 4% of total Mn in *Δmtm1* mitochondria was in the form of soluble Sod2p, and this corresponded to 26% of total SOD2 activity. The other 74% of the Sod2p protein (in the pellet) must have included another 12% of the total Mn. Thus, 15% of total Mn in *Δmtm1* mitochondria (4% + 11%) was probably MnSod2p-associated. The only other species observed in the soluble fraction was $Mn_{2\text{-}3}$, suggesting that >80% of the Mn in *Δmtm1* mitochondria arise from LMM species. As mentioned above, the concentration of Mn in *Δmtm1* mitochondria was about twice that of WT mitochondria. Our analysis indicates that most of the

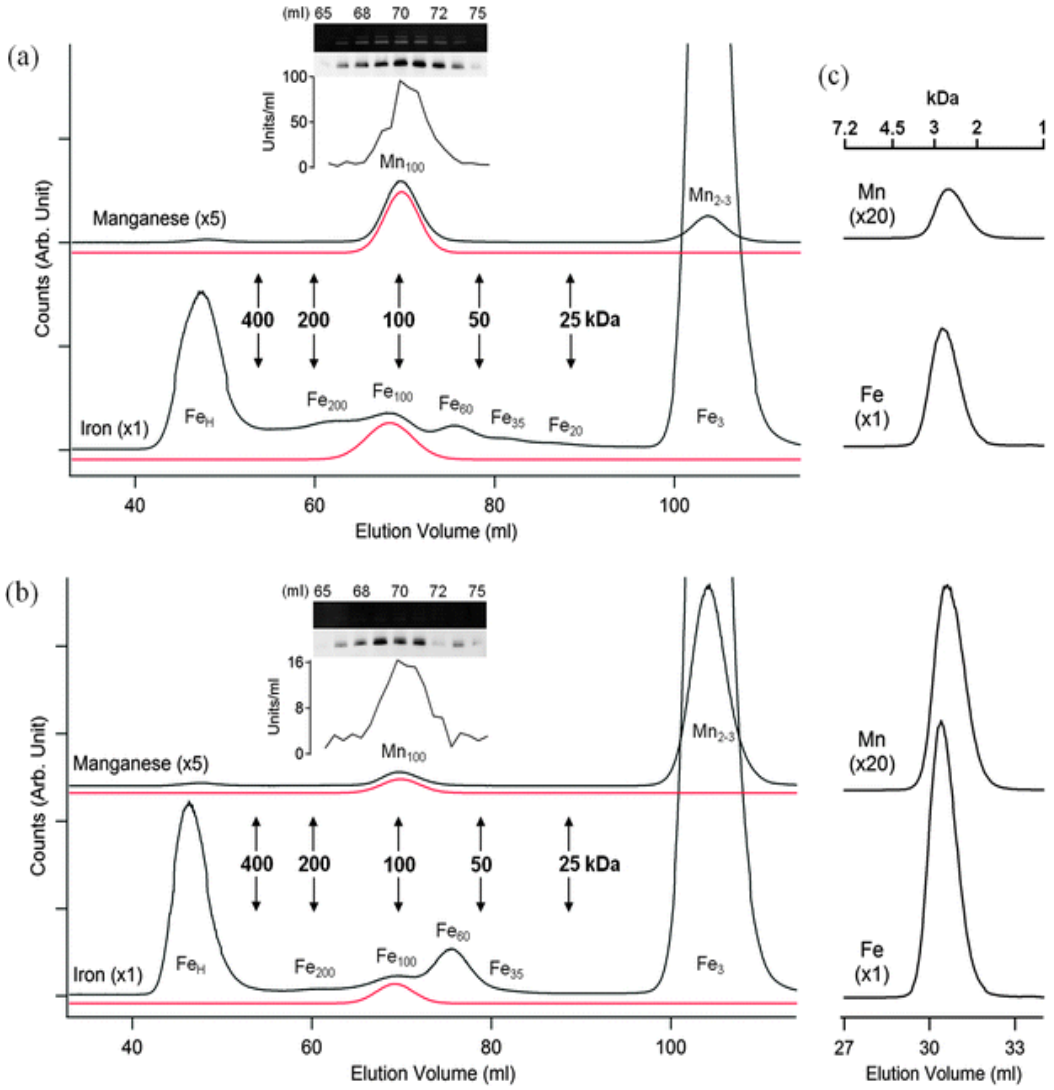

Figure 3.1. Mn and Fe traces from SEC-ICP-MS chromatography of soluble fractions of W303 and *Δmtm1* mitochondria. (a) HMM chromatograms of W303 mitochondria; (b) HMM chromatograms of *Δmtm1* mitochondria, Experiment 1. Red solid lines simulate Mn and Fe species that co-eluted with Sod2p. The inset shows images of SOD2 activity gel, Western blot membrane against Sod2p for each fraction labeled with fraction volume, and SOD2 unit activities determined spectrophotometrically. Metal peaks were labeled according to their approximate molecular weight. Molecular mass was determined using a calibration plot for the Hi-Load Superdex 200 column. (c) LMM chromatograms of W303 (top) and *Δmtm1* (bottom) mitochondria, Experiment 4. Chromatographic intensities were adjusted proportionally to mitochondrial LMM Mn and Fe concentrations, and then WT-Mn and *Δmtm1*-Mn were amplified 20-fold for easier comparison.

additional Mn in *Δmtm1* mitochondria was present as $Mn_{2\text{-}3}$. Also, the MnSod2p protein level in *Δmtm1* mitochondria was diminished relative to WT levels. Assuming 13 μM [Mn] in WT mitochondria, this corresponds to 12 μM MnSod2p and 1 μM $Mn_{2\text{-}3}$. In *Δmtm1* mitochondria, with 26 μM [Mn], we calculate 4 μM MnSod2p and 22 μM $Mn_{2\text{-}3}$. Thus, deleting MTM1 caused a 3-fold reduction in active MnSod2p and a 22-fold increase in the size of the LMM Mn pool in the mitochondria.

In the second experiment, for mitochondria isolated from WT cells grown on medium supplemented with 200 μM $MnCl_2$, the Mn trace (Figure 3.2) again showed two major peaks, Mn_{100} (23%) and $Mn_{2\text{-}3}$ (68%). In this case, 15% of the total Mn in the sample was soluble, and of this, 23% corresponded to MnSod2p. This means that 0.23 × 15% = 3.5% of total Mn in the sample corresponded to 10% of the SOD2 activity. The remaining 90% of the activity must have represented another 31% of total Mn. Thus, nearly 35% (3.5% + 31%) of total Mn in the sample was associated with MnSod2p. The only other species present in the chromatogram was $Mn_{2\text{-}3}$, suggesting that it corresponded to the remaining 65% of the total Mn in WT mitochondria grown on excess Mn. With 35 μM = [Mn], we conclude that 12 μM was MnSod2p and 23 μM was $Mn_{2\text{-}3}$. Thus, the MnSod2p level remained about the same while the LMM Mn pool increased dramatically. Thus, the size of the LMM Mn pool in mitochondria is sensitive to the Mn concentration in the medium.

Finally, we consider the Mn distribution in mitochondria from *Δmtm1* cells grown on 200 μM Mn (Figure 3.2). In this case, Mn_{100} represented 5% of the Mn in the chromatogram while $Mn_{2\text{-}3}$ was 94%. 28% of total Mn was soluble, and so (0.05 × 28%

=) 1.4% of total Mn corresponded to 31% of MnSOD2 activity. The remaining 69% of the SOD activity must correspond to another 3.1% of the total Mn in the sample, suggesting that 4.5% of total Mn was MnSod2p. The sample had 80 μM Mn, and so there was 4 μM (80 × 0.045) MnSod2p in mitochondria from *Δmtm1* cells grown with 200 μM Mn. The remaining 76 μM was associated with $Mn_{2\text{-}3}$. This analysis indicates that the concentration of MnSod2p did not change with Mn supplementation in the growth medium, but that the LMM Mn pool concentration increased more than 2-fold. The results of these calculations are visually summarized in Figure 3.3.

The corresponding Fe traces exhibited 7 distinguishable features, with significant concentrations in the void volume (FeH), 5 minor-intensity peaks in the central region (Figure 3.1 a and b, lower traces; F_{200}, Fe_{100}, Fe_{60}, Fe_{35}, and Fe_{20}), and an intense LMM feature (Fe_3) that has a slightly higher mass than $Mn_{2\text{-}3}$. Fe_3 is a viable candidate for Fe_{ASR}. For the first two experiments, an average of 25% of the total Fe was solubilized from mitochondrial extracts. Of this, Fe_H represented 67% of total mitochondrial Fe in one experiment and 17% in the other. The Fe_3 intensity corresponded to 19% of total Fe in the first experiment and 74% in the second. Despite the large variations, these two peaks collectively dominated the Fe chromatograms of soluble WT mitochondrial extracts. The intermediate-molecular-mass (IMM) Fe species corresponded to ca. 10% of the soluble Fe – representing 2.5% of the total Fe. With a total Fe concentration of 880 μM in WT mitochondria, these IMM Fe species were present at ca. 20 μM collectively, with Fe_{100} corresponding to a concentration of ca. 9 μM.

An average of 7% of total Fe was solubilized in the corresponding *Δmtm1* mitochondria samples. Since the Fe concentration in these mitochondria was 3500 μM, this corresponded to 245 μM Fe injected onto the column. Fe_H and Fe_3 again dominated the chromatograms. Fe_{100} represented 2% of the overall chromatogram intensity, corresponding to a concentration of 5 μM. Thus, upon deleting MTM1, Fe_{100} declined nearly 2-fold.

Under high Mn nutrient conditions, 14% of WT mitochondrial Fe was solubilized; this corresponded to 87 μM Fe (620 μM × 0.14) in the soluble sample. Fe_{100} represented 3% of that Fe (ca. 3 μM). For *Δmtm1* mitochondria, 8% of mitochondrial Fe was solubilized. At 5200 μM Fe, this corresponded to 416 μM soluble Fe loaded on the column. Fe_{100} represented 0.4%, corresponding to 2 μM. Thus, deleting MTM1 under high Mn caused a slight decline of Fe_{100}. This was the same qualitative effect as seen under normal Mn growth conditions.

Fe_{100} approximately coeluted with Mn_{100} raising the possibility that it corresponded to FeSod2p. The absolute concentration of Fe_{100} in mitochondria and the percentage of Fe that it represented would indeed make it impossible to detect by either Mössbauer or XAS spectroscopies. If the percentage of Fe-misincorporated Sod2p is defined as = $100[Fe_{100}]/([Fe_{100}] + [Mn_{100}])$, then the percentage of FeSod2p was 75 ± 4% and 79 ± 3% for WT and *Δmtm1* mitochondria (average of 3 experiments). Assuming that Fe_{100} corresponds to FeSod2p, these percentages show that there was no significant difference in the extent of Fe misincorporation into apo-Sod2p between WT and *Δmtm1* mitochondria. Although these results cannot exclude the possibility that Fe_{100}

corresponds to FeSod2p, the results of other LC experiments (e.g. see Figure 3.5) discount this possibility. Thus, we suggest that only minor portions of Sod2p in our WT and *Δmtm1* preparations may be misincorporated with Fe.

We performed SOD2 activity gels and Western blots against Sod2p using pooled Sod2p-containing fractions and as-isolated mitochondria. In all three experiments, pooled fractions of SOD2-active *Δmtm1* extracts revealed specific activities corresponding to 100 ± 14% of WT levels. This again indicated that the extent of Fe-misincorporation in *Δmtm1* and WT cells is similar.

The situation was different using isolated mitochondria. The SOD2 specific activity of *Δmtm1* mitochondrial extracts, prepared from cells grown without Mn supplementation, was ca. 20% of the SOD2 specific activity of equivalent WT mitochondrial extracts. This suggested that a large percentage of Sod2p in *Δmtm1* mitochondria is inactive but is not associated with the MnSod2p in the Mn100-containing fractions. The inactive Sod2p probably migrates differently through the column or remains in the pellet during solubilization. We performed Western blots on various fractions that eluted from the column, but could not identify any that contained Sod2p, suggesting that the inactive form is in the pellet. This form could be Fe-misincorporated, misfolded or modified in some manner.

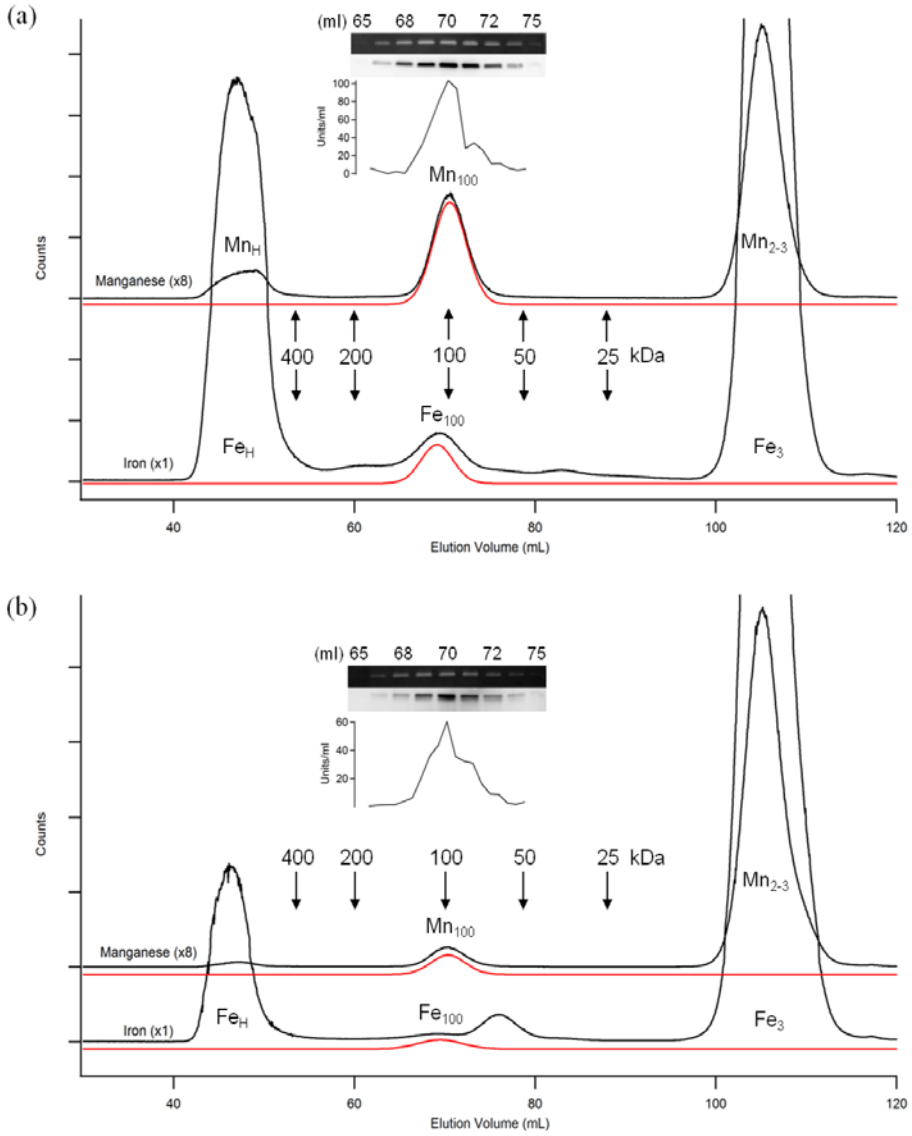

Figure 3.2. Mn and Fe traces from Experiment 2 (200 µM $MnCl_2$ supplimented in media) of the first group of LC-ICP-MS studies. The inset shows the SOD2 activity gels. Western blots against Sod2p and SOD2 activity unites determined spectrophometrically. (a) W303; (b) Δ*mtm1*

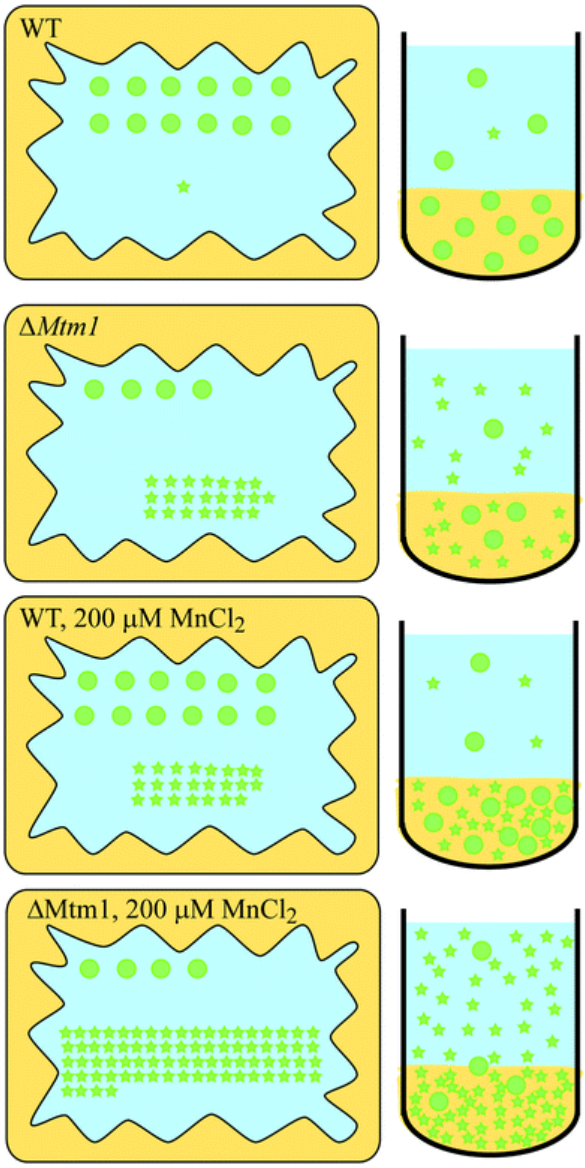

Figure 3.3. Visualization of Mn distribution. Left side, concentrations of MnSod2p (circles) and $Mn_{2\text{-}3}$ (stars) in intact mitochondria from WT and *Δmtm1* cells grown on media with ~2 and 200 μM Mn. Right side, the Mn content of corresponding mitochondrial extracts after sonication and centrifugation. Each circle and star represents 1 μM Mn concentration.

There was some recovery in SOD2 specific activity in mitochondria isolated from cells grown on Mn supplemented medium, similar to that reported previously.1 In this case, the SOD2 specific activity of *Δmtm1* mitochondria was ca. 70% relative to WT mitochondria. This might be caused, not by an increase of MnSod2p, but a decrease in Sod2p expression such that only ~30% of Sod2p in *Δmtm1* mitochondria is inactive. Further studies are required to examine this possibility.

LC-ICP-MS of LMM Species

We initially collected the $Mn_{2\text{-}3}$ and Fe_3 fractions from the first group of experiments, and subjected them to the LMM size-exclusion column to determine their molecular masses with greater accuracy. The results indicated multiple overlapping species, with poor reproducibility from batch to batch. More consistent (and simpler) results were obtained by disrupting isolated mitochondria by adding detergent (deoxycholate) rather than by sonication. Supernatant fractions were passed through the 10 kDa cut-off membrane and the flow-through was injected onto the column. $Mn_{2\text{-}3}$ and Fe_3 dominated (Figure 3.1 c, Experiment 4), and they eluted in accordance with molecular masses between 2–3 kDa (explaining the subscripts used). Taken together, these results suggest that the major LMM Mn and Fe species in yeast mitochondria have similar ligand environments (at least in terms of the collective masses of the ligands).

Anion Exchange Chromatography

We repeated previous LC experiments using the same column (MonoQ) and run conditions (except that we performed our LC under anaerobic conditions). Due to the high salt concentration involved at the end of the gradient, individual fractions were analyzed (after dilution) for metals using the ICP-MS off-line. Soluble mitochondrial extracts from sonicated WT and *Δmtm1* mitochondria afforded an intense Mn peak at ~14 mL, another less intense peak (or group of incompletely resolved peaks centered) at ~19 mL, and unassigned peaks at 2, 36, and 62 mL (Figure 3.4, Experiment 5). We tentatively assign the dominant peak to $Mn_{2\text{-}3}$, based on results of the LMM size-exclusion study in which MnSod2p and $Mn_{2\text{-}3}$ peaks dominated. SOD2 activity assays and Western blots against Sod2p demonstrated that Sod2p co-eluted with the second peak(s) (Figure 3.4, insets i, ii). The specific SOD2 activity in the five fractions containing most Sod2p was 2-fold lower in *Δmtm1* than in WT fractions, suggesting that one or more inactive forms of Sod2p co-eluted with the active form. The Fe concentrations in these fractions were also determined. One major Fe peak was observed in both *Δmtm1* and WT chromatograms, which we tentatively assign to Fe_3, with similar justification. There were low intensity features in the vicinity of the SOD2-active Mn peaks (Figure 3.4, insets iii, iv), but nothing that comigrated exactly with the SOD2-active fractions or with an intensity that would suggest massive Fe-misincorporation.

The experiment was repeated but using a shallower salt gradient and with the ICP-MS on-line. Sod2p and SOD2 activity co-eluted with Mn around 30 mL in both of WT and *Δmtm1* chromatograms (Fig. 3.5, Experiment 6) whereas the nearest Fe species

eluted at a somewhat greater elution volume. These results again indicate that the extent of Fe mis-incorporation is not significant in *Δmtm1* cells, and is no greater than in WT cells. SOD2 activity is diminished in *Δmtm1* mitochondria, but not because of excessive Fe-misincorporation.

The Sod2p in fractions collected from the MonoQ column migrated in four different positions in native gels (see Figure 3.5b, bottom insets). Sod2p is active as a homotetramer,1 suggesting that subunits may have different charge, with each combination migrating slightly differently through the column. The situation differs for Sod2p in fractions from size-exclusion columns (Figure 3.5a), because the molecular masses of the different tetrameric forms are so similar. Sod2p tetramers in earlier Mono Q fractions are less negatively charged, and more Sod2p in *Δmtm1* mitochondria eluted earlier compared with WT mitochondria. Although most Sod2p eluted at ~30 mL (Figure 3.5), an Sod2p band was observable down to 20.6 mL (0.14 M NaCl) in the *Δmtm1* chromatogram (Figure 3.5b), whereas Sod2p was visible only down to 24.7 mL (0.17 M NaCl) in the WT chromatogram (Figure 3.5a). This suggests that Sod2p might acquire a charge-altering post-translation modification such as phosphorylation, and that this process is somehow diminished in *Δmtm1* mitochondria. Consistent with this, threonine (T147 and T149) residues in Sod2p can be phosphorylated.

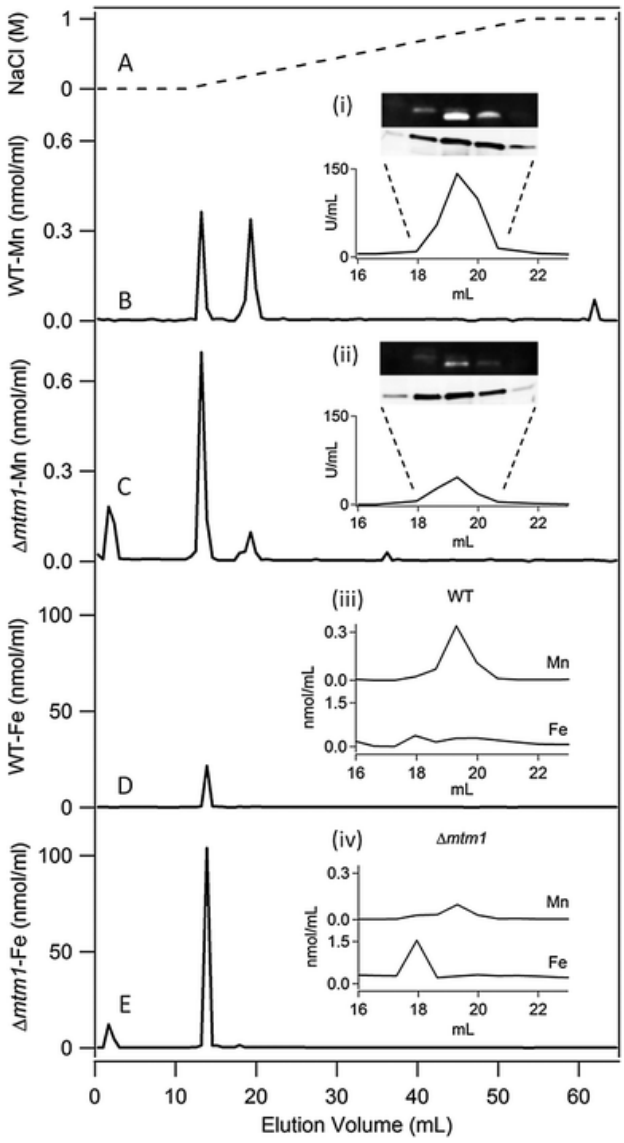

Figure 3.4. Off-line ICP-MS anion-exchange chromatograms of soluble W303 and *Δmtm1* mitochondria, Experiment 5. (A) dotted line, salt gradient; (B) W303, Mn concentrations in eluted fractions; (C) *Δmtm1*, Mn; (D) W303, Fe; (E) *Δmtm1*, Fe. Insets, (i) W303, SOD2 activity gel and Western blot membrane against Sod2p from five adjacent fractions containing most Mn (top), SOD2 unit activity from corresponding fractions (bottom); (ii) *Δmtm1*, same as (i); (iii) W303, close-up view of Mn and Fe profiles in 16–23 mL region; (iv) *Δmtm1*, same as (iii).

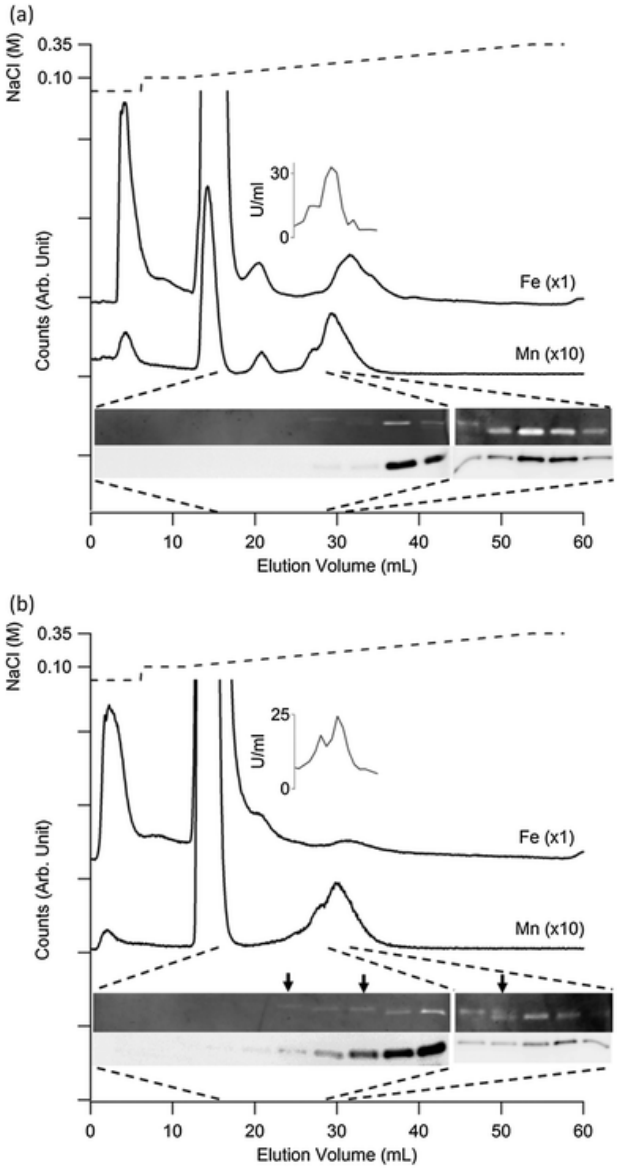

Figure 3.5 On-line anion-exchange chromatograms of soluble (a) W303 and (b) *Δmtm1* mitochondria in Experiment 6. Salt gradient is shown as the dashed lines above the data. Mn detector responses are multiplied by 10. Insets, SOD2 unit activity of the 15 fractions centered at 30 mL (above Fe trace); images of SOD2 activity gel and Western blot membrane against Sod2p (below Mn trace), from every other fraction in 16–28 mL (left), from five adjacent fractions (28–31 mL) containing most Mn (right). Differently-migrating MnSod2p bands in native gel are indicated by arrows above the lane exhibiting a differently charged form (reading from right to left). Contrast for the Western blots of the 16–28 mL fractions are greater than for the 28–31 mL blots.

Discussion

The early studies by Dr. Park suggested that Fe_{ASR} should be present at very low concentrations with no chance of being characterized or even detected by Mössbauer spectroscopy. Thus, we turned our attention to LC-ICP-MS with the goal of identifying Fe_{ASR} and the Fe-mismetallated FeSod2p. We regard Fe_3 as a viable candidate for Fe_{ASR}, because it is a LMM species with a molecular mass similar to that of $Mn_{2\text{-}3}$. In this case, the mismetallation reaction would be

$$Fe^{II}\ L_3 + \text{apo-Sod2p} \rightarrow L_3 + \text{FeSod2p}$$

The most likely candidate for FeSod2p was Fe_{100}, based on molecular mass. However, the fraction of mismetallated Sod2p present in *Δmtm1* mitochondria, assuming Fe_{100} to be this species, was no different than in WT mitochondria. This was unexpected, and it casts doubt on this assumption.

We were also unable to reconcile our size-exclusion LC-ICP results with a previous study. The previous MonoQ chromatograms of WT mitochondrial extracts displayed only one Mn peak (MnSod2) which was absent in chromatograms of *Δmtm1* mitochondria. In contrast, we observed the MnSod2 peak in chromatograms from both WT and *Δmtm1* mitochondria. Moreover, our chromatograms exhibited a second major Mn species that has not been observed previously.

In the earlier study, no Fe peaks were observed in the WT chromatogram while two Fe peaks were observed in the *Δmtm1* chromatogram (one that comigrated with Sod2p and one that eluted in the void volume). We observed a major Fe species in both WT and *Δmtm1* chromatograms that did not comigrate with Sod2p, as well as minor Fe peaks that comigrated in the vicinity of MnSod2p. We did not observe an Fe species that comigrates precisely with MnSod2p. We cannot explain these differences. In the previous study, the bulk of Fe in *Δmtm1* mitochondria was concluded to be associated with Sod2p (as FeSod2p). Based on our results, we conclude that only a tiny amount of mitochondrial Fe could be associated with Sod2p, and that the level of FeSod2p in *Δmtm1* cells is similar to that in WT cells.

Observed differences may arise from differences in the yeast strain (W303 vs. BY4741), growth medium (minimal vs. YPD), growth conditions or preparation methods, but we have no supporting evidence for any of these possibilities. It is also possible that additional FeSod2p formed in *Δmtm1* mitochondria but that it was less stable than MnSod2p and that it localized primarily in the pellet of our samples. However, yeast FeSod2p is sufficiently stable and soluble for crystallization studies, casting doubt on this explanation.

Determining the function of Mtm1p – defined by the species transported by this IM mitochondrial carrier – is a continuing challenge. Our results suggest that the lower SOD2 activity observed in *Δmtm1 S. cerevisiae* arises, not because of excessive mismetallation, but because a significant portion of Sod2p is misfolded or degraded, and/or because the expression-level of SOD2 is diminished. One possibility is that

Mtm1p imports a Maturation Factor (MF) required to help mature apo-Sod2p (Figure 3.6). Other proteins that exhibit this phenotype (Ssq1p, Grx5p and Atm1p) might also be involved in apo-Sod2p maturation, which includes installing Mn and folding the protein. In the absence of Mtm1p (or these other proteins), the rate of maturation might slow such that apo-Sod2p misfolds or does not become metallated as fast as observed in WT cells. The slow rate of maturation might cause the Mn species that is used for metallation (e.g. $Mn_{2\text{-}3}$) to accumulate. Under Mn-supplemented conditions, this Mn species would be imported at a greater rate.

Another possibility, suggested by the results of Figure 3.5, is that Mtm1p helps regulate MnSod2p activity and/or stability by promoting a reaction that affects the charge on the protein. Phosphorylation reactions are used to regulate numerous mitochondrial enzymes,[122, 123] and are involved in the H_2O_2 stress response.[124] Our results are consistent with the possibility that in the absence of Mtm1p, the degree of phosphorylation declines. However, further studies are required to interpret these results more definitively.

In WT cells, Sod2p is mainly metallated with Mn. Fridovich purified Sod2p from *S. cerevisiae*, and found sufficient Fe in the purified Mn-protein solution for no more than 6% of it to be Fe-bound.[125] Approximately 80% of the Sod2p isolated by Whittaker and Whittaker[126] from the same organism contained Mn, with ~20% containing Fe. Jeong et al.[127] purified the Sod2p from the closely-related *Schizosaccharomyces pombe* and was unable to detect any Fe (or Cu, Zn, or Ni) in the purified enzyme; the only metal detected was Mn.

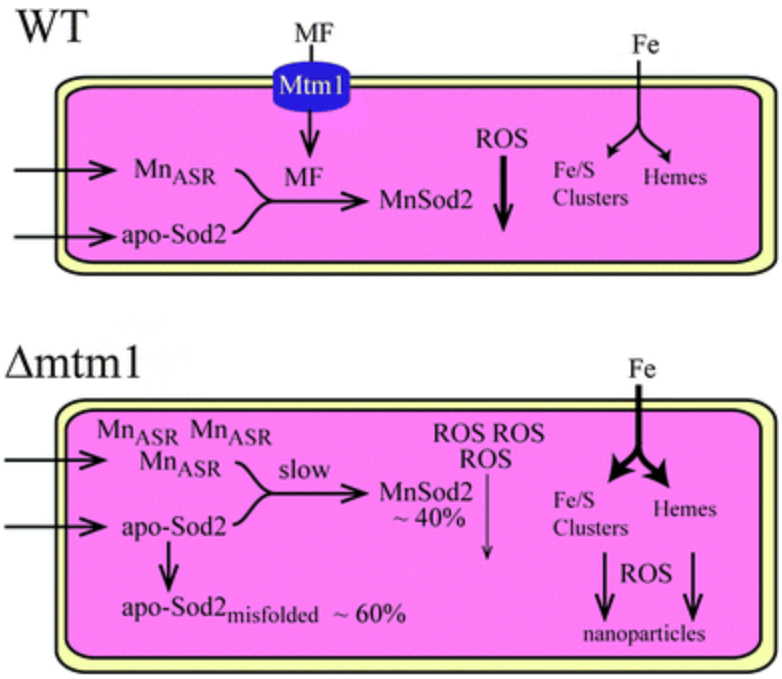

Figure 3.6 Model of Mtm1p Function. Mtm1p as an importer of a factor (presumed to be a small molecule) that helps mature apo-Sod2p, perhaps involving Mn insertion or protein folding. In the absence of Mtm1p, the rate of maturation slows which causes a build-up of Mn_{ASR} and immature Sod2p that eventually misfolds. The lack of functional MnSod2p increases the concentration of ROS in the matrix, which triggers the Fe accumulation phenotype.

On the other hand, Kang et al.[128] determined the X-ray diffraction crystal structure of the Fe-metallated *S. cerevisiae* Sod2p to 1.79 Å resolution. In cell grown under normal conditions, the extent of mismetallation seems to vary from 0% to 20%. The mismetallated protein used for crystallography was obtained by overexpressing yeast apo-Sod2p in E. coli grown in medium supplemented with 100 μM Fe, which may have increased the level of mismetallation. Using Mössbauer spectroscopy, Fleischhacker et al.[129] found that 40% of the Fe in whole E. coli cells (grown on medium supplemented with just 10 μM ^{57}Fe) was mononuclear NHHS Fe^{II}. Higher levels of such Fe might be present in cells grown with 100 μM Fe in the medium. Such Fe, consisting of one or more octahedral complexes with a coordination environment dominated by O and/or N ligands, is the type of Fe expected for mismetallation.

There is no doubt that apo-Sod2p can and does mismetallate with Fe, but our results do not support the view that there is an increased level of Fe mismetallation in *Δmtm1* cells. Rather, they suggest that in *Δmtm1* cells there is a decline in the degree to which apo-Sod2p is activated, folded, metallated or matured. Establishing the molecular details of this will be a future challenge, but one that is needed to provide further insight into the physiological role of this fascinating protein.

CHAPTER IV

DIRECT DETECTION OF LOW-MOLECULAR-MASS METAL SPECIES IN MITOCHONDRIA

Introduction

There is no doubt that eukaryotic cells contain low-molecular-mass (LMM) non-proteinaceous transition metals complexes, yet these so-called *labile* or *chelatable* metal pools are poorly understood in terms of composition, structure and function. Transition metal complexes generally exhibit rapid ligand-exchange, making them "moving targets" in terms of structural and functional characterization. Low-molecular-mass metal complexes (LMMMCs) are thought to participate in metal-ion regulation, trafficking, storage and/or signaling in cells. Such cellular processes are often dysfunctional in metal-associated diseases. Thus, it is important to characterize such complexes, these difficulties notwithstanding.

The most popular approach to studying LMMMCs is to treat intact cells with custom-designed fluorescence-based chelators (also called sensors or probes) that target such species when incubated with cells. These probes can penetrate cells and organelles without destroying them, a major advantage. However, the sought-after complexes are destroyed in the process, since endogenous ligands associated with these complexes must dissociate when the probes coordinate the metal. This is a major disadvantage. Also, the binding-strength required to chelate a particular pool of LMMMCs is generally unknown. Thus, a probe that is too strong might overestimate the size of the pool and a

probe that is too weak might underestimate it. LMMMC pools may also be heterogeneous, with multiple LMMMCs contributing. Probes are championed as being specific for a particular metal ion, but ideally they should be specific for a particular LMM complex. Without this specificity, it would be difficult to decipher the function of each component of a pool from the bulk properties of the pool.

Since the structures and properties of LMMMCs in cells have not been determined, the extent to which they are labile or chelatable also remains uncertain. If the ligands exchanged very fast, such complexes would lack a defined shape, raising questions of how the cell could recognize and use such complexes in regulation, trafficking or signaling. Moreover, the coordination sites of rapidly-exchanging metal complexes would allow for fluxional binding and uncontrolled reactions (e.g. the Fenton and Haber-Weiss reactions) that could damage the cell. The cell likely reduces the rates of ligand-exchange by using tight-binding polydentate ligands. Perhaps this is why transition metal ions coordinated solely by waters, erroneously called "free" metal ions, are not found in cells.[(130)]

Conversely, it is probably inappropriate to view LMMMC as intracellular "siderophores" that bind metal ions exceedingly tightly. If LMMMCs in cells are involved in trafficking, regulation and signaling, *intermediate* rates of ligand-exchange would seem to be required. These characteristics suggest that it might be possible (though perhaps not easy) to detect, isolate and characterize such complexes.

We are attempting to do exactly this using liquid chromatography (LC) in conjunction with an on-line inductively coupled plasma mass spectrometer (LC-ICP-

MS). In our system, the eluent from an LC column is split such that a portion is sent to the ICP-MS for detection; the rest is sent to a fraction collector. This system will allow us to isolate LMMMCs, presuming that they exist and are sufficiently stable to be isolated. Such an approach, if successful, would offer a major advantage relative to the use of probes since the complexes would not be destroyed.

The LC-ICP-MS method should also separates LMMMCs into individual complexes such that the vague "pool" concept could be discarded. The disadvantage of the LC-based approach is that cells must be disrupted during the preparation of extracts. Doing so could alter the pH and redox state of the environment in which the LMMMC exists. This might, in turn, induce ligand-exchange or other reactions. The resulting artifacts could easily be mistaken for *bona fida* endogenous LMMMCs. Clearly, both approaches will ultimately be required to detect, catalog and fully characterize these recalcitrant cellular components.

In this study we focus on LMMMCs in mitochondria, especially the organelle from *Saccharomyces cerevisiae*. Virtually all mitochondrial proteins are nuclearly encoded and many are targeted to the mitochondria by a signal sequence. Proteins typically thread through the TIM/TIM protein complexes on the outer and inner membranes as unfolded polypeptides. Once in the matrix, the signal sequence is clipped and the protein folds. Metalloproteins must be metallated during this process, and so the metal ions used for this should be available in the matrix. Given that the IM is very "tight", such metal species would need to enter this space through transporter proteins on the IM. Doing so would seem to require small LMMMCs that could pass through such

channels.[60] The situation for metalloproteins in the IMS is probably somewhat different. The IMS protein Mia40 binds both Cu and Zn, and may be involved in metallating incoming protein.[131] Pores in the OM allow species with Mol. wt < 1 kDa to pass unassisted. In this respect cytosolic LMMMCs could serve as metal donors without restriction.[60]

A LMM Mn complex has been detected in soluble mitochondrial extracts (Mtm1). When grown on minimal medium and harvested at the end of exponential growth phase (OD of 1.0 ± 0.1), a Mn complex with Mol. wt of 2-3 kDa was detected in yeast mitochondria.[132] About 1 μM out of 13 μM Mn total in WT mitochondria was due to this species, called $Mn_{2\text{-}3}$. When cells were grown with 200 μM $MnCl_2$ in the medium, the concentration of $Mn_{2\text{-}3}$ increased to 23 μM. Thus, the concentration of $Mn_{2\text{-}3}$ in mitochondria is sensitive to the concentration of Mn in the medium. $Mn_{2\text{-}3}$ was the only LMM Mn complex detected in the soluble fraction of mitochondria. The concentration of $Mn_{2\text{-}3}$ increased (from 1 μM $\rightarrow$ 22 μM) when Mtm1, an mitochondrial IM carrier protein suspected of being involved in activating, maturing or stabilizing apo-SOD2, was deleted. Since MnSOD2 is the only known Mn-containing protein in mitochondria, and since it is imported into the matrix in an apo- form, $Mn_{2\text{-}3}$ likely functions as the Mn donor to apo-SOD2.[132]

LMM Fe complexes in mitochondria have also been detected. Using an assay for Fe/S cluster assembly in intact mitochondria, Lutz et al.[133] discovered that 1,10-phenanthroline (phen), a strong membrane-soluble chelator of Fe^{II} ions, inhibits Fe/S cluster assembly in intact mitochondria. Similar results were obtained by Amutha et

al.[134] and Pandey et al.[135] who speculated that mitochondria must contain a pool of Fe^{II} that is used as feedstock for Fe/S cluster assembly. Accordingly, phen was thought to penetrate into the matrix and coordinate that pool, making it unavailable for Fe/S cluster assembly. Unaware of those results, Holmes-Hampton et al.[121] performed the equivalent experiment in which phen was added to intact ^{57}Fe-enriched mitochondria. Using Mössbauer spectroscopy, they discovered a pool of nonheme high-spin Fe^{II} that was selectively chelated by phen, which implied that this pool is used for Fe/S biosynthesis. In fermenting mitochondria, the concentration of the pool was ~ 150 μM Fe^{II} whereas in respiring mitochondria, it was much lower. Since the concentrations of respiratory complexes are 3-times higher in respiring mitochondria, Holmes-Hampton et al.[121] speculated that this decline was due to an increased rate of Fe/S cluster assembly under respiration conditions. This Fe^{II} pool is probably that inferred by Amutha and Pandey. The associated Mossbauer parameters indicate an Fe^{II} species with 5-6 oxygen and nitrogen donors but no sulfurs. This HS $Fe^{II}(O/N)_{5-6}$ species appears to be in equilibrium with a HS Fe^{III} species and with Fe^{III} oxyhydroxide nanoparticles. The same complex may have also been detected by Rauen et al.[136] using rhodamine-based fluorescence sensors. These researchers found that the concentration of labile Fe in the organelle was ~ 16 μM.[136-138] Consistent with this, a single LMM Fe complex with Mol. Wt of ~ 3 kDa was detected in soluble mitochondrial extracts using the LC-ICP-MS approach.[132] However, further work is required to determine whether this complex is the same as that detected by the sensor, by Mössbauer spectroscopy, or by the Fe/S cluster assays.

Mitochondria also contain a labile Zn pool that is probably involved in metallating various Zn proteins[139], and it may be involved in other functions. Mitochondria can accumulate Zn, but this inhibits respiration and causes other problem.[140, 141] Cytosolic Zn enters mitochondria through a Ca uniporter.[140] Mitochondria from neuronal cells contain Zn that can be mobilized and released when the IM is depolarized.[142] Mitochondria in normal prostate epithelial cells accumulate high levels of Zn whereas tumorogenic cells do not.[141, 143, 144] Using LC, Winge, Eide and coworkers[145] detected a labile Zn pool in the matrix. This pool expanded when they increased the concentration of Zn in the medium. Mzm1, a 13.9 kDa soluble matrix protein, is involved in maintaining that pool. Zn-specific fluorescence sensors have provided further evidence for labile Zn in mitochondria. Palmer and coworkers used FRET-based sensors to detect labile Zn in the mitochondria of HeLa cells.[68] Using human carbonic anhydrase II variants, McCranor et. al.[146] detected labile Zn in rat mitochondria. Labile Zn was detected in mitochondria from mammalian cells using modified GFP fused to calmodulin.[141, 142, 147] Chyan et al.[143] used a synthetic fluorescent probe to detect labile Zn in prostate cells. When the medium was spiked with 50 uM Zn, the fluorescence intensity of the mitos in normal cells increased 2.3 times whereas there was no effect on mitochondria in cancer cells. The mitochondria of tumerogenic prostate cells do not accumulate labile Zn. Mitochondrial Zn probably originates from the Zn-bound to metallothionin in the cytosol. Costello[148] concluded that Zn is transferred from donor to acceptor without going through the aquated Zn^{2+}

state. The IM protein ferrochelatase may use the Zn pool in the matrix to insert into porphyrins.

There is also evidence that mitochondria contain labile Cu. Cobine and Winge have reported that > 70% of the Cu in mitochondria is in the form of a non-proteinaceous species (named Cu_L) that might serve trafficking and/or metallating functions. They refer to the species as being "low molecular weight" but it migrates in accordance with a 13 kDa globular protein [149] this is larger than the range of molecular masses that we define as low molecular mass (200 – 10,000 Da). Ligand L is fluorescent and is present in non-limiting concentrations in the mitochondrial matrix.[150, 151] The complex has been detected in both yeast and mouse liver mitochondria. The concentration of Cu_L is sensitive to the concentration of Cu in the medium, increasing 6-fold in cells grown in medium supplemented with 0.5 mM Cu. Yang[152] used a custom-designed fluorescent sensor along with synchrotron x-ray fluorescence to detect labile Cu in mitochondria. Their data suggest a low-coordinate (linear or trigonal geometry) Cu^I species primarily coordinated by sulfur donors. Dodani et al.[153]developed a fluorescent sensor (Mito-CS1) that selectively binds Cu^I and targets to the mitochondria of HEK293T cells and human fibroblasts. Cells imported extra Cu when supplemented with 300 uM $CuCl_2$, and this Cu was sensed by these probes. Cu is thought to be imported into the matrix via Pic2, a mitochondrial carrier family protein.[154] Whether CuL metallates the Cu-containing proteins in the IMS has been considered but the issue remains undecided.[151, 155]

Considered collectively, these studies indicate the presence and importance of LMM transition metal complexes in mitochondria, yet much remains to be done to detect, identify and characterize them. In this study, we have used the LC-ICP-MS approach to investigate the LMM Mn, Fe, Cu and Zn complexes in mitochondria from yeast and to some extent mammalian cells. Our focus has been on detecting such species, establishing reproducibility, estimating molecular masses, and quantifying the concentrations of such species in the organelle.

Results

Six independent batches of mitochondria were isolated from WT yeast cells that had been grown on minimal medium containing 10 μM Fe (mostly as Fe^{III} citrate), 10 μM Zn, 2 μM Co, 1 μM Cu (mostly as $CuSO_4$), and 4 nM Mo. We will refer to these batches as A, C, D, F, K and P. Four other batches (G, H, I and J) were prepared from WT yeast cells grown on the same medium except spiked with a 10-fold increased concentration of either Fe, Cu, Zn or Mn. In 8 of these batches, cells were harvested during exponential phase (OD_{600} = 0.8) whereas in 2 of them (A and K), cells were harvested during post-exponential phase (OD_{600} = 1.1 and 1.6, respectively). Three other batches of mitochondria were prepared, one each from mouse brain (M), human Jurkat cells (N), and mouse liver (O).

The phosphorus, sulfur, Fe, Zn, Cu, Mn, Co and Mo concentrations of all batches were determined by acid digestion and (off-line) ICP-MS (Table 4.1). The approximate averaged concentration of phosphorus was highest (26 mM – yeast numbers), followed

Table 4.1. Table of concentrations and %'s of various metals and nonmetals in isolated mitochondria. Yeast of OD 0.8 consists of 5 independent preps, the other samples are from 1 independent prep of each condition. The concentration of Mo in the sample is in pM units.

Sample	P	S	Mn	Fe	Co	Cu	Zn	Mo
				Mitochondrial Extract (μM)				
Yeast, OD 0.8	25,500 ± 5,800	5,800 ± 1,200	15 ± 3	440 ± 70	0.075±0.004	52±16	270 ±180	2,000 ± 1,000
Relative error	23%	21%	20%	16%	5%	31%	66%	50%
Yeast, OD 1.6	28,600	6,450	20	725	0.125	80	365	1,000
10× Fe yeast	26,300	6,200	12	780	0.081	83	280	2,000
10× Cu yeast	23,100	6,000	13	410	0.065	140	240	2,000
10× Zn yeast	27,600	6,000	14	460	0.056	35	480	1,000
10× Mn yeast	29,400	6,000	25	460	0.049	64	250	2,000
Jurkat	28,400	7925	18	1,020	0.120	120	220	6,000
Liver	34,400	8621	16	420	0.080	21	320	8,000
Brain	32,900	7867	13	380	0.060	25	210	5,000
				Flow-Through Solution				
Yeast, OD 0.8	20,700 ± 600	4,900 ± 1100	2 ± 1	100 ± 30	0.060 ± 0.01	26 ± 5	120 ± 40	20
Yeast, OD 1.6	24,600	5,400	3	150	0.095	34	180	30
10x Fe Mito	21,400	5,300	3	170	0.072	21	120	20
10x Cu Mito	19,700	5,500	2	100	0.058	120	120	10
10x Zn Mito	21,200	5,000	2	120	0.049	27	280	20
10x Mn Mito	23,300	4,900	8	110	0.045	20	120	20
Jurkat Mito	26,200	6,500	4	110	0.100	22	110	1,000
Liver Mito	28,400	6,400	3	60	0.072	5	120	1,000
Brain Mito	26,700	6,300	4	50	0.050	3	110	1,000

Table 4.2. Table of percentages of LMM forms of various metals and nonmetals in isolated mitochondria. Yeast of OD 0.8 consists of 5 independent preps, the other samples are from 1 independent prep of each condition. The concentration of Mo in the sample is in pM units.

Sample	P	S	Mn	Fe	Co	Cu	Zn	Mo
Percentage of mitochondrial extract due to FTS								
Yeast, OD 0.8	83	84	13	24	85	50	44	1
Yeast, OD 1.6	85	84	15	21	76	43	50	2
10x Fe Mito	81	86	25	22	89	25	43	1
10x Cu Mito	85	92	15	25	89	85	51	1
10x Zn Mito	77	83	14	27	88	77	59	2
10x Mn Mito	79	81	32	25	92	31	50	1
Jurkat Mito	92	83	22	11	83	18	49	16
Liver Mito	83	75	19	15	90	24	39	13
Brain Mito	81	80	31	14	83	12	52	20

by that of sulfur (6 mM), Fe (440 μM), Zn (270 μM), Cu (52 μM), Mn (15 μM), Co (80 nM) and Mo (100 pM). Previously reported concentrations are similar; Morales et al.[3] obtained Fe, Zn, Cu and Mn concentrations of 770, 290, 50 and 15 μM, respectively. The higher [Fe] probably arises because the cells of Morales et al. were grown with 40 μM Fe^{III} citrate added to the medium and were harvested at an OD_{600} ~ 1.2. *S. cerevisiae* was recently found to load with Fe when cells are allowed to grow beyond exponential phase. Holmes-Hampton et. al.[156] reported concentration of 544, 236, 48, and 12 μM, respectively, for cells grown in 10 μM Fe and harvested at OD = 1.2.

The concentrations of all of these elements were similar in mouse tissues. In the human cell sample, P, S, Mn, and Zn concentrations were similar to the other samples while Fe, Co and Cu were higher. However, additional batches of these mammalian cells are needed before such differences can be considered significant.

In the current study, increasing Mn, Fe, Cu, and Zn one-by-one in the growth medium for yeast cells 10-fold approximately *doubled* the concentration of the same element in the corresponding isolated mitochondria. This shows proportionality between the concentration of these metals within the mitochondria and the corresponding concentration in the medium. This information would appear to be transferred via the cytosol. The regulation of metals in the mitochondria is not so tight as to make the mitochondrial concentrations insensitive to environmental changes.

Also interesting is that the environmentally-induced change in the mitochondrial concentration of one metal did not affect the mito concentrations of the other metals.

This shows that the homeostatic systems regulating Fe, Cu, Mn and Zn are, at least at this level, independent of each other.

Isolated mitochondria were then treated with the detergent triton, and then centrifuged. The soluble fraction was passed through a 10 kDa cutoff membrane and the metal content of the flow-through solution (FTS) was determined (Table 4.1). The percentages of mitochondrial metals that were contained in the FTS are given in Table 4.2. Over 80% of phosphorus, sulfur and Co in mitochondria are LMM species. In contrast, only ~20% of mitochondrial Mn, Fe and Cu are LMM species (in the table, the % of LMM Cu is listed as 35% but approximately 12% of this is actually Cu-containing species that we regard as not being LMM because they have masses > 10 kDa). Slightly less than half of mitochondrial Zn is LMM species. This is consistent with Eide et al.[157] who reported that > 40% of the Zn in sonicated yeast mitochondrial homogenates was soluble (assuming that most of the soluble Zn is also LMM).

Chromatograms of yeast mito extracts (n=5) exhibited four LMM phosphorus species with approximate masses of 1000, 800, 520, and 200 Da (Figure 4.1, Table 4.4). We will refer to these species as P_{1000}, P_{800}, P_{520} and P_{200}. These masses were estimated by calibrating the column with various LMM species mention in the previous chapter.

P_{520} exhibited the greatest intensity, followed distantly by P_{1000}, P_{800} and P_{200}. The concentrations of these species within mitochondria were as follows. Each peak in the chromatogram was fitted using a Gaussian function. Each function was integrated, and the area under each peak was normalized to the sum of all of the areas for all peaks in the chromatogram. The fractional area associated with a given peak was then

multiplied by the absolute concentration of that element in the FTS, affording the absolute concentration of the associated species (Table 4.3). Calculated in this manner, the concentration of P_{520} in isolated mitochondria was approximately 20 mM. ATP and ADP, with masses of 507 and 427, respectively, approximately comigrated with P_{520}. The P_{520} peak was broader than other peaks, suggesting that more than one species contribute. We conclude that the majority of the P_{520} peak is due to ATP with perhaps with some ADP contributing to the tailing. Since P_{520} accounts for ~ 90% of the chromatographic intensity, we calculate that P_{520} has a (phosphorus-based) concentration of ~ 20 mM. Assuming that this peak represents ATP, the actual concentration of P_{520} in mitochondria is ~ 7 mM. Yeast mitochondria reportedly contain 7.8 mM ATP.[158] The similarity of these two concentrations not only supports our assignment but also indicates that our method of calculating concentrations (at least for phosphorus compounds) is relatively accurate.

P_{1000}, P_{800} or P_{200} were not assigned. The estimated mass of P_{200} is similar to pyrophosphate (174 Da) while masses of P_{1000} and P_{800} are similar to NADPH (744 Da).The phosphorus-based concentrations of these three species are 400, 300, and 200 μM, respectively.

The phosphorus content of mammalian mitochondria was quite similar to that of yeast mitochondria; P_{520} and the same minor-intensity species were evident. In the chromatogram of mitochondria from Jurkat cells, the same minor-intensity peaks were present but their intensities were lower than in the others. The chromatograms of liver

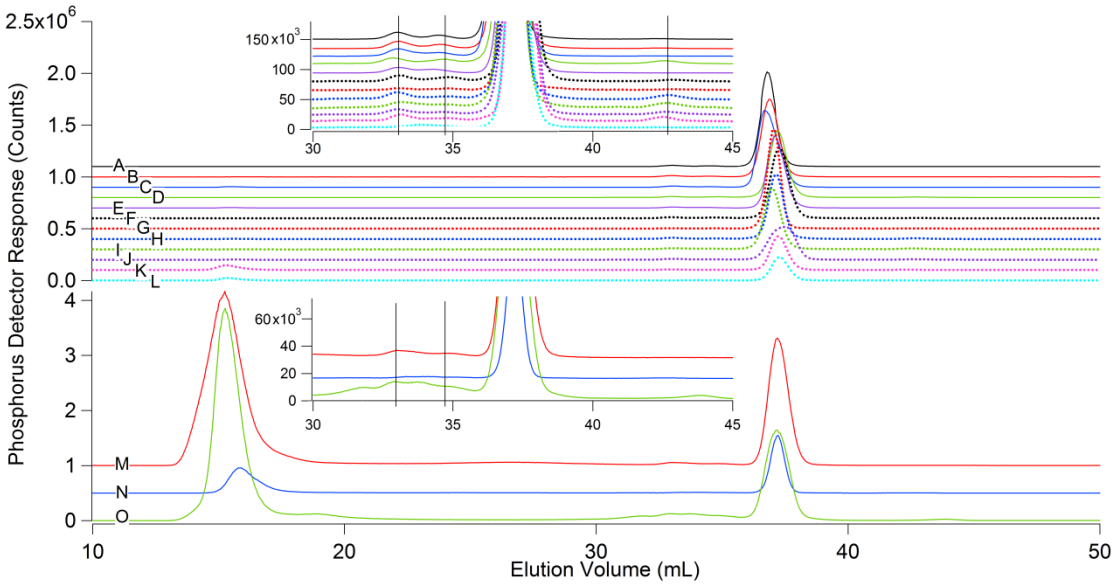

Figure 4.1. Phosphorus Chromatograms for LMM Mitochondrial Extracts. Traces A-L extracts prepared from yeast mitochondria. A) Trial 1, B) Trial 1 – 5 days aged, C) Trial 2, D) Trial 3, E) Trial 2 - 5 days aged, F) Trial 4, G) Mitochondria grown on 10x Fe, H) G) Mitochondria grown on 10x Cu, I) Mitochondria grown on 10x Zn, J) Mitochondria grown on 10x Mn, K) Mitochondria grown to OD_{600} = 1.6, L) Mitochondria grown to OD_{600} = 1.6 aged for 5 days, M) Mitochondria isolated from Mice brains, N) Mitochondria isolated from Human Jurkat cells, O) Mitochondria isolated from Mice Livers

Table 4.3. LMMMC's detected in mitochondrial extracts. Peaks were fit using manual peak fitting to minimize the deviation between data and simulation. The appearance of each peak in seen in the far right column with Y = Yeast, M= Mice, H=Human Jurkat mitos.

Peak Name	Peak Center (mL)	Peak Width (mL)	Molecular Mass (Da)	Area (%)	$[Metal]_{mito}$ (μM)	R-value (%)	Organism
P_{1000}	33.4 ± 0.2	0.9 ± 0.1	1000 ± 200	1.7 ± 0.7	400 ± 100	100	Y,M,H
P_{800}	34.6 ± 0.1	1.3 ± 0.2	800 ± 200	1.5 ± 0.5	300 ± 100	100	Y,M,H
P_{520}	37.1 ± 0.2	0.7 ± 0.1	520 ± 100	95 ± 18	20000 ± 4000	100	Y,M,H
P_{200}	42.7 ± 0.2	1.4 ± 0.1	200 ± 50	1.1 ± 0.8	230 ± 140	80	Y,M,H
S_{1100}	32.8 ± 0.3	1.0 ± 0.1	1100 ± 150	98 ± 1	4900 ± 39	100	Y,M,H
S_{780}	34.8 ± 0.1	1.4 ± 0.5	780 ± 200	10 ± 9	500 ± 400	60	Y
Mn_{2000}	30.5 ± 0.2	1.2 ± 0.1	2000 ± 200	45	~1-2	NA	M,H
Mn_{1500}	30.8 ± 0.2	0.9 ± 0.2	1500 ± 200	4.0 ± 2.0	0.08 ± 0.05	50	Y
Mn_{1100}	32.6 ± 0.1	0.9 ± 0.1	1100 ± 160	95 ± 7	1.9 ± 0.2	100	Y,M,H
Fe_{1500}	30.8 ± 0.1	0.8 ± 0.2	1500 ± 300	20	~22	NA	M
Fe_{1100}	32.7 ± 0.1	1.3 ± 0.2	1100 ± 250	6 ± 2	6 ± 2	80	Y,M
Fe_{870}	34.1 ± 0.5	0.7 ± 0.1	870 ± 100	11 ± 9	12 ± 9	60	Y,M
Fe_{680}	35.6 ± 0.4	1.1 ± 0.4	680 ± 130	16 ± 14	20 ± 10	50	Y,M
Fe_{575}	36.6 ± 0.3	1.4 ± 0.1	575 ± 150	82 ± 17	90 ± 20	100	Y,M,H

Table 4.3. (continued.) LMMMC's detected in mitochondrial extracts. Peaks were fit using manual peak fitting to minimize the deviation between data and simulation. The appearance of each peak in seen in the far right column with Y = Yeast, M= Mice, H = Human Jurkat mitos.

Peak Name	**Peak Center (mL)**	**Peak Width (mL)**	**Molecular Mass (Da)**	**Area (%)**	**$[Metal]_{mito}$ (µM)**	**R-value (%)**	**Organism**
Fe_{200}	43.3 ± 0.2	1.2 ± 0.8	200 ± 40	1.7 ± 1.5	2 ± 1	90	Y,M
Co_{1200}	32.3 ± 0.2	0.9 ± 0.1	1200 ± 180	36 ± 29	0.03 ± 0.02	90	Y,M,H
Co_{840}	34.3 ± 0.3	1.7 ± 0.6	840 ± 270	29 ± 23	0.02 ± 0.01	90	Y,M,H
Co_{620}	36.2 ± 0.5	1.6 ± 0.7	620 ± 180	8 ± 4	0.01 ± 0.003	50	Y,M,H
Co_{450}	38.2 ± 0.5	2.4 ± 0.9	450 ± 200	20 ± 34	0.013 ± 0.22	70	Y,M,H
Co_{340}	39.8 ± 0.2	1.8 ± 0.4	340 ± 100	9 ± 7	0.006 ± 0.004	90	Y,M,H
Co_{300}	41.1 ± 0.4	2.0 ± 1.5	300 ± 10	3 ± 2	0.002 ± 0.001	80	Y
Cu_{8000}	20.4 ± 0.5	3 ± 2	8000 ± 4000	42 ± 38	11 ± 10	40	Y
Cu_{5000}	23.1 ± 0.1	1.4 ± 0.2	5000 ± 1000	60 ± 26	16 ± 7	90	Y
Zn_{1500}	30.8 ± 0.2	0.7 ± 0.1	1500 ± 0.2	6	~7%	NA	M,H
Zn_{1150}	32.2 ± 0.2	0.6 ± 0.5	1150 ±100	85 ± 20	110 ± 20	100	Y,M,H
Zn_{900}	34.1 ± 0.1	1.8 ± 1.3	900 ± 300	5 ± 1	6 ± 1	100	Y

and brain mitochondrial extracts exhibited additional features indicating additional phosphorus-containing species.

Sulfur-detected chromatograms (Figure 4.2) exhibited two major peaks, corresponding to species (S_{1100} and S_{780}) with masses of 1100 and 780 Da. S_{1100} dominated and was observed in all chromatograms; the concentration of this species in mitochondria was nearly 5 mM. S_{780} was present more sporadically. Neither species comigrated with glutathione or glutathione disulfide (GSH or GSSG) and no peaks in the chromatogram comigrated with GSH or GSSG! This was and is a puzzling result that implies the absence of these well-known sulfur-containing species in mitochondria. Numerous published studies report millimolar concentrations of GSH in mitochondria.[159] Further studies are needed to resolve this discrepancy.

One peak dominated the Zn-detected chromatograms (Figure 4.3), corresponding to a mass of 1100 Da. The so-called Zn_{1100} species was present at a concentration of 110 uM (nearly half of the total Zn present in mitos). A minor-intensity peak at 900 Da was present at a concentration of ~ 1 uM. Zn_{1100} is almost certainly the species described by Eide, Winge and Cobine, who found that this is a cationic species (suggesting that the ligands, on average, are uncharged) and based on their data elutes on a G-25 SEC column at a MM of just lower than coenzyme B_{12}.[145] Mitochondria from yeast grown on medium containing 10-times more Zn than is normally present in minimal media exhibited a 2.5-fold increase in the intensity of the Zn_{1100} peak. Signal intensities for the other peaks were only slightly affected. A higher-mass species Zn_{2000} was not observed in yeast

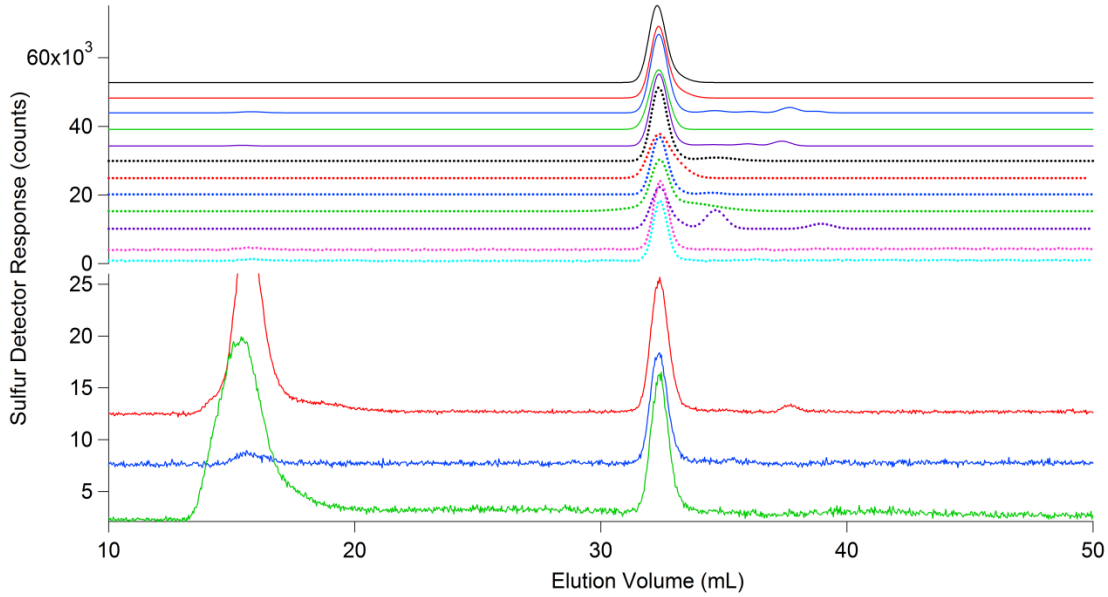

Figure 4.2. Sulfur Chromatograms for LMM Mitochondrial Extracts. Traces A-L extracts prepared from yeast mitochondria. A) Trial 1, B) Trial 1 – 5 days aged, C) Trial 2, D) Trial 3, E) Trial 2 - 5 days aged, F) Trial 4, G) Mitochondria grown on 10x Fe, H) G) Mitochondria grown on 10x Cu, I) Mitochondria grown on 10x Zn, J) Mitochondria grown on 10x Mn, K) Mitochondria grown to OD_{600} = 1.6, L) Mitochondria grown to OD_{600} = 1.6 aged for 5 days. M) Mitochondria isolated from Mice brains, N) Mitochondria isolated from Human Jurkat cells, O) Mitochondria isolated from Mice Livers

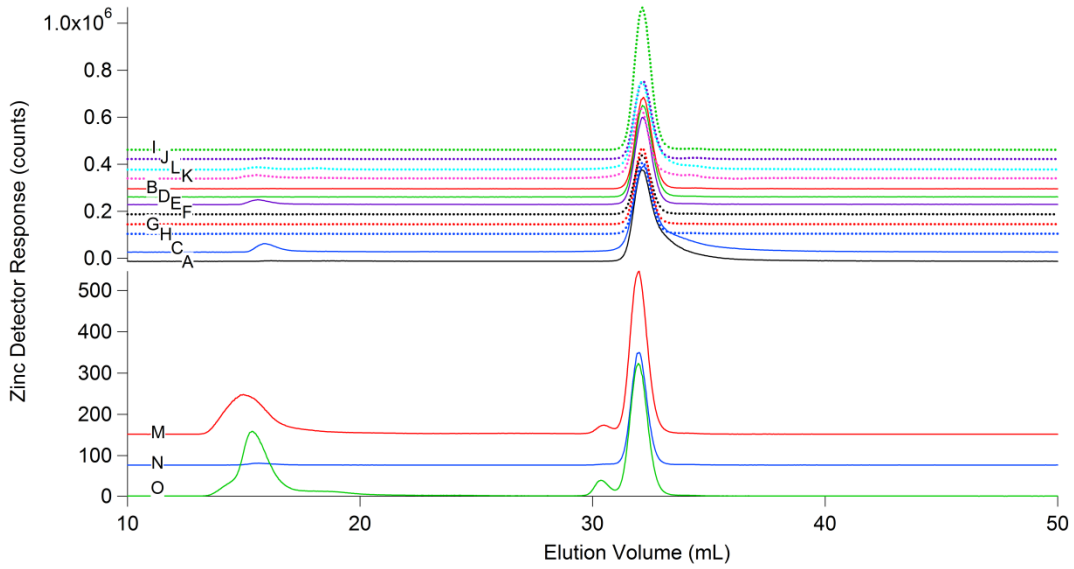

Figure 4.3. Zinc Chromatograms for LMM Mitochondrial Extracts. Traces A-L extracts prepared from yeast mitochondria. A) Trial 1, B) Trial 1 – 5 days aged, C) Trial 2, D) Trial 3, E) Trial 2 - 5 days aged, F) Trial 4, G) Mitochondria grown on 10x Fe, H) G) Mitochondria grown on 10x Cu, I) Mitochondria grown on 10x Zn, J) Mitochondria grown on 10x Mn, K) Mitochondria grown to OD_{600} = 1.6, L) Mitochondria grown to OD_{600} = 1.6 aged for 5 days. M) Mitochondria isolated from Mice brains, N) Mitochondria isolated from Human Jurkat cells, O) Mitochondria isolated from Mice Livers

mitochondria chromatograms but was found in mitochondria from mouse samples. In Jurkat cells, Zn_{2000} could be detected but at very low intensity.

A single Mn species, with a mass of 1100 Da, dominated the chromatograms of yeast mitochondrial FTSs. A second minor-intensity species of slightly higher molecular mass (Mn1500) was evident in some yeast mitochondrial chromatograms (Figure 4.4). The mitochondrial FTS from yeast cells grown in media containing 10-times the normal concentration of Mn afforded a chromatogram in which the Mn_{1100} intensity was 4-times greater; the intensity of the Mn_{1500} species was also increased albeit more modestly. The concentration of Mn_{1100} within yeast mitochondria was ca. 2 uM, while that of Mn_{1500} was 23-times less. In our previous study of LMM Mn species in yeast mitochondria (Park Mtm1), we observed a single LMM Mn species ($Mn_{2\text{-}3}$) estimated to have a molecular mass between 2-3 kDa. This is slightly discordant with our current results in which the major LMM Mn species has a mass of 1100 Da. $Mn_{2\text{-}3}$ and Mn_{1100} may be the same species (with one set of calibrations in error). Alternatively, subtle differences in the growth of the cells or in preparation of mitochondrial FTSs may have resulted in different Mn species being present. We have also considered that Mn_{1500} and $Mn_{2\text{-}3}$ are the same species, and that Mn_{1100} is a different species that is present in higher concentrations under particular growth conditions. Further studies are required to resolve this issue.

Both Mn_{1500} and Mn_{1100} were present in mitochondrial FTSs from human cells and mouse tissues, but the relative intensities differed relative to those in yeast mitochondria. In mitochondria from Jurkat cells, the Mn_{1500} peak accounted for ~95% of

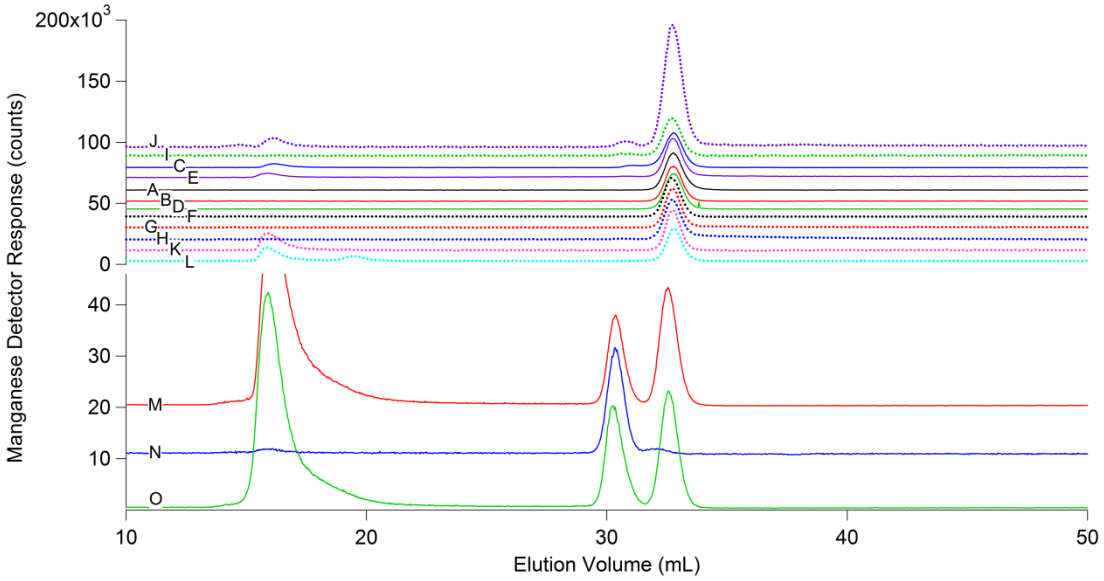

Figure 4.4. Manganese Chromatograms for LMM Mitochondrial Extracts. Traces A-L extracts prepared from yeast mitochondria. A) Trial 1, B) Trial 1 – 5 days aged, C) Trial 2, D) Trial 3, E) Trial 2 - 5 days aged, F) Trial 4, G) Mitochondria grown on 10x Fe, H) G) Mitochondria grown on 10x Cu, I) Mitochondria grown on 10x Zn, J) Mitochondria grown on 10x Mn, K) Mitochondria grown to OD_{600} = 1.6, L) Mitochondria grown to OD_{600} = 1.6 aged for 5 days. M) Mitochondria isolated from Mice brains, N) Mitochondria isolated from Human Jurkat cells, O) Mitochondria isolated from Mice Livers

the overall chromatogram with minor contributions from Mn_{1100}. Mitos from mouse brain and liver exhibited a more equal distribution between the two peaks, affording concentrations of ~1.5 and ~1.5 μM, respectively.

Yeast mitochondrial TFSs exhibited one major Fe-detectable peaks, but the mass associated with it depended upon the growth phase of the cell when they were harvested and whether or not the FTS was injected into the LC-ICP-MS system immediately after preparing it or 5 days later. Mitochondrial FTSs isolated from cells that were harvested during exponential growth phase (at OD_{600} = 0.8) exhibited an Fe-detected chromatogram dominated by a peak from a species (Fe_{580}) corresponding to a mass of 580 Da. The chromatogram from a mitochondrial FTS isolated from cells grown on media containing a 10-fold increase in Fe^{III} citrate exhibited a 1.7-fold increase in the intensity of Fe_{580}. Other minor Fe peaks were evident in the spectra, including a low-intensity peak corresponding to a mass of 1100 Da.

Fe-detected chromatograms from FTSs isolated from cells harvested during post-exponential growth phase (at OD600 = 1.6) differed significantly. They also exhibited one major Fe peak but it corresponded to a species (Fe_{1100}) with a mass of 1100 Da. The Fe_{580} peak was present, but at low intensity. Surprisingly, when the FTS dominated by Fe_{1100} was left in the refrigerated glove box for 5 days, the resulting chromatogram was dominated by the Fe_{580} peak, with Fe_{1100} a minor component. Another Fe containing species (Fe_{870}) corresponding to a mass of 870 Da was also evident. We hypothesis that Fe_{1100} spontaneously converted into Fe_{580} via an intermediate Fe_{870}. The only other Fe species present gave rise to a very low intensity peak associated with a mass of 200 Da.

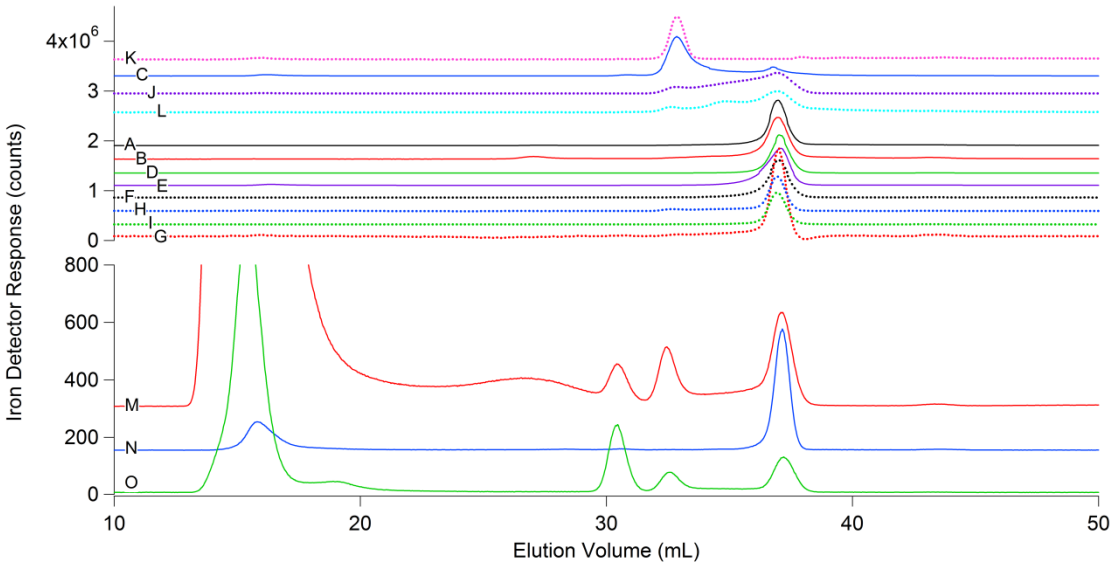

Figure 4.5. Iron Chromatograms for LMM Mitochondrial Extracts. Traces A-L extracts prepared from yeast mitochondria. A) Trial 1, B) Trial 1 – 5 days aged, C) Trial 2, D) Trial 3, E) Trial 2 - 5 days aged, F) Trial 4, G) Mitochondria grown on 10x Fe, H) G) Mitochondria grown on 10x Cu, I) Mitochondria grown on 10x Zn, J) Mitochondria grown on 10x Mn, K) Mitochondria grown to OD_{600} = 1.6, L) Mitochondria grown to OD_{600} = 1.6 aged for 5 days. M) Mitochondria isolated from Mice brains, N) Mitochondria isolated from Human Jurkat cells, O) Mitochondria isolated from Mice Livers

Since hexaqua iron complexes have masses of ca. 160 Da, we assign this peak as such. The concentration of Fe_{200} in our isolated mitochondria samples was 1 – 3 uM which we regard as an upper limit of what might be present in mitochondria in cells (one half of 1% of the Fe in mitochondria). Alternatively, Fe_{200} might be an artifact of our isolation procedure such that mitochondria in cells might be devoid of hexaqua iron complexes.

Fe chromatograms of FTSs from mitochondria isolated from mammalian cells and tissues showed some correspondence to yeast mitochondria but also some additional peaks. The chromatogram of FTS from mitochondria isolated from Jurkat cells was similar to that of yeast harvested during exponential growth phase, with Fe_{580} dominating. That from mouse tissues exhibited three major peaks corresponding to masses of 2000, 1200, and 580 Da. The peak at 580 Da probably arises from the same species present in yeast mitochondria (Fe_{580}), while that at 2000 Da arises from a species (Fe_{2000}) not present in yeast mitochondria. Whether the peak at 1200 Da arises from the Fe_{1100} species in yeast mitochondria is uncertain; the two peaks migrate near to each other but they do not seem to co-migrate precisely. The concentrations of these species in mammalian mitochondria range from 10-30 μM.

Careful analysis of the copper-detected chromatograms revealed deviations in the baseline past 30 mL of the elution volume that detracted from the reliability beyond that volume (Figure 4.6). As a result, we decided not to analyze that region and have presented Cu chromatograms truncated at 30 mL (corresponding to a mass of ~ 2000 Da. Further studies will be required to determine whether LMM Cu complexes with masses

< 2000 Da are present in mitochondria. On the other end of these chromatograms, our soluble mitochondrial extracts were passed through a 10 kDa cutoff membrane such that Cu species with masses > 10,000 Da will not be considered. Since the Cu_L species described by Winge and Cobine has a mass of ~ 13,000 Da, our study was not designed to detect this species.[150]

Within these limitations, the Cu-detected chromatograms of the FTS of mitochondria from yeast cells still yielded new insights. The chromatograms were dominated by a peak corresponding to a mass of 5000 Da. The concentration of Cu_{5000} in yeast mitochondria was ca. 16 μM. It accounts for ca. 60% of the Cu in the FTS (with much of the remainder high-molecular mass Cu species that eluted in the void volume). With a mass of 5000 Da, we are uncertain whether Cu_{5000} is a Cu protein. However, there was no major UV (280 nm) peak at 5000 Da, suggesting that it might be non-proteinaceous. The Cu_{5000} peak increased 4-fold in intensity when the Cu concentration in the medium was increased 10 fold. Interestingly, the Cu-detected chromatograms of the mammalian system did not exhibit peaks in the region between 2000 – ca. 10,000 Da (though some Cu species with masses > 10,000 Da were evident). This was similar to the results of our previous study of mouse brain LMM extracts, in that no LMM Cu species were evident.

The Co-detected chromatograms exhibited many peaks, albeit with somewhat greater batch-to-batch variability than that observed for other metals (Figure 4.7). FTSs from yeast mitochondria exhibited peaks between 300 – 1200 Da with the dominant peak at 1200 Da. The concentration of the Co_{1200} species was just 30 nM, a

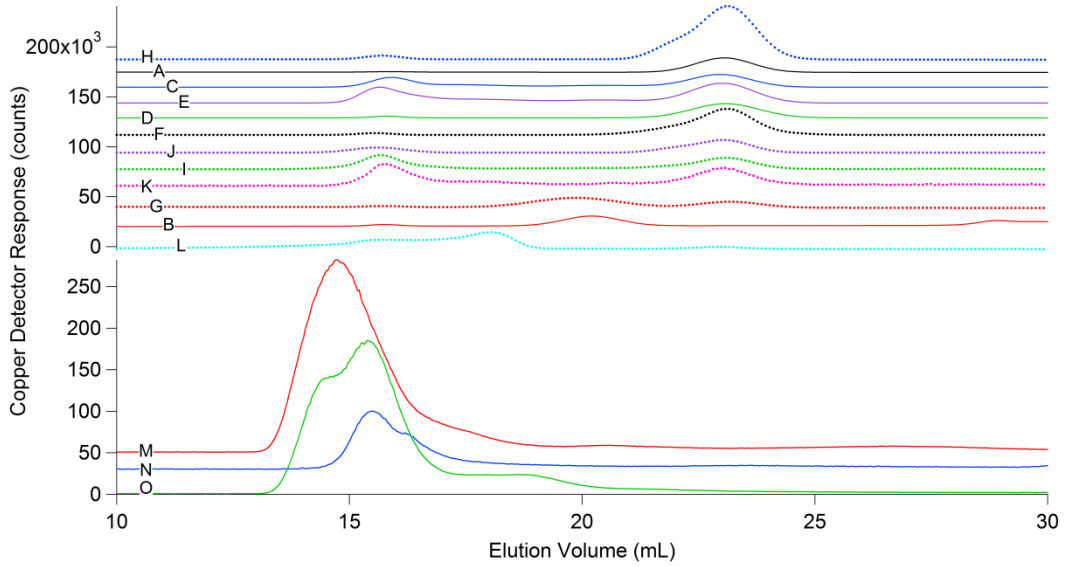

Figure 4.6. Copper Chromatograms for LMM Mitochondrial Extracts. Traces A-L extracts prepared from yeast mitochondria. A) Trial 1, B) Trial 1 – 5 days aged, C) Trial 2, D) Trial 3, E) Trial 2 - 5 days aged, F) Trial 4, G) Mitochondria grown on 10x Fe, H) G) Mitochondria grown on 10x Cu, I) Mitochondria grown on 10x Zn, J) Mitochondria grown on 10x Mn, K) Mitochondria grown to OD_{600} = 1.6, L) Mitochondria grown to OD_{600} = 1.6 aged for 5 days. M) Mitochondria isolated from Mice brains, N) Mitochondria isolated from Human Jurkat cells, O) Mitochondria isolated from Mice Livers

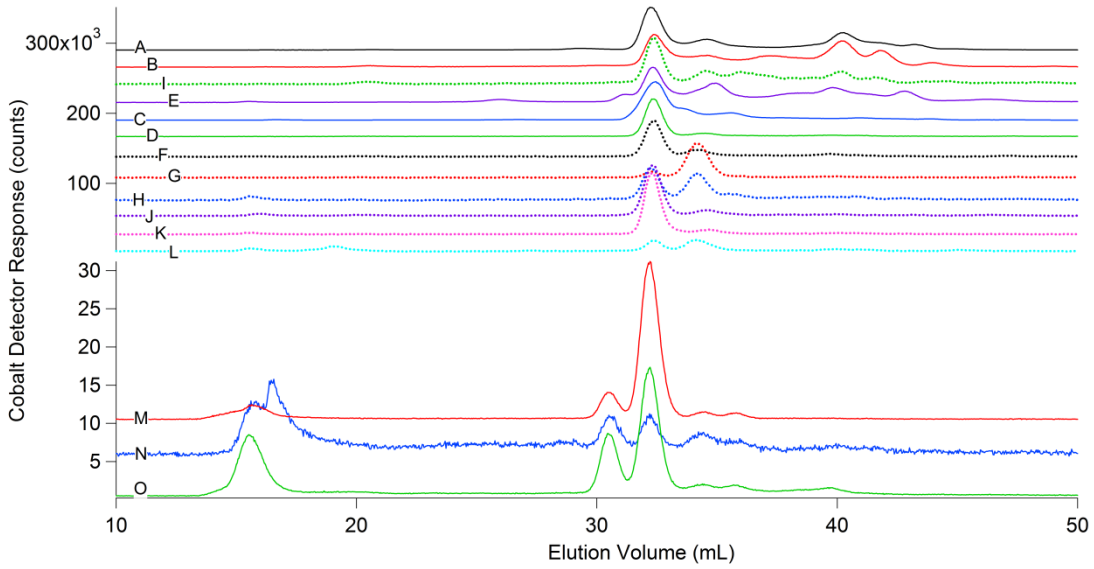

Figure 4.7. Cobalt Chromatograms for LMM Mitochondrial Extracts. Traces A-L extracts prepared from yeast mitochondria. A) Trial 1, B) Trial 1 – 5 days aged, C) Trial 2, D) Trial 3, E) Trial 2 - 5 days aged, F) Trial 4, G) Mitochondria grown on 10x Fe, H) G) Mitochondria grown on 10x Cu, I) Mitochondria grown on 10x Zn, J) Mitochondria grown on 10x Mn, K) Mitochondria grown to OD_{600} = 1.6, L) Mitochondria grown to OD_{600} = 1.6 aged for 5 days. M) Mitochondria isolated from Mice brains, N) Mitochondria isolated from Human Jurkat cells, O) Mitochondria isolated from Mice Livers

Factor of 1000 less than many other LMM metal species. Co_{1200} is probably a member of the cobalamin family. Cobalamins have masses in this range, or actually slightly higher. Cyanocobalamin (vitamin B_{12}), has a mass of 1355 Da while adenosylcobalamin (coenzyme B_{12}) has a mass of 1580 Da. FTS from yeast mitochondria exhibit other lower mass species, ranging from 840 to ~ 200 Da, however the batch-to-batch variation in these peaks was significant. Peaks in the 200 Da region are probably aqueous Co ions; higher mass species from say 340 – 840 Da, are Co complexes, with ligands heavier than water, but probably not cobalamins as their masses are too low.

Co chromatograms of the mammalian samples were similar to each other, except that the intensities of the Co peaks in the Jurkat sample were very low. In comparison to the yeast mitochondrial FTSs, those from mammalian cells and tissues exhibited not only a peak due to Co_{1200} but also a peak corresponding to a mass of 1700 Da. The associated Co_{1700} species is probably a member of the cobalamin family. Cobalamins are not covalently bound to proteins, and our treatment of mitochondria with the detergent Triton could have released some of these centers. Thus, we are uncertain whether these chromatograms provide evidence for free cobalamins in intact mitochondria within cells. Even if they are artifact of our isolation procedure, they can be used as internal molecular mass markers.

Mitochondria from *S. cerevisiae* are not known to contain any molybdenum enzymes, whereas mammals contain at least two – mARC1/2. These enzymes are found on the outer mitochondrial membrane[(160)] and function to generate nitric oxide from nitrites. This is congruent with our study, in which a LMM Mo species was present in

the FTSs of mammalian mitochondria, but not in that from yeast. The mass associated with that species is 720 Da. Molybdopterins bind molybdenum in different conformations depending on the enzyme sight they originate from ranging from ~560 – 980 Da.

In summary the work in this chapter provides the foundation for further studies to characterize these LMMMCs for both their structure and function. Using a novel LC-ICP-MS approach labile metals in the mitochondria no longer need to be approached from the prospective of being lumped into generalized pools of metals but can be discussed in terms of different species or complexes.

CHAPTER V

LOW MOLECULAR MASS METAL COMPLEXES IN THE MOUSE BRAIN*

Introduction

Transition metals such as iron, copper, manganese, molybdenum, and cobalt are critical components of cells and super-cellular structures like the brain. They tend to be redox-active and have excellent catalytic properties that render them common residents in the active-sites of enzymes. However, many of those same properties can be deleterious to the cell, especially when their ligands are coordinated weakly. Labile Fe^{II} and Cu^{I} complexes in particular can react with H_2O_2 to generate $^{\cdot}OH$ via the Fenton reaction.[11, 12] Hydroxyl radicals and other reactive oxygen species (ROS) can damage DNA, proteins and membranes. Thus, trafficking newly-imported metal ions from the plasma membrane to various apo-protein targets requires chaperones that bind these metal ions weakly enough so that they can be transferred from one species to another while simultaneously avoiding dangerous side-reactions. Substantial progress has been made in understanding metal ion trafficking, but many molecular-level details remain unknown.[13] Nowhere is metal ion trafficking more important than in the brain, since many neurodegenerative diseases are associated with metal ion accumulation.[161, 162]

---

* This chapter is reproduced with permission from "Low Molecular Mass Metal Complexes in Mice Brains" by Sean P. McCormick, Myrinmoy Chakrabarti, Allison L. Cockrell, Jinkyu Park, Lora S. Lindahl, and Paul A. Lindahl 2013, Metallomics, 5, 232-241, copyright 2013 Royal Chemical Society

The concentration of Fe in the brains of mice fed standard (50 mg Fe per kg) chow is ca. 350 μM, with ~50% present as ferritin, ~40% as Fe/S clusters and heme centers, and 5%–9% as mononuclear nonheme high-spin (NHHS) Fe^{II} and Fe^{III} species.[156] Most Fe/S clusters and heme centers reside in mitochondrial respiratory complexes where they help provide chemical energy for the brain. Some NHHS Fe^{II} ions are found in the active sites of enzymes while others may be involved in trafficking. NHHS Fe^{II} complexes often have weakly-coordinating ligands and engage in Fenton chemistry.

Trafficking of metals involves protein chaperones that bind metal ions in one location of the cell and release them in another, e.g. to an apo-protein binding site during folding and maturation.[8] Whether trafficking also involves low-molecular-mass (LMM) metal complexes is less certain. Such species may exist in aqueous regions of a cell, where they might interact with protein chaperones and/or pass through membrane-bound transporters. For example, Mrs3p/Mrs4p are membrane-bound mitochondrial proteins that transport Fe from the cytosol to the mitochondrial matrix.[163] Although the structures of these two proteins are unknown, homologous structures suggest that the channels that pass through them are too small to accommodate a protein. This suggests that LMM Fe complexes, consisting of the metal ion coordinated by small organic or inorganic ligands, and/or by waters, pass through these transporters.

If LMM metal complexes are involved in trafficking, they should have weakly coordinating ligands that can be displaced by strong chelating agents. Pamp et al.[164] concluded that labile Fe constitutes 0.2–3% of overall cellular Fe. In human cells

containing 400 μM Fe,[106] this corresponds to a collective labile Fe concentration of 1–10 μM. Using fluorescence sensors, Petrat et al. found that the concentration of chelatable iron in the cytosol of intact hepatocytes was in the same range, namely 5.8 ± 2.6 μM.[165] According to Rauen et al. about 1% of cellular Fe exists in a pool that is not bound to ferritin or other proteins.[136] They estimate that the concentration of chelatable Fe in liver mitochondria and in the cytosol is 12 μM[137] and 6 μM,[165] respectively. Using chelators of different Fe affinities had no effect on the apparent size of the mitochondrial chelatable Fe pool, suggesting that the determined pool concentration (16 ± 2 μM) represents its "true" size. These estimates are substantially less than the concentration of NHHS Fe^{II} ions present within yeast mitochondria, as quantified by Mössbauer spectroscopy.[121] Some Mössbauer-detectable NHHS Fe^{II} species may be protein-bound and not labile. Differences may also arise from the different organisms probed and/or different cellular metabolic growth modes. The Mössbauer-detected NHHS Fe^{II} ions in yeast are chelated by 1,10-phenantroline (Phen).[121] This attenuates Fe/S cluster synthesis,[135] strongly suggesting that these ions serve as feedstock for this process.

The roles of LMM Fe complexes in cells and the brain are unknown, but patterns are emerging suggesting involvement in development, aging and neurodegenerative diseases. Kaur et al.[166] found an increase in the labile iron pool (LIP) in the brains of older mice, suggesting that such ions might be involved in aging. Wypijewska et al.[84] found increased LIP in the Substantia nigra region of PD brains. Sohal et al.[167] and Magaki et al.[168] reported that 20%–30% of nonheme Fe in the developing mouse brain

was labile. Meguro et al.[169] found that chelatable nonheme Fe^{II} and Fe^{III} species were distributed heterogeneously throughout the rat brain and that the concentration of these species increased with age. Huang et al.[65] reported that psychological stress expands the LMM Fe^{III} and Fe^{II} pools in particular regions of the brain, as detected by Perl's and Turnbull's stains. Nothing is known regarding the particular complexes involved.

Although not formally a transition metal, Zn plays critical roles in brain metabolism.[101] The concentration of Zn in the mouse brain is ca. 320 μM,[156] most of which is bound to metalloproteins. Metallothioneins are the primary intracellular Zn-buffering proteins. Metallothionein III in the brain has a molecular mass (MM) of ca. 7 kDa and contains 8–11 Zn binding sites.[170] Zn is also found in aggregated amyloid beta protein filaments in Alzheimer's Disease (AD), and is associated with amyotrophic lateral sclerosis, epilepsy, strokes, depression, and schizophrenia.[171] Protein-based and non-protein-based fluorescent probes have been used to image mobile Zn ions in cells and tissues.[172, 173] Palmer and coworkers targeted protein-based FRET fluorescence sensors to the mitochondria, ER and Golgi of HeLa cells, and estimated the presence of such pools at low pM concentrations.[68, 69] The detected concentration of cytosolic Zn was also extremely low, namely 80 pM. In contrast, high concentrations of Zn (estimated to be mM levels) are found in synaptic vesicles within neurons that use glutamate as a neurotransmitter.[174] The synaptic Zn pool has been detected by Zn-specific fluorescent dyes.[66, 67] These vesicles are located primarily in the cerebral cortex and limbic structures. Labile Zn ions enter these vesicles via the membrane-bound protein ZnT3 and are released upon synaptic activation.[175] This pool modulates the

overall excitability of the brain, and is involved in signal transduction, memory and learning.

Copper is present in the mouse brain at low concentrations (~5 μM)[156] but it is no less important than Fe or Zn. Cu plays essential roles in respiration, oxidative stress response, and other enzymatic activities.[176] Cu ions in the brain parenchyma are involved in the metabolism of neurotransmitters and myelination.[177]

Numerous proteins are known to be involved in Cu trafficking. Ctr1 is a transporter on the plasma membrane that brings Cu into the cell.[178] Cellular Cu can be stored in metallothionein, transported to mitochondria, incorporated into apo-Cu/Zn SOD, or transported to the Golgi apparatus for export from the cell.[177] Cu-containing ceruloplasmin helps distribute and metabolize Cu, and it may help Fe efflux from the brain.[179] Cox17 is an 8.0 kDa protein that transfers cytosolic Cu to mitochondria for incorporation into apo-cytochrome c oxidase.[180] CCS1 is a trimer with 9 kDa subunits which functions to insert Cu into apo-Cu/Zn SOD.[181, 182] The concentration of CCS1 is sensitive to intracellular levels of Cu. Atx1 is an 8.2 kDa copper-binding chaperone that transports Cu to the Cu-ATPases in the trans-Golgi network. These proteins, Atp7a and Atp7b, deliver Cu for incorporation into proteins.[58] When intracellular Cu concentration exceeds some setpoint value, they export Cu from the cell.

The presence of a labile Cu pool is less certain than that for Fe or Zn. Using highly selective ratiometric fluorescent reporters for Cu^{I} ions, Domaille et al. found an ascorbate-induced increase in the labile Cu^{I} pool in HEK 293 T cells.[58] Hirayama et al. used a fluorescent sensor to visualize labile Cu^{I} pools in mice.[183]

The mouse brain contains ~14 μM Mn, ~400 nM Mo, and ~30 nM Co, respectively.[156] Some Mn is incorporated into mitochondrial superoxide dismutase which functions to diminish oxidative stress.[181] Mn levels in the brain are elevated in patients with AD and Prion disease.[184] Mo is coordinated to the molybdopterin cofactor in molybdenum hydroxylases.[43] A deficiency of this cofactor causes seizures and death in newborns.[44, 45] Cobalt metabolism in the brain includes lipid biosynthesis and C1 metabolism.[39, 40] Co is present in coenzyme B_{12} bound in methionine synthase.[41] This enzyme functions in methionine metabolism, which includes methyl group transfer reactions involving choline, folate and S-adenosyl-methionine.[185]

In this study, we have evaluated the presence of LMM metal complexes in the mouse brain. Rather than using specific chelators to identify such species, we have detected them using anaerobic liquid chromatography with an on-line ICP-MS following the approach of Adams and coworkers who explored the metalloproteome of a prokaryote.[186] We report here that the brain contains a limited number of LMM Fe, Co, Mn, Mo, Cu and Zn complexes. These complexes were enumerated and characterized in terms of concentration and approximate MM. A few species were tentatively assigned.

Results

The objective of this study was to determine whether the mouse brain contained LMM transition metal complexes detectable by LC-ICP-MS. We avoided oxidizing Fe^{II}-containing species due to concern that endogenous ligands might dissociate upon oxidation and be replaced by waters, rendering insoluble aqueous Fe^{III} ions that would

adsorb to the column. Once animals were euthanized, all procedures involving samples were performed in a refrigerated Ar-atmosphere glove box. In each experiment, isolated brains were homogenized and centrifuged, and then supernatants were passed through a 10 kDa cut-off membrane. Because such complexes could potentially be highly dynamic and unstable, samples were prepared for the LC as fast as possible; FTSs were injected onto the LC column ca. 3 h after animals were euthanized. Experiments were performed 13 times to assess reproducibility.

Elemental concentrations in the FTSs were determined and corrected for dilution, affording estimates for the collective concentrations of all the LMM species for these elements in the brain. The results were (in μM): Co, 0.06 ± 0.01; Mo, 0.3 ± 0.1; Mn, 0.8 ± 0.1; Cu, 4.2 ± 0.2; Fe, 18 ± 1; Zn, 44 ± 7; S, 1500 ± 70; and P, 11,000 ± 1000 (Table 5.1). Assuming the total metal concentrations in the brain mentioned in the Introduction (except for Co, which was found in the current study to be present in the brain at 88 ± 5 nM), the percentages of these elements in the brain that passed through the LMM membrane were: Co, 66 ± 10; Mo, 67 ± 25; Mn, 6 ± 1, Cu, 84 ± 12; Fe, 5 ± 0.4; Zn, 14 ± 2; S, 9 ± 2; P, 12 ± 3. Thus, LMM species represent large percentages of total Co, Mo and Cu ions in the brain, but small percentages of Mn, Fe, Zn, S and P. For Fe in particular, the calculated percentage is comparable to previous chelation-based determinations in human cells (see Introduction).

Given the potential liability of these metal complexes, we evaluated the percentage of the metals that eluted from the column, normalized to the amount loaded. The averages of three runs were: Mo, 74 ± 12; Mn, 93 ± 4; Fe, 89 ± 7; Co, 93 ± 4; Cu,

84 ± 6; Zn, 92 ± 3; P, 91 ± 3 and S, 92 ± 6, respectively. These values indicate that the majority of the metal-containing species in the FLSs eluted from the column. The small percentage of each metal that did not elute demonstrates the importance of washing the column extensively between runs.

A total of 13 runs were performed; of these, 11 were analyzed. The two excluded runs had peak linewidths 2–3 fold greater than the others (suggesting a problem with the column). Thus, our analyses were essentially free of subjective bias. Reproducibility was acceptable but there were noticeable variations. P and S chromatograms were the most reproducible, in that the same sets of peaks, with similar relative area-ratios, were observed in each run. The V_e associated with each peak were not perfectly matched from one chromatogram to another, and so small shifts in the volume dimension, corresponding to no more than 0.24 mL, were allowed to align S and P peaks to the greatest extent possible. The identical alignment offsets were used for the corresponding Mo, Mn, Co, Fe, Cu and Zn chromatograms generated in the same run. In this way, the S and P chromatograms served as an internal calibration to align the metal-based chromatograms. Data sets were not adjusted further.

We considered that some peaks might arise from degradation products of the brain, despite using freshly prepared FTS and working quickly. To examine this, a FTS was left for 13 days in a refrigerated box prior to passage through the column. The resulting chromatograms, compared to those obtained using fresh FTS, revealed virtually no change in relative peak areas and distributions (Figure 5.1). We conclude that our samples did not degrade on the time scale of the experiment.

Table 5.1. Concentrations of LMM metal ions in the brain.

	Brain LMM Concentrations (μM)							
Trace	P	S	Mn	Fe	Co	Cu	Zn	Mo
A	10117.78	1577.20	0.910	18.014	0.058	4.564	56.339	0.251
B	10228.06	1427.36	0.764	17.512	0.051	4.154	38.416	0.168
C	11644.15	1558.52	0.728	16.653	0.048	4.469	44.594	0.210
D	10385.55	1490.66	0.692	18.336	0.064	4.092	45.450	0.189
E	11303.93	1430.73	0.947	18.980	0.058	4.406	38.416	0.293
F	12312.71	1500.22	0.874	17.763	0.075	4.186	53.250	0.398
G	11904.76	1573.58	0.692	18.515	0.064	3.903	41.138	0.230
H	10063.02	1417.55	0.983	18.085	0.051	4.312	39.609	0.147
I	11363.47	1465.79	0.910	17.405	0.058	4.249	53.127	0.377
J	11968.04	1436.23	0.837	17.834	0.054	4.123	39.211	0.440
K	9448.96	1464.04	0.874	16.187	0.061	4.312	40.495	0.335
L	8771.42	1365.06	0.874	17.369	0.051	4.154	39.303	0.168
Average	10792.65	1475.58	0.840	17.721	0.058	4.244	44.112	0.267
Std. Dev	1112.10	66.98	0.099	0.774	0.008	0.181	6.540	0.100

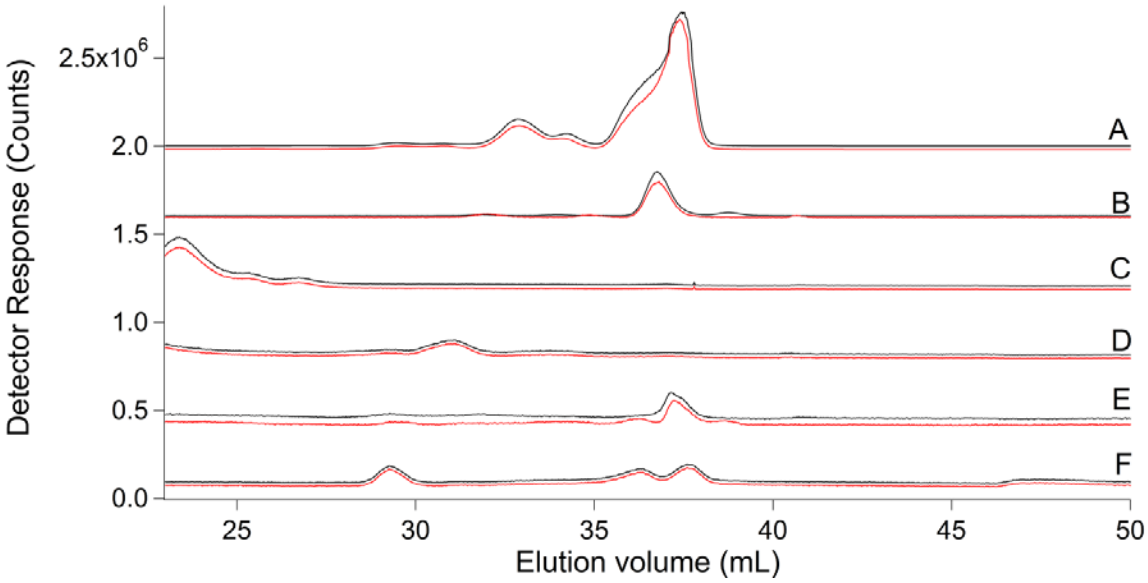

Figure 5.1. Chromatograms Obtained Testing for Sample Degradation. Fresh brain extract (black) and 13 Day old (red) refridgerated and stored anearobically were analysized as described in the methods section. The traces for P (A), S (B), Cu (C), Zn (D), Fe (E), Mn (F) are provided.

We also considered that our results might depend on the FTS buffer employed. To examine this, the buffer was switched from Tris to HEPES (both 20 mM at pH 7.4). The resulting chromatograms revealed no significant differences (Figure 5.2). Remaining run-to-run variations probably arose from animal-to-animal differences. To minimize these, mice were euthanized at approximately the same time of day (10 am–12 noon). Age and gender differences were considered as variational factors, but no correlations were obvious. In analyzing datasets, we assumed that any peak observed in ≥50% of the metal-matched datasets represented a real species in the brain. Peaks observed in >25% and <50% of chromatograms were viewed as probably reflecting real species. Peaks observed in ≤25% of chromatograms were considered artifacts and were not included in downstream analyses. Averages for peaks that were reproducibly present, according to these criteria, are summarized in Table 5.2. MMs for each species were estimated from V_e and the best-fit linear regression standard-curve line.

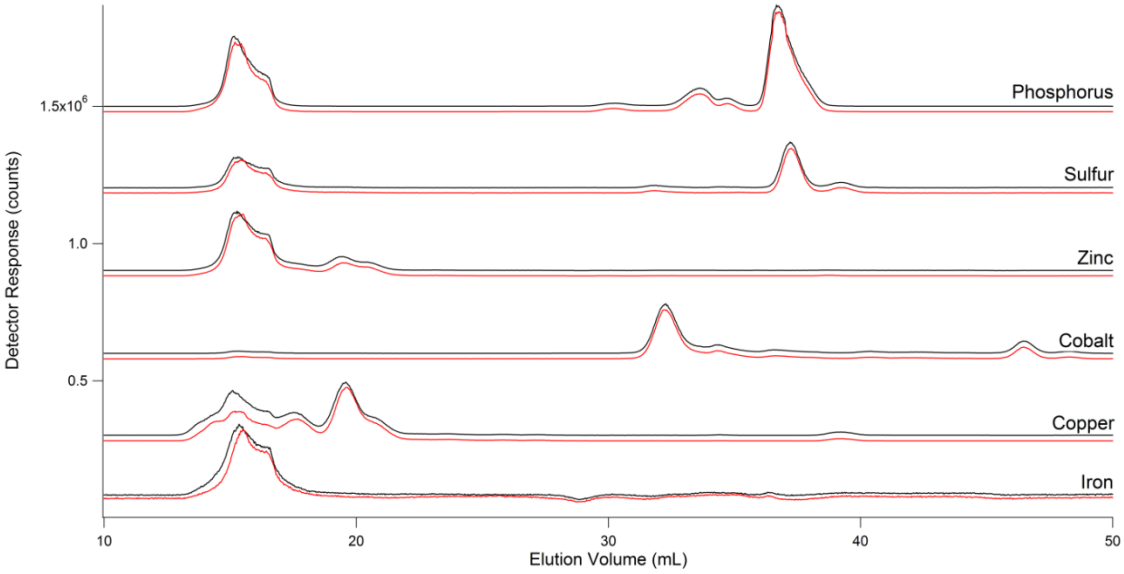

Figure 5.2. Chromatograms Obtained using HEPES (red) and Tris (black).

Table 5.2 Low-molecular-mass metal complexes in the mouse brains. Confidence was defined as the number of chromatograms for a given element in which the peak was present divided by the total number of chromatograms for that element, multiplied by 100

Assigned Name	Peak Center (mL)	Peak Width (mL)	Molecular Mass (Da)	Area (%)	$[Metal]_{Brain}$ (μM)	R-factor (%)
P_{HMM}	V < 18 mL	N/A	24-48 kDa	43 ± 14	4641 ± 1510	100
P_{2490}	29.5 ± 0.3	0.6 ± 0.2	2490	0.8 ± 0.5	86 ± 54	67
P_{1950}	30.7 ± 0.6	1.0 ± 0.5	1950	1.18 ± 1	127 ± 112	92
P_{1240}	32.9 ± 0.4	0.7 ± 0.1	1240	7 ± 3	755 ± 323	100
P_{1060}	33.7 ± 0.2	0.5 ± 0.1	1060	4 ± 3	432 ± 323	41
P_{900}	34.5 ± 0.3	0.42 ± 0.06	900	3 ± 2	324 ± 216	92
P_{630}	36.2 ± 0.2	0.5 ± 0.2	630	19 ± 13	2051 ± 1403	83
P_{570}	36.7 ± 0.2	0.5 ± 0.2	570	15 ± 11	1619 ± 1187	67
P_{530}	37.1 ± 0.1	0.5 ± 0.1	530	14 ± 10	1510 ± 1079	50
P_{490}	37.5 ± 0.1	0.5 ± 0.2	490	13 ± 13	1403 ± 1403	58
S_{HMM}	V < 18 mL	n/a	24-48 kDa	54 ± 10	797 ± 148	100
S_{1540}	31.84 ± 0.24	0.59 ± 0.10	1540	2.4 ± 1	35 ± 15	100
S_{940}	34.28 ± 0.38	0.81 ± 0.36	940	1.4 ± 1	21 ± 15	100
S_{570}	36.70 ± 0.04	0.41 ± 0.06	570	22 ± 13	325 ± 192	92
S_{520}	37.14 ± 0.07	0.48 ± 0.09	520	17 ± 11	251 ± 162	100
S_{370}	38.81 ± 0.19	0.67 ± 0.18	370	5 ± 1	74 ± 74	100
Co_{HMM}	V < 18 mL	n/a	24-48 kDa	8 ± 7	4.64 ± 4	100
Co_{1640}	31.54 ± 0.75	0.52 ± 0.06	1640	38 ± 16	22.04 ± 9	100
Co_{1380}	32.38 ± 0.29	0.75± 0.31	1380	18 ± 8	10.44 ± 4	100
Co_{1130}	33.38 ± 0.61	0.9± 0.5	1130	15 ± 11	8.7 ± 6.4	100
Co_{920}	34.38 ± 0.49	0.49± 0.18	920	3 ± 2	1.7 ± 1.2	92
Co_{900}	34.48 ± 0.33	1.17±1.04	900	1.8 ± 0.8	1.044 ± 0.46	50
Co_{630}	36.20 ± 0.30	1.25±1.22	630	4.7 ± 4.6	2.726 ± 2.66	75
Co_{500}	37.40 ± 0.33	1.22±1.29	500	3.2 ± 3	1.856 ± 1.74	75
Co_{400}	38.45 ± 0.28	0.74 ±0.69	400	2 ± 2	1.16 ± 1.16	58
Co_{300}	39.72 ± 0.46	0.77 ±0.47	310	1.4 ±0.6	0.812 ± .35	75
Co_{210}	41.57 ± 0.47	1.10 ±0.93	210	2.0 ± 1.8	1.16 ± 1.04	85
Co_{aq}	43.88 ± 0.53	1.05 ±1.27	< 200	2.5 ± 2.8	1.45 ± 1.62	50

Table 5.2 (continued) Low-molecular-mass metal complexes in the mouse brains. Confidence was defined as the number of chromatograms for a given element in which the peak was present divided by the total number of chromatograms for that element, multiplied by 100

Assigned Name	Peak Center (mL)	Peak Width (mL)	Molecular Mass (Da)	Area (%)	$[Metal]_{Brain}$ (μM)	R-factor (%)
Cu_{HMM}	V < 19.4 mL	n/a	24-48 kDa	60 ±16	2.55 ± 0.68	100
Cu_{19390}	19.46 ± 0.11	0.82 ± 0.6	19390	23± 12	0.98 ± 0.51	100
Cu_{15670}	20.5 ± 0.19	0.64 ± 0.13	15670	13 ± 5	0.55 ± 0.21	100
Cu_{8650}	23.41 ± 0.28	1.03 ± 0.23	8650	2 ± 0.7	0.08 ± 0.03	100
Cu_{5680}	25.47 ± 0.24	0.63± 0.17	5680	0.5 ± 0.3	0.02 ± 0.01	100
Cu_{4230}	26.91 ± 0.4	0.71 ± 0.32	4230	0.5 ± 0.2	0.02 ± 0.008	100
Cu_{1020}	33.86 ± 0.66	0.42 ± 0.19	1020	0.2 ± 0.6	0.01 ± 0.03	92
Cu_{370}	38.90 ± 0.23	0.60 ± 0.20	370	0.8 ± 0.8	0.03 ± 0.03	100
Zn_{HMM}	V < 18 mL	n/a	24-48 kDa	86 ± 3	37.94 ± 1.32	100
Zn_{19630}	19.4 ± 0.4	0.6 ± 0.2	19,630	8.5 ± 4	3.75 ± 1.76	100
Zn_{16000}	20.4 ± 0.5	0.8 ± 0.4	16,000	5 ± 2	2.21 ± 0.88	92
Zn_{1760}	31.2 ± 0.5	0.6 ± 0.5	1,760	0.4 ± 0.2	0.18 ± 0.09	42
Zn_{400}	38.5 ± 0.1	0.4 ± 0.1	400	0.2± 0.1	0.09 ± 0.04	67
Fe_{HMM}	V < 18 mL	n/a	24-48 kDa	98 ± 2	17.37 ± 0.35	100
Fe_{3320}	28.1 ± 0.4	0.6 ± 0.5	3320	1.4 ± 1.2	0.25 ± 0.21	58
Fe_{1720}	31.3 ± 0.1	0.6 ± 0.2	1720	0.3 ± 0.2	0.05 ± 0.03	58
Fe_{510}	37.3 ± 0.3	0.6 ± 0.4	510	0.5 ± 0.3	0.09 ± 0.05	75
Mn_{HMM}	V < 18 mL	n/a	24-48 kDa	77 ± 22	0.65 ± 0.18	100
Mn_{3810}	27.42 ± 0.24	0.64 ± 0.10	3810	3 ± 1	0.025 ± 0.008	50
Mn_{2710}	29.08 ± 0.54	0.68 ± 0.24	2710	3± 2.0	0.025 ± 0.017	85
Mn_{2040}	30.48 ± 0.76	1.38 ± 0.94	2040	11 ± 5	0.09 ± 0.04	58
Mn_{1680}	31.43 ± 0.3	0.67 ± 0.40	1680	17 ± 9	0.14 ± 0.08	50
Mn_{1270}	32.81 ± 1.29	1.25 ± 1.08	1270	8 ± 7	0.07 ± 0.06	50
Mo_{HMM}	V < 18 mL	n/a	24-48 kDa	82 ± 12	0.22 ± 0.03	100
Mo_{940}	34.3 ± 0.5	0.5 ± 0.2	940	2.0 ± 1.6	0.005 ± 0.004	50
Mo_{410}	38.4 ± 0.6	1.21 ± 0.7	410	5.3 ± 3	0.01 ± 0.008	58
Mo_{350}	39.1 ± 0.7	0.94 ± 0.4	350	8.6 ± 5	0.02 ± 0.013	67
Mo_{240}	41.0 ± 0.6	1.6 ± 0.7	240	4 ± 3	0.01 ± 0.008	67

Representative chromatograms of the FLS for each element, along with various standard compounds, are shown in Figures. 7.3–10. The P chromatogram (Fig. 5.1) exhibited two major regions of peaks. The high-molecular-mass (HMM) region corresponds to P-containing compounds with MMs between ca. 13–6 kDa (21–25 mL). P-compounds with MMs between 4–0.2 kDa (27–41 mL) are included in the LMM region. The intermediate-molecular-mass (IMM) region between 4–6 kDa was effectively devoid of peaks.

The ill-resolved shape of the HMM region suggested that multiple overlapping species contributed, and we did not attempt to decompose it. In contrast, the peaks in the LMM region were better resolved. These were simulated using the equation

$$I_V = I_0 + \mathrm{I}_{\max}\, e^{-\left(\frac{V - V_0}{\omega}\right)^2} \qquad (5.1)$$

where ω is the width of the peak and I_V, I_0, and I_{max} are the detector responses at any volume V, at volume V = 0, and at the volume corresponding to the peak maximum, respectively. We integrated the total area under the chromatogram along with the relative areas under the individual LMM peaks such that the percentage of the total eluent P due to each LMM peak ($f_{cpd\text{-}i}$) could be determined. The concentration of each P-containing species represented by the LMM peaks in the brain ([Cpdi]) was calculated using the equation

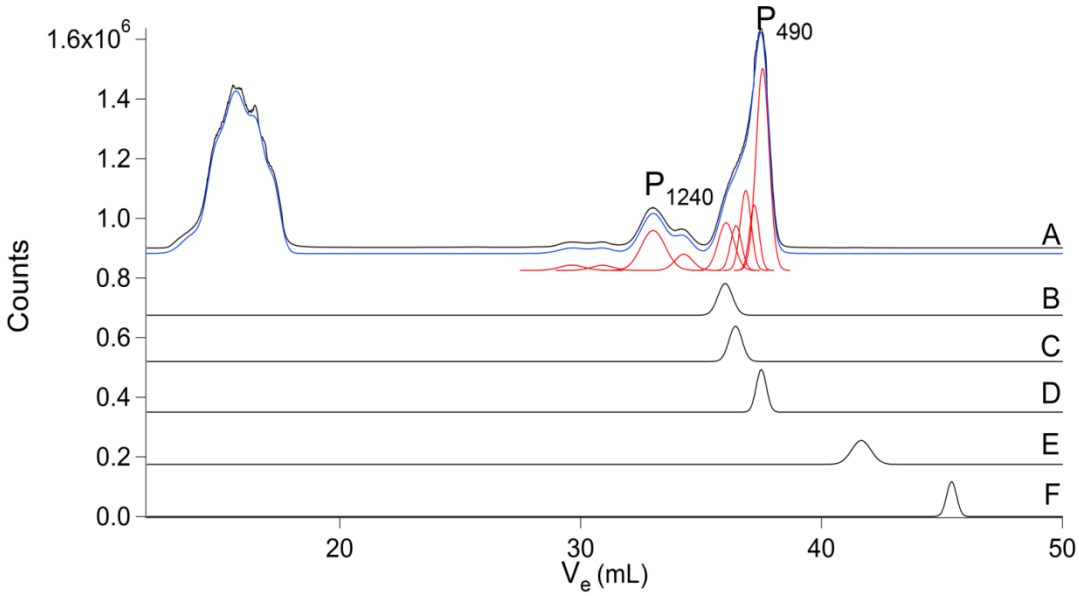

Figure 5.3. Phosphorus Chromatograms of Brain FTS and Various Phosphorus-containing Compounds. (A) Brain FTS; (B) IP_6; (C) ATP; (D) ADP; (E) AMP, and (F) HPO_4^{2-}. Red lines in Fig. 5.3–5.10 are simulations representing the LMM species listed in Table 5.1. The blue line is the overall simulation.

$$[Cpd_i] = f_{cpd-i} \cdot [P]_{fts} \cdot FD \qquad (5.2)$$

where $[P]_{fts}$ is the concentration of P in the FTS and FD is the fold-dilution used to prepare the FTS starting from the intact brain. Similar equations were used to estimate the concentrations of all LMM metal and S compounds. Eqn (5.2) assumes that the same proportion of each P compound was retained by the column. Maximum and minimum concentrations for each compound (Table 5.2) were estimated by assuming that the P retained by the column was exclusively either the P species of interest, or other P-containing species, respectively.

Eight species were used to simulate the LMM region of the P chromatogram (Figure 5.3, Table 5.2). Each was designated by the element followed by a subscript indicating its approximate MM. The dominant P peak (P_{490}) comigrated with ADP and was assigned as such. Authentic ATP migrated at a slightly smaller V_e and its peak fit in the left-side shoulder of P_{490} as long as the linewidth was increased. Alternatively, the peak for ATP and another species could both fit into this shoulder if narrower linewidths were assumed. IP_6 binds Fe in cells and is thought to be involved in trafficking. However, no Fe peaks comigrated with Fe-bound IP_6. The remaining P peaks were not assigned. Curiously, no peaks comigrated with AMP or orthophosphate.

Peaks in the representative S chromatogram (Figure 5.4) again segregated into HMM, IMM and LMM regions. Again, there were few, if any, S-containing species present in the IMM region.

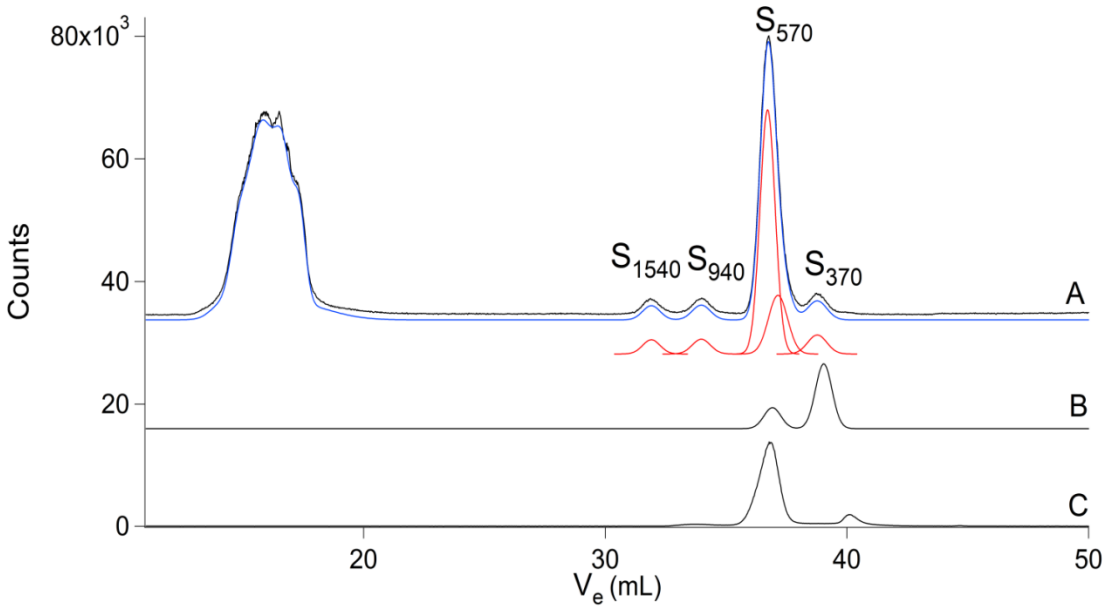

Figure 5.4. Sulfur Chromatograms of Brain FTS and Various S-containing Compounds. (A) Brain FTS; (B) glutathione, GSH; (C) oxidized glutathione, GSSG. The authentic glutathione solution contained some GSSG, while the GSSG solution contained a contaminant.

As with P, the S-containing species in the HMM region were poorly resolved and only the overall response in this region was determined by simulation. The LMM region contained 4 major resolved peaks. The dominant peak (S_{570}) comigrated with GSSG. However, its broad linewidth suggested that GSSG and another S species with a similar MM contributed. Another peak (S_{370}) nearly comigrated with GSH, and was assigned as such. The remaining two species, S_{1540} and S_{940} were not assigned. The ratio of peak areas for the oxidized and reduced glutathione species was ca. 4:1 GSSG: GSH, assuming that one of the two species that contributed to S_{570} was GSSG. This suggests a molar ratio of *ca.* 2: 1 which is reasonably close to previously reported molar ratios for brain samples.[187]

The Co chromatogram (Figure 5.5) displayed numerous species in the LMM region, some HMM peak intensity, and little if any peaks in the IMM region. Of all metals detected, Co exhibited the greatest number of LMM species. Cyanocobalamin migrated just slightly slower than the dominant Co peak (Co_{1640}), suggesting that Co_{1640} might arise from a related complex (e.g. adenosylcobalamin). Aqueous Co^{II} ions migrated as multiple species, consistent with rapid ligand/proton exchange reactions.

The representative Cu chromatogram (Figure 5.6) indicated a HMM region containing ca. 5–6 reasonably resolved peaks, with MMs between 19 and 48 kDa. The IMM region was devoid of peaks, and the LMM region contained only ca. 2 peaks. Although the trace in Figure 7.6 suggests a miniscule amount of aqueous Cu, this feature was not reliably present in other traces.

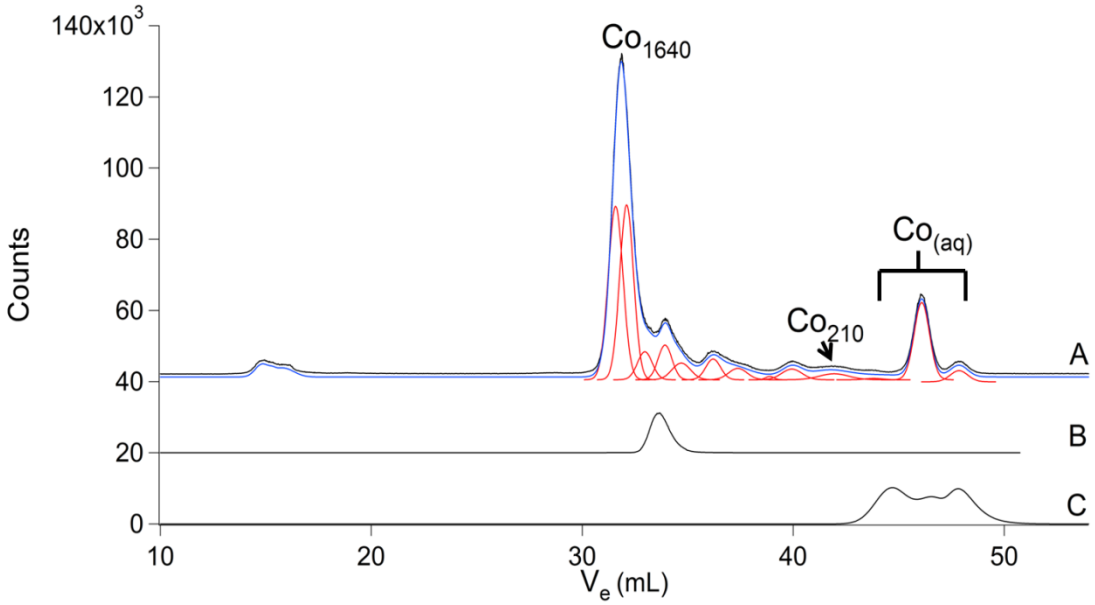

Figure 5.5. Cobalt Chromatograms of Brain FTS and Other Co Species. (A) Brain FTS; (B) cyanocobalamin; and (C) aqueous Co. The three lowest MM simulations in the figure are considered a single species (Coaq) in Table 5.2.

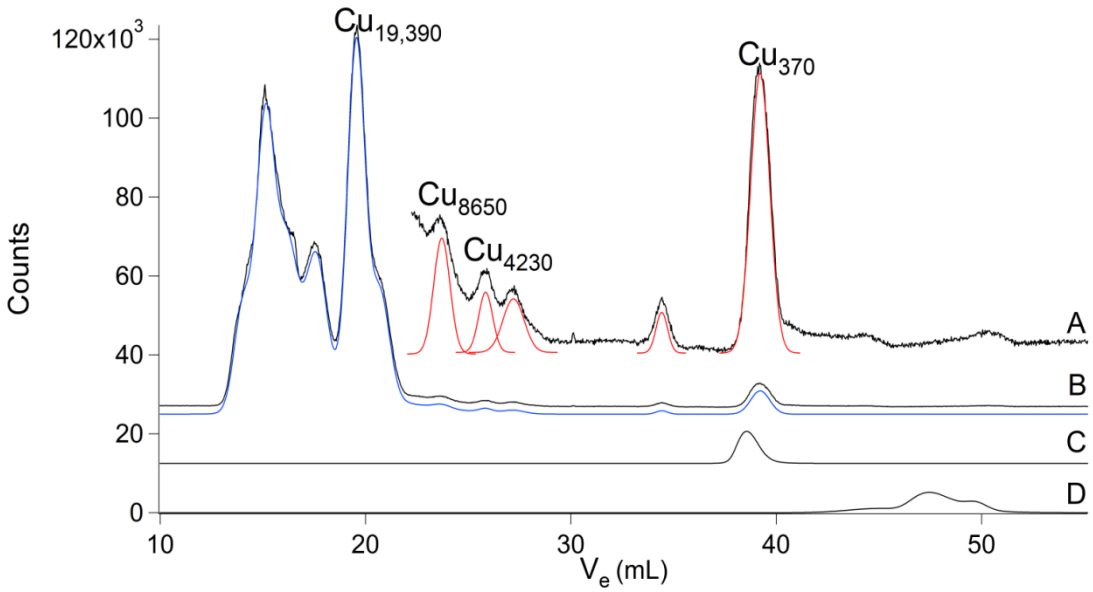

Figure 5.6. Copper Chromatograms of Brain FTS and Other Cu Species. (A) Brain FTS × 15; (B) brain FTS × 1; (C) Cu^{II}(EDTA); and (D) aqueous Cu.

The Zn chromatogram (Figure 5.7) showed a well-resolved HMM region that included ca. 5 species. The IMM and LMM regions were virtually devoid of peaks.

The Fe chromatogram (Figure 5.8) showed a poorly resolved HMM region and an IMM region largely devoid of peaks. The LMM region included two significant peaks (Fe_{1720} and Fe_{510}), but these were only observed in 58% and 75% of the chromatograms, respectively. In general, there was more variability in the Fe (and Mn) chromatograms than in chromatograms from the other metals. In most traces, the ultra LMM region was devoid of features (the trace shown in Figure 6.8 shows such a feature, but it was not routinely observed).

The Mn chromatogram (Figure 5.9) included poorly resolved features in the HMM region, no features in the IMM region, and a few peaks in the LMM region. Mn_{1270} and the broad feature centered at ca. 28 mL were present in about half of the traces. The Mo chromatogram (Figure 5.10) exhibited peaks in the HMM and LMM regions, while the IMM region was largely devoid of peaks. The major LMM peak (Mo_{350}) comigrated with molybdopterin isolated from xanthine oxidase, suggesting that these peaks arise from the same or a closely related species.

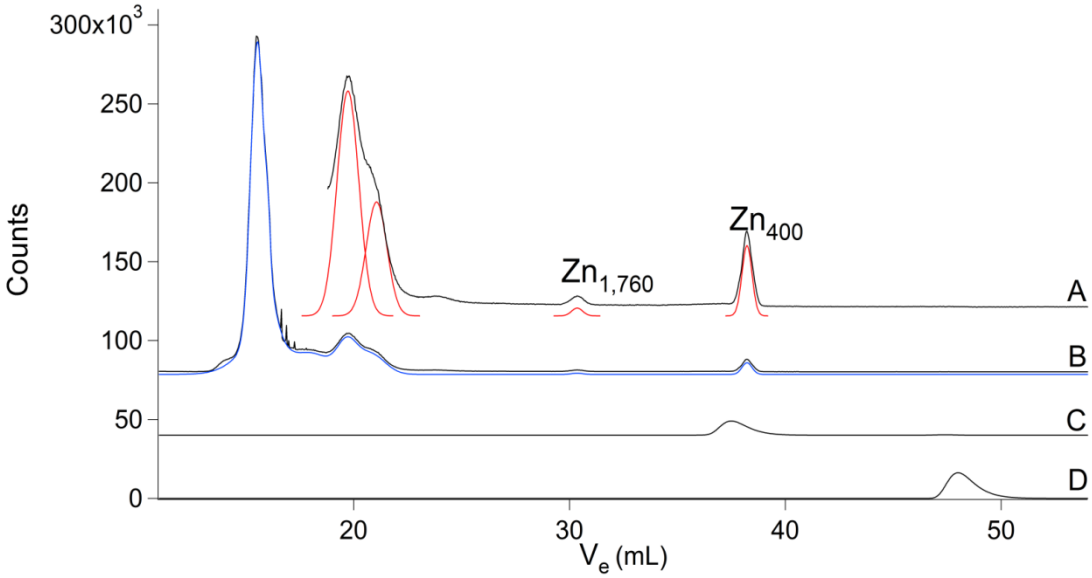

Figure 5.7 Zinc Chromatograms of Brain FTS and Other Zinc Species. (A) Brain FTS ×16; (B) brain FTS × 1; (C) Zn^{II}(TPEN); and (D) aqueous Zn.

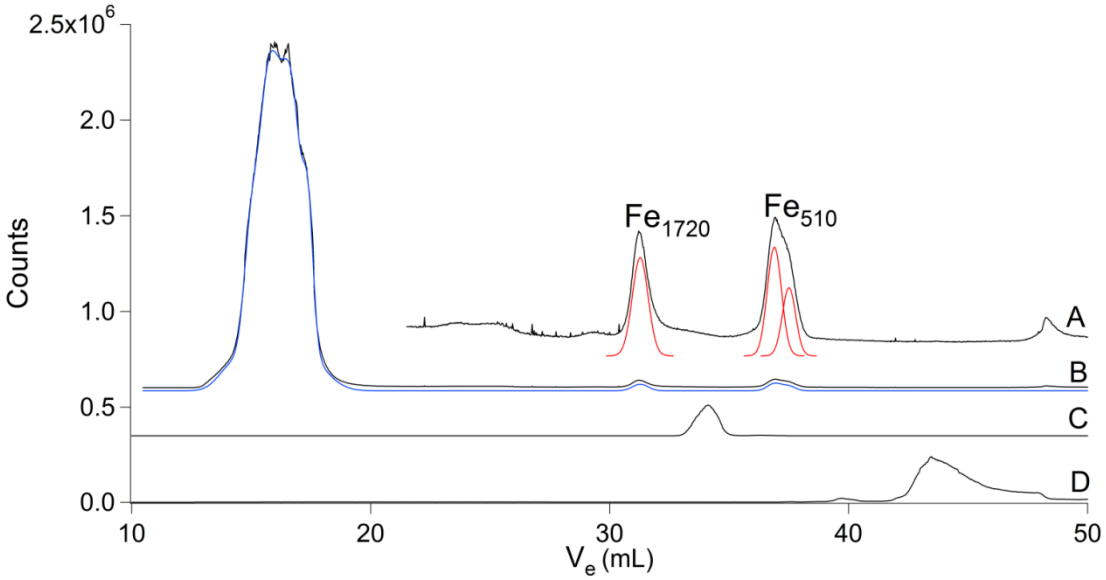

Figure 5.8. Iron Chromatograms of Brain FTS and Other Iron Species. (A) Brain FTS × 15; (B) brain FTS × 1; (C) Fe^{II}(ATP); and (D) aqueous Fe.

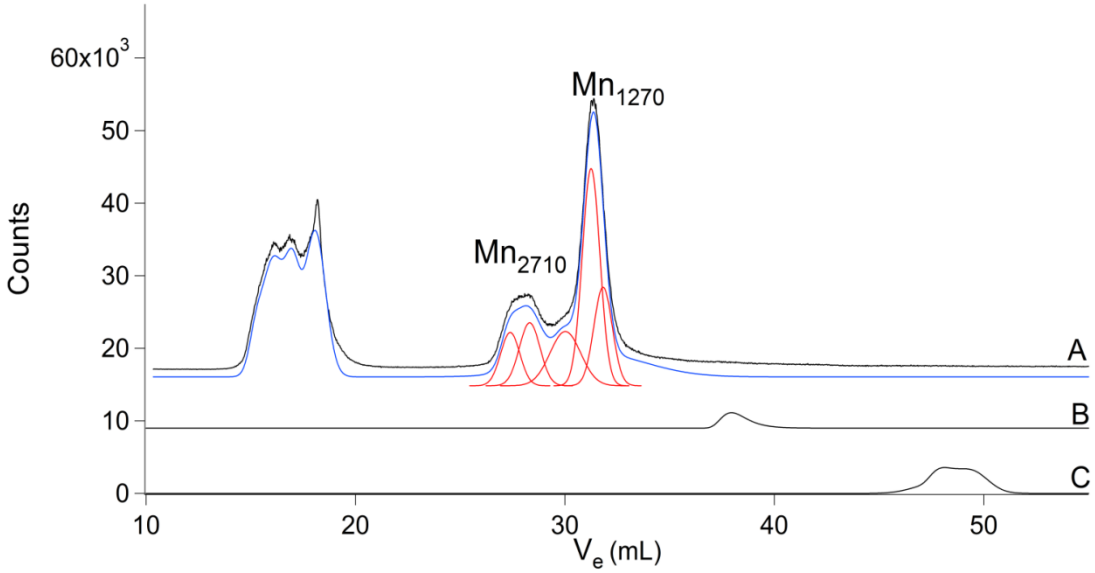

Figure 5.9. Manganese Chromatograms of Brain FTS and Other Mn Species. (A) Brain FTS; (B) Mn^{II}(EDTA); and (C) aqueous Mn.

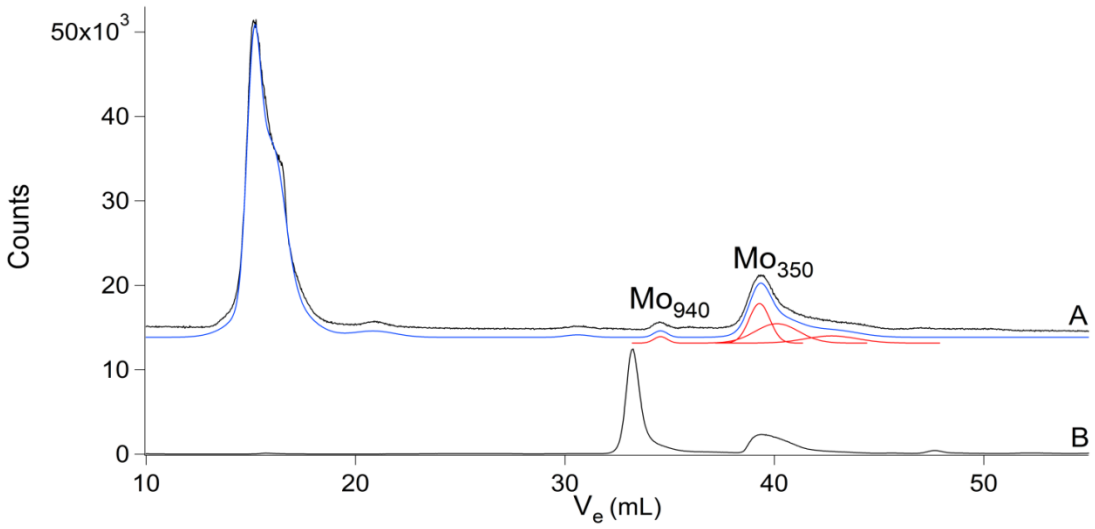

Figure 5.10. Molybdenum Chromatograms of Brain FTS and Molybdopterin Extract From Xanthine Oxidase. (A) Brain FTS; and (B) molybdopterin. The intense peak in B with MM ~1.5 kDa was not assigned.

Discussion

The objective of this study was to determine whether the mouse brain contains LMM metal complexes, defined as Mo, Mn, Fe, Co, Cu and Zn complexes possessing MMs <10 kDa. Rather than using chelators, our approach was to detect such species directly, using ICP-MS to monitor metals eluting from our LMM size-exclusion chromatography column. We were careful to avoid oxidation of any redox-active complexes, by working in an inert-atmosphere glovebox. We attempted to limit ligand substitution reactions by minimizing the time between euthanizing the animals and loading the LC column, and by running the column at low temperature. We distinguished "real" from artifactual complexes by repeating the experiment 13 times and assigning a confidence probability to each species in accordance with the proportion of runs in which the species was observed (Table 5.2). Our results were independent of buffer used. The vast majority of metal ions loaded on the column did not adhere to it.

By these criteria, our results indicate that there are 11 Co, 5 Cu, 5 Mn, 4 Mo, 3 Fe, and 2 Zn LMM complexes in the mouse brain. Of these 30 LMM metal complexes, only 2–3 have masses suggesting protein ligation (Cu_{8650}, Cu_{5680} and perhaps Cu_{4230}). The rest have lower MMs which suggest either small peptides as ligands or perhaps organic and/or inorganic ligands.

Except for Cu, all of the metals displayed a significant gap between one edge of the HMM region (with MMs > ~20 kDa) and one edge of the LMM region (with MMs <4 kDa). The absence of metal complexes between these two regions implies that the division into such groups is not arbitrary. Zhuang et al. reported that the shortest (non-

alternatively spliced) protein in the mouse genome is 38 residues, which corresponds to 4.2 kDa.[188] This suggests that the complexes in the HMM region are exclusively protein-based and it raises the possibility that the metal complexes in the LMM region are either non-proteinaceous or have peptides arising from post-translational truncations. Large natural products and siderophores (e.g. actinomycin D, glycosylated antibiotics, pyoverdine) have MMs of ca. 1.5 kDa.

Of the metals examined, Co exhibited the most LMM complexes and perhaps the least protein-based species. Cu and Zn displayed the opposite pattern, with numerous well-resolved metal-bound proteins and few non-proteinaceous complexes.

Our results impact the issue of whether cells contain "free" aqueous metal ions. They indicate that there are significant concentrations of aqueous Co ions in the brain, but do not provide clear evidence of aqueous Cu, Zn, Mn, Mo or Fe ions. ICP-MS is quite sensitive, such that the concentration of aqueous metal ion would need to be <10 nM (ca. 103 ions per cells) to escape detection. In a seminal study published over a decade ago, O'Halloran and coworkers argued that there are no "free" or aqueous Cu ions in the cell, and that Cu trafficking exclusively involves transferring Cu ions from one protein chaperone to the next.[130] Their conclusion was based on ability of the Cu-loaded chaperone CCS to donate Cu into apo-SOD1 even in the presence of bathocuproine sulfate, a strong Cu^{I} chelator. Using thermodynamic binding constants, they estimated that there is <1 aqueous Cu ion per cell. They rationalized that the intracellular milieu must have a large capacity for binding aqueous Cu ions, and that aqueous Cu would be dangerous to the cell, due to its tendency to engage in Fenton

chemistry. To the limited extent that our results can detect aqueous Cu (down to ~300 Cu ions per cell), they support the conclusion that there are no "free"/aqueous Cu ions in the mouse brain.

Similar thermodynamic calculations involving aqueous Zn ions in the cell yield concentrations of tens to hundreds of pM. Like Cu, this translates into <1 aqueous Zn ion per cell assuming a cell volume of 10^{-14} L. Aqueous Zn ions also inhibit human receptor protein-tyrosine phosphatase in accordance with $K_I = 21 \pm 7$ pM,[189] again suggesting very few if any intracellular aqueous Zn ions. Our results suggest the absence of aqueous Zn in the mouse brain and provide substantial evidence for protein-based Zn complexes. We propose that the Zn species released during the firing of synaptic vesicles have one or more non-aqueous ligands. The species released are almost certainly not "free"/aqueous Zn.

Aqueous metal ions rapidly exchange bound waters with the solvent, with rate-constants that vary in the order $Ni^{II} < Co^{II} < Fe^{II} < Mn^{II} < Zn^{II} < Cu^{II}$.[190] The waters on such complexes have average residence times ranging from 10^{-4}–10^{-10} sec. At moments when a coordinated water dissociates, thousands of potential ligands in the cellular milieu could interact with the metal at the vacant coordination site. This would promote the formation of a new complex. In the likely event that the new ligand would coordinate stronger than water, the complex would become less dynamic. Even if no permanent complexes formed, the result of this dynamic exchange-reaction would be a population-distribution of closely related and rapidly interconverting species rather than a single entity. Indeed the broad structured peaks obtained from the chromatographic migration

of aqueous metal ions in our study suggest such a population of species. Could such dynamical populations serve discrete physiological functions in a cell, or would they be deleterious, engaging in uncontrolled side reactions that produce toxic species? We suspect that cells could not survive the uncontrollable behavior of most aqueous transition metal ions. Moreover, the cell would be unable to regulate such ions since the coordinating ligands would not be under genetic control. Chaos would result.

Accordingly, aqueous metal ions with the fastest water exchange-dynamics would seem to be the least likely to exist in a cell, while those with slower exchange-dynamics might be sufficiently stable. Our detection of aqueous Co ions in FTSs supports this possibility, since, of the metals examined, aqueous Co^{II} exchanges water ligands slowest. To test this idea further, aqueous Ni^{II} ions, which exhibit even slower water exchange-dynamics, were added to a FTS prior to passage through the column. A single peak with the MM of aqueous Ni^{II} was detected. When other aqueous metal ions, including Fe, Cu, Zn and Mn were added to the FTS, the only aqueous ion detected in the resulting chromatograms was Co (data not shown). Alternatively, or in addition, our detection of aqueous Co may arise from the greater sensitivity of Co relative to the other metals.

The fast ligand exchange-dynamics inherent to metal ions are slowed with polydentate ligands. Polydentate metal complexes would likely exist as single autonomous entities that are not in a dynamic equilibrium with other potential ligands in the cell. Slower exchange dynamics would minimize toxic side reactions because they would not have dynamically-free sites. Moreover, such ligands would need to be

synthesized and thus regulated by the cell. The shape of such large complexes would allow other cellular components (e.g. membrane-bound protein transporters) to recognize and distinguish one complex from another. All of these factors favor the occurrence in the cell of metal complexes with polydentate ligands. Undoubtedly all of the LMM metal complexes characterized in this study are of that type.

We are particularly interested in metal complexes involved in metal ion trafficking – assuming such complexes exist. For such complexes, the coordinating polydentate ligands must bind strong enough to avoid the problems mentioned above, yet also allow the metal to be transferred to downstream acceptors. In some well-documented cases, altering the redox state of the metal[(191)] or the pH[(192)] of the solution are sufficient to labilize the ligands. Binding to a protein or macromolecular complex might also labilize the ligands coordinating a metal. One future task will be to identify the complexes and the LMM metal-containing proteins that we have detected here.

Determining the physiological role of each LMM metal complex in the brain that we have described in this study will be a challenge that will require multiple "orthogonal" approaches. The LC-ICP-MS approach used here is complementary to that of treating cells or tissues with custom-designed chelators that react with and sense labile metal complexes. The advantage of the chelator-based method is the ability to detect labile metal ions in intact live cells. The disadvantages are that such chelators may react with multiple species in the cell, and that the process of detection destroys the complexes of interest. The advantage of the LC-ICP-MS approach is that individual metal complexes can be detected undisturbed (barring potential degradation reactions

occurring during workup). The disadvantage is that the cell itself must be disrupted such that critical information regarding cellular compartmentalization is lost. Merging these approaches, e.g. using LC-ICP-MS to assess which particular complexes react with designer metal sensors, will undoubtedly yield the greatest insight into metal ion metabolism in cells and super-cellular structures such as the brain.

CHAPTER VI

INSIGHTS INTO IRON UPTAKE IN MOUSE PLASMA USING LC-ICP-MS

Introduction

Iron is a redox-active metal that plays essential roles in mammalian physiology and disease.[193] Fe-containing hemoglobin binds and transports O_2 to tissues where mitochondrial respiratory complexes, packed with Fe-rich cytochromes and Fe/S clusters, catalyze O_2 reduction. Iron in the brain helps synthesize neurotransmitters and myelin that insulates neurons.[194] Iron is critical for the developing hippocampus.[195] Young rodent brains experience a growth-associated Fe deficiency due to the inability of Fe to be imported fast enough to counterbalance the diluting effect of brain growth. [156, 196]

The liver plays a central role in Fe metabolism.[197] Hepatocytes synthesize hepcidin, the master regulator of Fe in the body. This peptide hormone controls the stability of ferroportin, a membrane-bound protein through which duodenal enterocytes, hepatocytes and macrophages export Fe^{II} into the blood. Hepatocytes also synthesize transferrin, a blood protein that binds Fe^{III} in the plasma. Transferrin is widely considered to be the dominant (or even exclusive) Fe component of the plasma, and the major (or exclusive) protein that transports plasma Fe into healthy tissues. Transferrin-bound-iron (TBI) enters cells through the receptor TfR1.[193] Ferritin is a spherically-shaped Fe-storage protein complex. Liver macrophages contain high levels of ferritin [197, 198] which can be exported into the blood. Hepatocytes also synthesize

ceruloplasmin, a blood protein that oxidizes the ferroportin-associated Fe^{II} that enters the blood. This oxidation to Fe^{III} is required for transferrin binding.

A significant portion of splenic Fe is found in red-pulp macrophages which degrade senescent erythrocytes.[199] The resulting nonheme Fe is released into the blood, coordinated to transferrin, and sent to the bone marrow for installation into nascent heme groups. As a result, plasma Fe exchanges rapidly. The concentration of Fe in the plasma (20 – 50 μM) is largely controlled by ferroportin and hepcidin [193, 198-201]

Transferrin has a high affinity for aqueous Fe^{III}, yet under normal dietary conditions, only_30% of plasma transferrin is Fe bound[201] which implies that the concentration of aqueous Fe^{III} in the blood must be very low. Indeed, apo-transferrin scavenges free Fe in the plasma. As long as sufficient apo-transferrin is available, virtually all $^{59}Fe^{III}Cl3$ or $^{59}Fe^{III}$citrate added to plasma will coordinate in minutes.[202-206] These results have been interpreted to mean that virtually all Fe in normal plasma is TBI. NTBI is thought to play an important (damaging) metabolic role, but only when transferrin is fully saturated, e.g. in Fe-overload diseases [201, 207, 208] for which NTBI concentrations are high. [209] However, healthy plasma reportedly contains other forms of Fe besides transferrin. [210] This contradiction stems from uncertainty or disagreement as to the composition, concentration and stability of NTBI. NTBI might be a population of Fe complexes, including heme groups, heme:hemopexin complexes, hemoglobin:haptoglobin complexes and ferritin [200, 201, 204] and/or Fe coordinated to citrate, ascorbate, acetate or albumin.[201, 211-213]

NTBI rapidly enters tissues, especially the live.[202, 205] In heart cell cultures, NTBI is imported 300-times faster than TBI.[214] The receptors that import NTBI include DMT1, ZIP14, and voltage-dependent Ca channels.[201, 215] The liver and kidney rapidly absorb ferritin via TIM2 [216] and Scara5 receptors, respectively. [217] The NTBI importer in hepatocytes exhibits an apparent Michaelis-Menten K_m of 1.25 μM.[218]

The kinetics of Fe import into organs has been evaluated by injecting radioactive ^{59}Fe into rodents, sacrificing the animals at various times, dissecting organs, and measuring how much radioactivity was incorporated. Dallman and Spirito [219] reported that the amount of radioactive $^{59}FeCl_3$ taken up per brain maximized at Postnatal day 18 (P18). Taylor and Morgan obtained similar results using ^{59}TBI.[200] Both groups concluded that the concentration of receptors for Fe import in the brain increased during the first 2 weeks of life and then declined. Craven et al. [205] saturated plasma transferrin in rodents and then injected ^{59}Fe citrate. ^{59}Fe citrate was absorbed into organs with a $t_{1/2}$ < 30 sec, compared to TBI (in controls) which had $t_{1/2}$ ~50 min. In a related study, Ueda et al. [203] blocked transferrin receptors in mice and then injected $^{59}FeCl_3$ into the blood. Within minutes, essentially all of this Fe converted into TBI as monitored by gel filtration LC. Malecki et al. [220] injected $^{59}FeCl_3$ into hypotransferrinemic mice. The rate of ^{59}Fe uptake into the brain was nearly 100× faster than with WT mice, confirming that NTBI imports faster than TBI. [221, 222]

The most critical period of mammalian development is from birth to young adulthood, yet this is also the most difficult to study using tracers. We developed a Pup Swapping method to determine the kinetics of Fe uptake during this period. ^{56}Fe and

^{57}Fe-enriched pups were swapped at birth, such that each nursed on milk containing the opposite isotope. Mathematical models were developed to quantify the rates of Fe import from the plasma into major organs. Surprisingly, NTBI rather than TBI was the dominant Fe-containing species that incorporated into the organs of healthy non-iron-overloaded mice at early stages of development.

Results and Discussion

Initial experiments using the pup swapping protocol resulted in kinetic data of iron uptake in mouse organs and mouse plasma over a long time interval (i.e., weeks). The concentration of Fe in blood is much higher than the endogenous Fe concentration in organs. This high concentration of Fe in blood is primarily located in the red blood cells in the form of hemoglobin. In order to understand iron trafficking in blood one must look at it in is most transient forms and that would be those found in the plasma portion of whole blood.

As expected, the starting isotope concentration in the plasma, [$^{s}Fe_P$], decreased with age while that of the enriching isotope, [$^{e}Fe_P$], increased. The sum of these concentrations, [$^{t}Fe_P$], increased slightly with time. The collection of adequate plasma volumes in animals under the age of 7 days was difficult due to their small blood volumes. In order to estimate [$^{t}Fe_P$] for ages 0-7 days it was necessary to use extrapoloation of all data collected.

Our collaborator, Dr. Barlas, using the data developed two models seen in figure 6.1. One model referred as the one component model made the assumption that a single

Fe-containing species called Fe_T was imported into the plasma and that Fe_T alone was deposited into the organs (Figure 6.1, top). At birth, all Fe_T in the plasma and tissues was assumed to be the starting isotope. ${}^{e}Fe_T$ enters the blood at rate E_{feed}. Both ${}^{e}Fe_T$ and ${}^{s}Fe_T$ compete for import into organs via a common receptor at the interface with the blood. Receptors were treated as Michaelis-Menten enzymes acting on substrates ${}^{e}Fe_T$ and ${}^{s}Fe_T$. Using the solutions to a system of ordinary differential equations we were unable to obtain simulations which demonstrated organs becoming enriched at a rate faster than that of plasma.

In order to postulate a system which could explain the enrichment of organs prior to plasma a two component model was developed assuming a) Fe enters the plasma exclusively as second species called Fe_{NT}; b) Fe_{NT} in the plasma converts to Fe_T; and c) Fe_{NT} and Fe_T are imported independently into the organs. Fe_{NT} could represent a single species or many. Using this model and its ODE's it was possible to simulate the observed phenomenon of organ enrichment occurring faster than the plasma as long as the rate of import of Fe_{NT} is faster than that of Fe_T .

In order to determine the feasibility of a two component plasma model we carried out an LC-ICP-MS experiment to determine what iron containing species are present in plasma of healthy mice. The liquid chromatogram (LC) exhibited ~6 Fe-associated peaks (Figure 5.2). Peaks at > 300, 90, and 55 kDa were assigned to ferritin, transferrin, and hemopexin, respectively; the other 3 peaks could not be assigned. The LC-ICP-MS experiment demonstrates that numerous Fe-containing species coexist with transferrin in healthy WT mouse plasma.

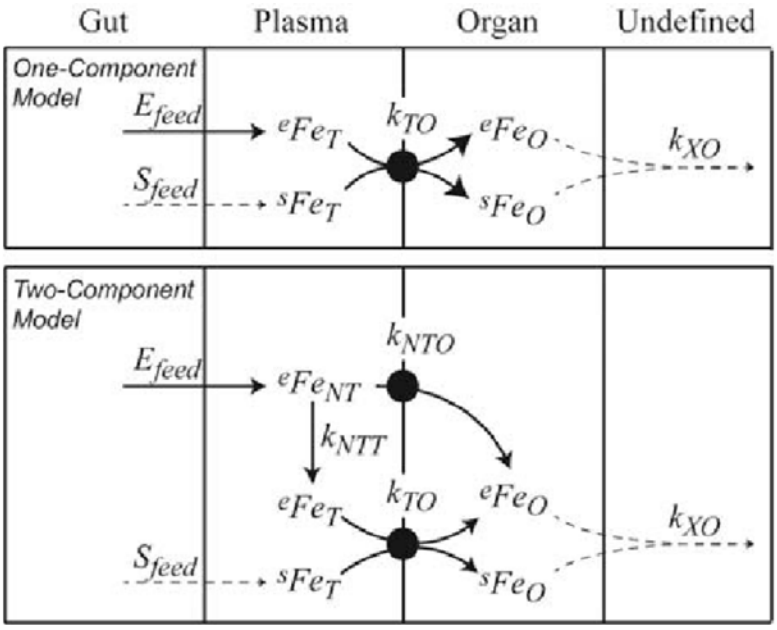

Figure 6.1. One Component Model (OCM, top) and Two Component Model (TCM, bottom) Describing Fe Import into Mouse Organs. For the OCM, enriching and starting isotopes are imported from the gut to the plasma to form species Fe_T which is imported into organs through a receptor. The resulting species Fe_O can be exported. The TCM is similar except that the enriching isotope enters the plasma as a second species Fe_{NT} which converts to Fe_T. Both Fe_{NT} and Fe_T can be imported into organs at independent rates.

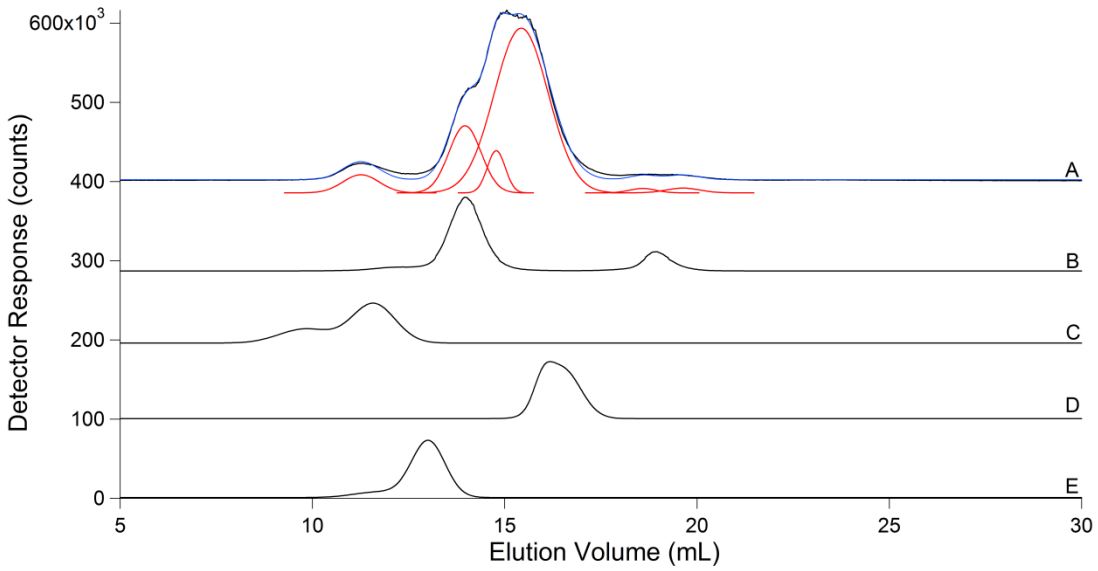

Figure 6.2. Chromatogram of Mouse Blood Plasma. (A), transferrin (B), ferritin (C) and hemopexin (D). Black lines are the data, red lines are simulations. The blue line is a composite simulation including, from left to right, ferritin (6% of the Fe), transferrin (17%), unidentified protein 1 (UP1, 6%), hemopexin (69%), and unidentified proteins UP2 and UP3 (1% each). UP1 has a molecular mass of 60-80 kDa, while UP2 and UP3 have masses < 7 kdDa.

The main form of iron known to be present in plasma is that of transferrin bound iron (TBI), which in our model would be Fe_T. However, Fe entering the plasma flows through the transporter DMT1 as an Fe^{II} species, and then is oxidized by ceruloplasmim and coordinated to apo-transferrin. If the Fe^{II} species exist in a nontransferrin form which we call $Fe_{NT,}$ could explain the model. These processes collectively account for the $Fe_{NT} \rightarrow Fe_T$ reaction. Second, NTBI is imported into organs faster than TBI, consistent with the more rapid import of Fe_{NT} vs. Fe_T as required by our simulations. Third, our analysis requires that plasma contain at least two forms of Fe; by LC, we found that plasma contains ca. 6 Fe-containing species only one of which can be TBI. Whether any of the other species reflects NTBI is uncertain; the concentration of the NTBI in the plasma which is imported rapidly into organs may be below the detection limit.

CHAPTER VII

CONCLUSIONS AND FUTURE WORK

Conclusions

The major objective of this dissertation was to detect and characterize low-molecular-mass labile metal complexes (LMMMCs) in eukaryotic cells, organelles and in mammalian tissues. Prior studies using metal sensors and chelators have been able to detect pools of such species but not distinct complexes. Despite the popularity of these methods, this is a serious deficiency. The approach used here was to build a novel liquid chromatography system (in a refrigerated inert-atmosphere glove box) in which a portion of the eluent flows to an in-line ICP-MS and the remainder flows to a fraction collector in the box. Using such a system, labile LMM metal complexes could be detected. The specific function of each species has not been determined, and this remains a challenge for the future. However, we anticipate that many of these detected species function in metal ion trafficking, metabolism, and/or regulation.

In collaboration with Dr. Jinkyu Park a study was conducted concerning a mitochondrial membrane protein MTM1 that appears to be associated with MnSOD2. Previous research suggested that the deletion of Mtm1p resulted in the accumulation of a "bioavailable" form of iron which mismetallated apo-SOD2 causing inactivation of the protein. Initial biophysical studies performed by Dr. Park failed to detect "bioavailable" iron uniquely present in mitochondria isolated from a Δmtm1 strain. However, large amounts of Fe nanoparticles were present. To investigate further, we isolated

mitochondria from the mutant and wild type strains, then solubilized them and subjected extracts to both SEC and AEX chromatography using the LC-ICP-MS system. The SEC analysis of Δ*mtm1* mitochondria showed a Fe species with a mass near that of MnSOD2. However, the peak did not co-elute precisely and the relative amounts of the putative FeSOD2 relative to that of MnSOD2 was no greater with the mutant strain than with the WT strain. Nor was the SOD activity in fractions any lower in the mutant strain than in the WT strain when normalized to the amount of SOD2 protein in those fractions. Analysis of the AEX chromatography results afforded a similar conclusion, namely that apo-SOD2 was not mismetallated to any greater degree in the mutant than in the WT strain. Mtm1p does not appear to be directly involved in iron metabolism. Mtm1 most likely is an importer of a factor (presumed to be a small molecule) that helps mature apo-Sod2p, perhaps involving Mn insertion or protein folding. In the absence of Mtm1p, the rate of maturation slows and immature Sod2p eventually misfolds. The lack of functional MnSod2p increases the concentration of ROS in the matrix, which triggers the formation of Fe nanoparticles. The formation of nanoparticles disregulates the import of iron in the mitochondria resulting in Fe accumulation.

A second major result of that study was the detection of a single LMM Mn complex that is present in both WT and Δ*mtm1* mitochondria. This species was initially assigned a mass of 2-3 kDa (current estimates are ~ 1100 Da). In WT mitochondria, the concentration of this Mn complex is proportional to the Mn concentration in the growth medium, with concentrations ranging from 1 – 10 μM when Mn nutrient concentrations of 2 and 200 uM are used. In Δ*mtm1* mitochondria, the concentration of the LMM Mn

complex is significantly higher (22 μM). This is the only LMM Mn complex observed in yeast mitochondria, and MnSOD2 is the only Mn-containing protein. Since SOD2 enters mitochondria unfolded, we hypothesized that the LMM Mn complex donated Mn to apo-SOD2 during metallation. This is the first description of such a LMM Mn complex in mitochondria.

LMMMCs from WT mitochondria were reinvestigated in Chapter 4, with a broader emphasis on all bio-relative metals and a greater emphasis on reproducibility. LMM extracts of yeast mitochondria were found to contain 6 Co, 3 Cu, 2 Mn, 5 Fe and 3 Zn LMM metal complexes and approximately 6 P- and S-containing LLM species. The major P-containing peak was broad and approximately comigrated with ATP and ADP. The Zn and Mn chromatograms each exhibited a dominate peak in the 1 kDa range. The LMM Mn species is probably the same as that observed previously; the exact mass of this species will require further study. The concentrations of the Zn and Mn complexes in mitochondria were estimated at ~120 and 2 μM, respectively. Numerous LMM cobalt species were observed, albeit with low concentrations (10 - 60 nM). The most reproducible cobalt peaks comigrated approximately with hydroxycobalmin or methylcobalmin. The low intensity of these species was congruent with the absence of any known Co-containing proteins in mitochondria. The major Cu species observed in WT yeast mitochondria had masses between 5,000 – 10,000 Da which suggests they might be Cu-containing peptides. Interestingly, such species were not present in mitochondria isolated from human cells or mouse brain or liver. Two major LMM Fe species were observed, with relative concentrations that varied with the cell culture

density at the time of harvesting. The major LMM Fe species in mitochondria isolated from cells harvested during post-exponential growth mode has a mass of ~1000 da while that from cells harvested during exponential growth had a mass of ~ 600 Da. Moreover, the 1000 Da Fe complex converted into the 600 Da Fe complex upon incubating samples for days in a refrigerated glovebox. Both Fe complexes appear to be present in mitochondria.

The LMM metal complexes in mouse brain were investigated (Chapter 5). In this case, 11 Co, 2 Cu, 5 Mn, 4 Mo, 3 Fe and 2 Zn complexes with molecular masses <4 kDa were detected. One LMM Mo complex comigrated with the molybdopterin cofactor. Most Cu and Zn complexes appeared to be protein-bound with masses ranging from 4–20 kDa. Co was the only metal for which the "free" or aqueous complex was reproducibly observed. Aqueous Co may be sufficiently stable in this environment due to its relatively slow water-exchange kinetics. Comparing the peaks observed in the isolate mice brain mitochondria and mice brain extracts provides some interesting findings. In the case of phosphorus the major peak is approximately the same MM in in each case. In sulfur, however the major mitochondria peak is a minor peak in the brain extract chromatograms. For metals like Zn, Co, and Mn the major peak in the mitochondria is approximately the same in the brain extract. Copper on the other hand is different and it appears that the brain extract has more HMM complexes than the ~5-8kDa complexes seen in mitochondria. Iron is surprisingly similar with the same 2 major peaks in the same approximate MM ranges. If the concentration of various species in the brain extract was corrected for the volume occupied by the mitochondria the

concentrations are within 10-20% of what we report for isolated brain mitochondria. In conclusion, these are among the first systematic studies of LMM metal complexes in yeast cells and mitochondria, and in mouse brain. Further efforts will be required to identify these LMM metal complexes unambiguously and to determine their functions.

The LC-ICP-MS system was also used to examine the Fe containing proteins in plasma from mouse blood (Chapter 6). This study investigated the mechanism of iron uptake in mice using a stable isotope animal switching method. Mouse organs were found to enrich faster than the blood plasma, suggesting the need for two components present in the plasma with different rates of exchange. Transferrin is the major protein in plasma which transports iron to organs and is thought to be the sole means of transport. Chromatograms exhibited ~6 Fe-associated peaks three of which were assigned to ferritin, transferrin, and hemopexin. The other 3 peaks could not be assigned. The LC-ICP-MS experiment demonstrated that numerous Fe-containing species coexist with transferrin in healthy WT mouse plasma and thus supports the main conclusion of the study.

Future Work

The studies of this dissertation lay the ground work for further investigations regarding the structure and function of LMMMCs. The ability to structurally characterize these complexes is primarily limited by the quantity of material available for analysis. These LMMMCs are typically present in cells and organelles at low micromolar concentrations. Since only a few hundred microliters of solution are loaded

onto the columns, very low molar quantities are available for downstream analysis. Thus, multiple runs must be performed, with common peak-containing fractions binned. Further work is required to determine appropriate methods for the pre and post chromatography sample concentrating without disrupting the structure of the complexes. Common methods used by protein chemists involve the use of ultrafiltration membranes, lyophilization, or RP prep cartridges. Ultrafiltration of LMMMC is problematic due to limited membrane sizes available. Lyophilization and RP methods both are effective but studies are need to identify and minimize ligand exchange processes. A second option to investigate would be the use of solid phase extraction techniques which use different solvents or stationary phase and could be optimized to the system of interest.

Increasing the purity of metal complexes is another means by which further characterizations might be forthcoming. Adding a second LC column (e.g. AEX after SEC) would undoubtedly help increase the purity of these complexes. In previous studies, peaks were present with similar masses have been resolved when a second dimension such as AEX or hydrophilic interaction liquid chromatography (HILIC) was applied.

Once a species is isolated in a concentrated and pure form, electrospray ionization ion mobility mass spectrometry (ESI-IM-MS) would be the method of choice to gain information on both the mass and collisional cross section of the complex. Once the mass is known structural information can be gained using NMR spectroscopy. The major issue with NMR of LMMMCs comes with paramagnetic metal centers. Paramagnetic metal centers cause line broadening which makes NMR features difficult

to detect. To alleviate this a background spectra could be acquired and then a chelator could be added causing release of the apo-ligand which could then be detected when the background spectra are subtracted. These techniques along with the standard biophysical techniques done in the Lindahl lab will provide vital structural information.

Establishing the function of LMMMCs will require a different type of investigation. Here, differences in the concentration of such species due to genetic changes in the organism will be a viable approach. For example, the disappearance of a LMM Fe complex in mitochondria isolated from a strain of yeast that lacks the mitochondrial Fe transporters Mrs3/4 would identify the LMM Fe complex as being imported by Mrs3/4. Similar inferences could be made by examining many genetic mutant strains and observing the effect on LMM metal complexes.

The field of metal ion trafficking and homeostasis is still in its infancy but is constantly developing as more information on metal transporters, metalloproteins, and metallochaperones become available. A void remains when it comes to understanding the structure and function of LMMMCS. The novel LC-ICP-MS system and the approach pioneered in this dissertation will hopefully provide a viable means of filling that void such that it will play an equally important role along with metal sensor and probe studies in revealing the structure and function of these intriguing metal complexes.

REFERENCES

1. Thomson, A. J., and Gray, H. B. (1998) Bio-inorganic chemistry, *Curr Opin Chem Biol 2*, 155-158.
2. Andreini, C., Bertini, I., Cavallaro, G., Holliday, G. L., and Thornton, J. M. (2008) Metal ions in biological catalysis: from enzyme databases to general principles, *J Biol Inorg Chem 13*, 1205-1218.
3. Morales, J. G., Holmes-Hampton, G. P., Miao, R., Guo, Y. S., Munck, E., and Lindahl, P. A. (2010) Biophysical Characterization of Iron in Mitochondria Isolated from Respiring and Fermenting Yeast, *Biochemistry-Us 49*, 5436-5444.
4. Giedroc, D. P., Keating, K. M., Martin, C. T., Williams, K. R., and Coleman, J. E. (1986) Zinc metalloproteins involved in replication and transcription, *J Inorg Biochem 28*, 155-169.
5. Wirstam, M., Lippard, S. J., and Friesner, R. A. (2003) Reversible dioxygen binding to hemerythrin, *J Am Chem Soc 125*, 3980-3987.
6. Bleackley, M. R., and MacGillivray, R. T. A. (2011) Transition metal homeostasis: from yeast to human disease, *Biometals 24*, 785-809.
7. Jonnalagadda, S. B., and Rao, P. V. V. P. (1993) Toxicity, Bioavailability and Metal Speciation, *Comparative Biochemistry and Physiology C-Pharmacology Toxicology & Endocrinology 106*, 585-595.
8. Finney, L. A., and O'Halloran, T. V. (2003) Transition metal speciation in the cell: Insights from the chemistry of metal ion receptors, *Science 300*, 931-936.

9. Cotruvo, J. A., and Stubbe, J. (2012) Meta nation and mismetallation of iron and manganese proteins in vitro and in vivo: the class I ribonucleotide reductases as a case study, *Metallomics 4*, 1020-1036.

10. Gu, M. Z., and Imlay, J. A. (2013) Superoxide poisons mononuclear iron enzymes by causing mismetallation, *Molecular Microbiology 89*, 123-134.

11. Galaris, D., and Pantopoulos, K. (2008) Oxidative stress and iron homeostasis: Mechanistic and health aspects, *Crit Rev Cl Lab Sci 45*, 1-23.

12. Valko, M., Rhodes, C. J., Moncol, J., Izakovic, M., and Mazur, M. (2006) Free radicals, metals and antioxidants in oxidative stress-induced cancer, *Chem-Biol Interact 160*, 1-40.

13. Ba, L. A., Doering, M., Burkholz, T., and Jacob, C. (2009) Metal trafficking: from maintaining the metal homeostasis to future drug design, *Metallomics 1*, 292-311.

14. Ganz, T. (2004) Hepcidin in iron metabolism, *Curr Opin Hematol 11*, 251-254.

15. Neufeld, L. M., Ramakrishnan, U., Rivera, J., Villalpando, S., Gonzalez-Cossio, T., and Martorell, R. (2001) Prevalence of anemia and iron deficiency during pregnancy of women supplemented with iron or iron and multiple micronutrients, *Faseb J 15*, A641-A641.

16. Pietrangelo, A. (2010) Hereditary Hemochromatosis: Pathogenesis, Diagnosis, and Treatment, *Gastroenterology 139*, 393-408.

17. Niederau, C., Fischer, R., Sonnenberg, A., Stremmel, W., Trampisch, H. J., and Strohmeyer, G. (1985) Survival and Causes of Death in Cirrhotic and in

Noncirrhotic Patients with Primary Hemochromatosis, *New England Journal of Medicine 313*, 1256-1262.

18. Balcerza.Sp, Mintz, D. H., and Westerma.Mp. (1968) Diabetes Mellitus and Idiopathic Hemochromatosis, *American Journal of the Medical Sciences 255*, 53-&.

19. Cutler, D. J., Isner, J. M., Bracey, A. W., Hufnagel, C. A., Conrad, P. W., Roberts, W. C., Kerwin, D. M., and Weintraub, A. M. (1980) Hemochromatosis Heart-Disease - an Unemphasized Cause of Potentially Reversible Restrictive Cardiomyopathy, *American Journal of Medicine 69*, 923-928.

20. Camaschella, C. (2008) Recent advances in the understanding of inherited sideroblastic anaemia, *British Journal of Haematology 143*, 27-38.

21. Delatycki, M. B., Williamson, R., and Forrest, S. M. (2000) Friedreich ataxia: an overview, *Journal of Medical Genetics 37*, 1-8.

22. Oshiro, S., Morioka, M. S., and Kikuchi, M. (2011) Dysregulation of Iron Metabolism in Alzheimer's Disease, Parkinson's Disease, and Amyotrophic Lateral Sclerosis, *Advances in Pharmacological Sciences 2011*, 8.

23. La Fontaine, S., and Mercer, J. F. B. (2007) Trafficking of the copper-ATPases, ATP7A and ATP7B: Role in copper homeostasis, *Arch Biochem Biophys 463*, 149-167.

24. de Bie, P., Muller, P., Wijmenga, C., and Klomp, L. W. J. (2007) Molecular pathogenesis of Wilson and Menkes disease: correlation of mutations with

molecular defects and disease phenotypes, *Journal of Medical Genetics 44*, 673-688.

25. Deng, H. X., Hentati, A., Tainer, J. A., Iqbal, Z., Cayabyab, A., Hung, W. Y., Getzoff, E. D., Hu, P., Herzfeldt, B., Roos, R. P., Warner, C., Deng, G., Soriano, E., Smyth, C., Parge, H. E., Ahmed, A., Roses, A. D., Hallewell, R. A., Pericakvance, M. A., and Siddique, T. (1993) Amyotophic - Lateral - sclerosis and Structural Defects in Cu,Zn Superoxide Dismutase *Science 261*, 1047-1051.

26. Rosen, D. R., Siddique, T., Patterson, D., Figlewicz, D. A., Sapp, P., Hentati, A., Donaldson, D., Goto, J., Oregan, J. P., Deng, H. X., Rahmani, Z., Krizus, A., McKennayasek, D., Cayabyab, A., Gaston, S. M., Berger, R., Tanzi, R. E., Halperin, J. J., Herzfeldt, B., Vandenbergh, R., Hung, W. Y., Bird, T., Deng, G., Mulder, D. W., Smyth, C., Laing, N. G., Soriano, E., Pericakvance, M. A., Haines, J., Rouleau, G. A., Gusella, J. S., Horvitz, H. R., and Brown, R. H. (1993) Mutations in Cu.Zn Superoxide Dismutase Gene are Associated with Familial Amyotophic - Lateral - Sclerosis, *Nature 362*, 59-62.

27. Seetharaman, S. V., Prudencio, M., Karch, C., Holloway, S. P., Borchelt, D. R., and Hart, P. J. (2009) Immature Copper-Zinc Superoxide Dismutase and Familial Amyotrophic Lateral Sclerosis, *Exp Biol Med 234*, 1140-1154.

28. Rasia, R. M., Bertoncini, C. W., Marsh, D., Hoyer, W., Cherny, D., Zweckstetter, M., Griesinger, C., Jovin, T. M., and Fernandez, C. O. (2005) Structural characterization of copper(II) binding to alpha-synuclein: Insights into the

bioinorganic chemistry of Parkinson's disease, *P Natl Acad Sci USA 102*, 4294-4299.

29. Maret, W., and Sandstead, H. H. (2006) Zinc requirements and the risks and benefits of zinc supplementation, *Journal of Trace Elements in Medicine and Biology 20*, 3-18.

30. Wang, F. D., Kim, B. E., Dufner-Beattie, J., Petris, M. J., Andrews, G., and Eide, D. J. (2004) Acrodermatitis enteropathica mutations affect transport activity, localization and zinc-responsive trafficking of the mouse ZIP4 zinc transporter, *Hum Mol Genet 13*, 563-571.

31. Walker, C. L. F., Ezzati, M., and Black, R. E. (2009) Global and regional child mortality and burden of disease attributable to zinc deficiency, *European Journal of Clinical Nutrition 63*, 591-597.

32. Prasad, A. S. (2009) Zinc: role in immunity, oxidative stress and chronic inflammation, *Current Opinion in Clinical Nutrition and Metabolic Care 12*, 646-652.

33. Fraker, P. J., Haas, S. M., and Luecke, R. W. (1977) Effect of Zinc - Deficiency on Immune Resoponse of Young Adult Mouse, *Journal of Nutrition 107*, 1889-1895.

34. Cuajungco, M. P., Goldstein, L. E., Nunomura, A., Smith, M. A., Lim, J. T., Atwood, C. S., Huang, X. D., Farrag, Y. W., Perry, G., and Bush, A. I. (2000) Evidence that the beta-amyloid plaques of Alzheimer's disease represent the

redox-silencing and entombment of A beta by zinc, *J Biol Chem 275*, 19439-19442.

35. Miller, Y., Ma, B., and Nussinov, R. (2010) Zinc ions promote Alzheimer A beta aggregation via population shift of polymorphic states, *P Natl Acad Sci USA 107*, 9490-9495.

36. Roth, J. A. (2006) Homeostatic and toxic mechanisms regulating manganese uptake, retention, and elimination, *Biological Research 39*, 45-57.

37. Martin, C. J. (2006) Manganese neurotoxicity: Connecting the dots along the continuum of dysfunction, *Neurotoxicology 27*, 347-349.

38. Choi, C. J., Anantharam, V., Saetveit, N. J., Houk, R. S., Kanthasamy, A., and Kanthasamy, A. G. (2007) Normal cellular prion protein protects against manganese-induced oxidative stress and apoptotic cell death, *Toxicological Sciences 98*, 495-509.

39. Stangl, G. I., Schwarz, F. J., and Kirchgessner, M. (1999) Cobalt deficiency effects on trace elements, hormones and enzymes involved in energy metabolism of cattle, *Int J Vitam Nutr Res 69*, 120-126.

40. Kalhan, S. C., and Marczewski, S. E. (2012) Methionine, homocysteine, one carbon metabolism and fetal growth, *Rev Endocr Metab Dis 13*, 109-119.

41. Dixon, M. M., Huang, S., Matthews, R. G., and Ludwig, M. (1996) The structure of the C-terminal domain of methionine synthase: Presenting S-adenosylmethionine for reductive methylation of B-12, *Structure 4*, 1263-1275.

42. Schroede.Ha, Balassa, J. J., and Tipton, I. H. (1970) Essential Trace Metals in Man - Molybdenum, *J Chron Dis 23*, 481-&.

43. Hille, R., Nishino, T., and Bittner, F. (2011) Molybdenum enzymes in higher organisms, *Coordin Chem Rev 255*, 1179-1205.

44. Carmi-Nawi, N., Malinger, G., Mandel, H., Ichida, K., Lerman-Sagie, T., and Lev, D. (2011) Prenatal Brain Disruption in Molybdenum Cofactor Deficiency, *J Child Neurol 26*, 460-464.

45. Vijayakumar, K., Gunny, R., Grunewald, S., Carr, L., Chong, K. W., DeVile, C., Robinson, R., McSweeney, N., and Prabhakar, P. (2011) Clinical Neuroimaging Features and Outcome in Molybdenum Cofactor Deficiency, *Pediatr Neurol 45*, 246-252.

46. Guerciolini, R., Szumlanski, C., and Weinshilboum, R. M. (1991) Human Liver Xanthine-Oxidase - Nature and Extent of Individual Variation, *Clin Pharmacol Ther 50*, 663-672.

47. Beemer, F. A., Duran, M., Wadman, S. K., Johnson, J. L., and Rajagopalan, K. V. (1980) Molybdenum Metabolism, *Am J Dis Child 134*, 1097-1098.

48. Palacios, O., Atrian, S., and Capdevila, M. (2011) Zn- and Cu-thioneins: a functional classification for metallothioneins?, *J Biol Inorg Chem 16*, 991-1009.

49. Tottey, S., Patterson, C. J., Banci, L., Bertini, I., Felli, I. C., Pavelkova, A., Dainty, S. J., Pernil, R., Waldron, K. J., Foster, A. W., and Robinson, N. J. (2012) Cyanobacterial metallochaperone inhibits deleterious side reactions of copper, *P Natl Acad Sci USA 109*, 95-100.

50. Giedroc, D. P., and Arunkumar, A. I. (2007) Metal sensor proteins: nature's metalloregulated allosteric switches, *Dalton T*, 3107-3120.

51. Banci, L., Bertini, I., Ciofi-Baffoni, S., Kozyreva, T., Zovo, K., and Palumaa, P. (2010) Affinity gradients drive copper to cellular destinations, *Nature 465*, 645-U145.

52. Gaither, L. A., and Eide, D. J. (2000) Functional expression of the human hZIP2 zinc transporter, *J Biol Chem 275*, 5560-5564.

53. Kakhlon, O., and Cabantchik, Z. I. (2002) The labile iron pool: characterization, measurement, and participation in cellular processes, *Free Radical Bio Med 33*, 1037-1046.

54. Schlief, M., and Gitlin, J. (2006) Copper homeostasis in the CNS, *Mol Neurobiol 33*, 81-90.

55. Bush, A. I. (2000) Metals and neuroscience, *Curr Opin Chem Biol 4*, 184-191.

56. Giroux, E. L., and Henkin, R. I. (1973) Macromolecular ligands of exchangeable copper, zinc and cadmium in human serum, *Bioinorganic Chemistry 2*, 125-133.

57. Jalla, S., Westcott, J., Steirn, M., Miller, L. V., Bell, M., and Krebs, N. F. (2002) Zinc Absorption and Exchangeable Zinc Pool Sizes in Breast-Fed Infants Fed Meat or Cereal as First Complementary Food, *Journal of Pediatric Gastroenterology and Nutrition 34*, 35-41.

58. Domaille, D. W., Zeng, L., and Chang, C. J. (2010) Visualizing Ascorbate-Triggered Release of Labile Copper within Living Cells using a Ratiometric Fluorescent Sensor, *J Am Chem Soc 132*, 1194-+.

59. Haas, K. L., and Franz, K. J. (2009) Application of Metal Coordination Chemistry To Explore and Manipulate Cell Biology, *Chem Rev 109*, 4921-4960.

60. Pierrel, F., Cobine, P., and Winge, D. (2007) Metal Ion availability in mitochondria, *Biometals 20*, 675-682.

61. Greenberg, G. R., and Wintrobe, M. M. (1946) A Labile Iron Pool, *J Biol Chem 165*, 397-398.

62. Jacobs, A. (1977) Low-Molecular Weight Intracellular Iron Transport Compounds, *Blood 50*, 433-439.

63. Perls, M. (1867) Nachweis von Eisenoxyd in gewissen Pigmenten, *Archiv f. pathol. Anat. 39*, 42-48.

64. Mallory, F. B., and Parker, F. (1939) Fixing and staining methods for lead and copper in tissues, *Am J Pathol 15*, 517-U518.

65. Huang, K., Li, H., Shen, H., and Li, M. (2012) Psychological Stress Expands Low Molecular Weight Iron Pool in Cerebral Cortex, Hippocampus, and Striatum of Rats, *Biol Trace Elem Res 146*, 79-85.

66. Chang, C. J., Nolan, E. M., Jaworski, J., Okamoto, K. I., Hayashi, Y., Sheng, M., and Lippard, S. J. (2004) ZP8, a neuronal zinc sensor with improved dynamic range; Imaging zinc in hippocampal slices with two-photon microscopy, *Inorg Chem 43*, 6774-6779.

67. Huang, Z., and Lippard, S. J. (2012) Illuminating Mobile Zinc with Fluorescence: From Cuvettes to Live Cells and Tissues, In *Methods in Enzymology, Vol 505: Imaging and Spectroscopic Analysis of Living Cells: Live*

Cell Imaging of Cellular Elements and Functions (Conn, P. M., Ed.), pp 445-468.

68. Dittmer, P. J., Miranda, J. G., Gorski, J. A., and Palmer, A. E. (2009) Genetically Encoded Sensors to Elucidate Spatial Distribution of Cellular Zinc, *J Biol Chem 284*, 16289-16297.

69. Qin, Y., Dittmer, P. J., Park, J. G., Jansen, K. B., and Palmer, A. E. (2011) Measuring steady-state and dynamic endoplasmic reticulum and Golgi Zn2+ with genetically encoded sensors, *P Natl Acad Sci USA 108*, 7351-7356.

70. Wegner, S. V., Arslan, H., Sunbul, M., Yin, J., and He, C. (2010) Dynamic Copper(I) Imaging in Mammalian Cells with a Genetically Encoded Fluorescent Copper(I) Sensor, *J Am Chem Soc 132*, 2567-+.

71. Chen, Z., Gao, C., Hua, Y., Keep, R. F., Muraszko, K., and Xi, G. (2011) Role of Iron in Brain Injury After Intraventricular Hemorrhage, *Stroke 42*, 465-470.

72. Major, J. L., Parigi, G., Luchinat, C., and Meade, T. J. (2007) The synthesis and in vitro testing of a zinc-activated MRI contrast agent, *Proceedings of the National Academy of Sciences 104*, 13881-13886.

73. Domaille, D. W., Que, E. L., and Chang, C. J. (2008) Synthetic fluorescent sensors for studying the cell biology of metals, *Nature Chemical Biology 4*, 168-175.

74. Que, E. L., and Chang, C. J. (2006) A smart magnetic resonance contrast agent for selective copper sensing, *J Am Chem Soc 128*, 15942-15943.

75. Que, E. L., Domaille, D. W., and Chang, C. J. (2008) Metals in neurobiology: Probing their chemistry and biology with molecular imaging, *Chem Rev 108*, 1517-1549.

76. Que, E. L., Gianolio, E., Baker, S. L., Wong, A. P., Aime, S., and Chang, C. J. (2009) Copper-Responsive Magnetic Resonance Imaging Contrast Agents, *J Am Chem Soc 131*, 8527-8536.

77. Zeng, L., Miller, E. W., Pralle, A., Isacoff, E. Y., and Chang, C. J. (2006) A selective turn-on fluorescent sensor for imaging copper in living cells, *J Am Chem Soc 128*, 10-11.

78. Que, E. L., and Chang, C. J. (2010) Responsive magnetic resonance imaging contrast agents as chemical sensors for metals in biology and medicine, *Chem Soc Rev 39*, 51-60.

79. Que, E. L., New, E. J., and Chang, C. J. (2012) A cell-permeable gadolinium contrast agent for magnetic resonance imaging of copper in a Menkes disease model, *Chemical Science 3*, 1829-1834.

80. Zhang, X. A., Lovejoy, K. S., Jasanoff, A., and Lippard, S. J. (2007) Water-soluble porphyrins imaging platform for MM zinc sensing, *P Natl Acad Sci USA 104*, 10780-10785.

81. Popescu, B. F. G., Robinson, C. A., Chapman, L. D., and Nichol, H. (2009) Synchrotron X-ray Fluorescence Reveals Abnormal Metal Distributions in Brain and Spinal Cord in Spinocerebellar Ataxia: A Case Report, *Cerebellum 8*, 340-351.

82. Popescu, B. F. G., Robinson, C. A., Rajput, A., Rajput, A. H., Harder, S. L., and Nichol, H. (2009) Iron, Copper, and Zinc Distribution of the Cerebellum, *Cerebellum 8*, 74-79.

83. Popescu, B. F. G., George, M. J., Bergmann, U., Garachtchenko, A. V., Kelly, M. E., McCrea, R. P. E., Luning, K., Devon, R. M., George, G. N., Hanson, A. D., Harder, S. M., Chapman, L. D., Pickering, I. J., and Nichol, H. (2009) Mapping metals in Parkinson's and normal brain using rapid-scanning x-ray fluorescence, *Phys Med Biol 54*, 651-663.

84. Wypijewska, A., Galazka-Friedman, J., Bauminger, E. R., Wszolek, Z. K., Schweitzer, K. J., Dickson, D. W., Jaklewicz, A., Elbaum, D., and Friedman, A. (2010) Iron and reactive oxygen species activity in parkinsonian substantia nigra, *Parkinsonism Relat D 16*, 329-333.

85. Ide-Ektessabi, A., and Rabionet, M. (2005) The role of trace metallic elements in neurodegenerative disorders: Quantitative analysis using XRF and XANES spectroscopy, *Anal Sci 21*, 885-892.

86. Becker, J. S., Matusch, A., Palm, C., Salber, D., Morton, K. A., and Becker, S. (2010) Bioimaging of metals in brain tissue by laser ablation inductively coupled plasma mass spectrometry (LA-ICP-MS) and metallomics, *Metallomics 2*, 104-111.

87. Hutchinson, R. W., Cox, A. G., McLeod, C. W., Marshall, P. S., Harper, A., Dawson, E. L., and Howlett, D. R. (2005) Imaging and spatial distribution of beta-amyloid peptide and metal ions in Alzheimer's plaques by laser ablation-

inductively coupled plasma-mass spectrometry, *Analytical Biochemistry 346*, 225-233.

88. Lear, J., Hare, D. J., Fryer, F., Adlard, P. A., Finkelstein, D. I., and Doble, P. A. (2012) High-Resolution Elemental Bioimaging of Ca, Mn, Fe, Co, Cu, and Zn Employing LA-ICP-MS and Hydrogen Reaction Gas, *Anal Chem 84*, 6707-6714.

89. Hare, D. J., Lee, J. K., Beavis, A. D., van Gramberg, A., George, J., Adlard, P. A., Finkelstein, D. I., and Doble, P. A. (2012) Three-Dimensional Atlas of Iron, Copper, and Zinc in the Mouse Cerebrum and Brainstem, *Anal Chem 84*, 3990-3997.

90. Becker, J. S., Kumtabtim, U., Wu, B., Steinacker, P., Otto, M., and Matusch, A. (2012) Mass spectrometry imaging (MSI) of metals in mouse spinal cord by laser ablation ICP-MS, *Metallomics 4*, 284-288.

91. Becker, J. S., Niehren, S., Matusch, A., Wu, B., Hsieh, H. F., Kumtabtim, U., Hamester, M., Plaschke-Schlutter, A., and Salber, D. (2010) Scaling down the bioimaging of metals by laser microdissection inductively coupled plasma mass spectrometry (LMD-ICP-MS), *Int J Mass Spectrom 294*, 1-6.

92. Salber, D., Uhlenbrock, F., Manuvelpillai, J., Wu, B., Palm, C., Matusch, A., and Becker, J. S. (2010) LMD-ICP-MS: A novel high resolution analytical technique for quantitative imaging of metal isotopes in tissue sections and single cells, *Eur J Cell Biol 89*, 54-55.

93. Weaver, J., and Pollack, S. (1989) Low-MR Iron Isolated from Guinea Pig Recticulocytes as AMP-Fe and ATP-Fe Complexes, *Biochem J 261*, 787-792.

94. Gercken, B., and Barnes, R. M. (1991) Determination of Lead and Other Trace-Element Species in Blood by Size Exclusion Chromatography and Inductively Coupled Plasma Mass-Spectrometry, *Anal Chem 63*, 283-287.

95. Boulyga, S. F., Loreti, V., Bettmer, B., and Heumann, K. G. (2004) Application of SEC-ICP-MS for comparative analyses of metal-containing species in cancerous and healthy human thyroid samples, *Analytical and Bioanalytical Chemistry 380*, 198-203.

96. Hare, D. J., Grubman, A., Ryan, T. M., Lothian, A., Liddell, J. R., Grimm, R., Matsuda, T., Doble, P. A., Cherny, R. A., Bush, A. I., White, A. R., Masters, C. L., and Roberts, B. R. (2013) Profiling the iron, copper and zinc content in primary neuron and astrocyte cultures by rapid online quantitative size exclusion chromatography-inductively coupled plasma-mass spectrometry, *Metallomics 5*, 1656-1662.

97. Morrison, J. G., White, P., McDougall, S., Firth, J. W., Woolfrey, S. G., Graham, M. A., and Greenslade, D. (2000) Validation of a highly sensitive ICP-MS method for the determination of platinum in biofluids: application to clinical pharmacokinetic studies with oxaliplatin, *J Pharmaceut Biomed 24*, 1-10.

98. Naranuntarat, A., Jensen, L. T., Pazicni, S., Penner-Hahn, J. E., and Culotta, V. C. (2009) The Interaction of Mitochondrial Iron with Manganese Superoxide Dismutase, *J Biol Chem 284*, 22633-22640.

99. Crichton, R. R., Dexter, D. T., and Ward, R. J. (2008) Metal based neurodegenerative diseases - From molecular mechanisms to therapeutic strategies, *Coordin Chem Rev 252*, 1189-1199.

100. Becker, J. S. (2010) Bioimaging of metals in brain tissue from micrometre to nanometre scale by laser ablation inductively coupled plasma mass spectrometry: State of the art and perspectives, *Int J Mass Spectrom 289*, 65-75.

101. Bitanihirwe, B. K. Y., and Cunningham, M. G. (2009) Zinc: The Brain's Dark Horse, *Synapse 63*, 1029-1049.

102. Drayer, B., Burger, P., Darwin, R., Riederer, S., Herfkens, R., and Johnson, G. A. (1986) Magnetic Resonance Imaging of Brain Iron, *American Journal of Neuroradiology 7*, 373-380.

103. Pozebon, D., Dressler, V. L., Mesko, M. F., Matusch, A., and Becker, J. S. (2010) Bioimaging of metals in thin mouse brain section by laser ablation inductively coupled plasma mass spectrometry: novel online quantification strategy using aqueous standards, *J Anal Atom Spectrom 25*, 1739-1744.

104. Lange, H., Kaut, A., Kispal, G., and Lill, R. (2000) A mitochondrial ferredoxin is essential for biogenesis of cellular iron-sulfur proteins, *P Natl Acad Sci USA 97*, 1050-1055.

105. Hudder, B. N., Morales, J. G., Stubna, A., Muenck, E., Hendrich, M. P., and Lindahl, P. A. (2007) Electron paramagnetic resonance and Mossbauer spectroscopy of intact mitochondria from respiring Saccharomyces cerevisiae, *J Biol Inorg Chem 12*, 1029-1053.

106. Jhurry, N. D., Chakrabarti, M., McCormick, S. P., Holmes-Hampton, G. P., and Lindahl, P. A. (2012) Biophysical Investigation of the Ironome of Human Jurkat Cells and Mitochondria, *Biochemistry-Us 51*, 5276-5284.

107. McCormick, S. P., Chakrabarti, M., Cockrell, A. L., Park, J., Lindahl, L. S., and Lindahl, P. A. (2013) Low-molecular-mass metal complexes in the mouse brain, *Metallomics 5*, 232-241.

108. Luk, E., Carroll, M., Baker, M., and Culotta, V. C. (2003) Manganese activation of superoxide dismutase 2 in Saccharomyces cerevisiae requires MTM1, a member of the mitochondrial carrier family, *P Natl Acad Sci USA 100*, 10353-10357.

109. Palmieri, F., Pierri, C. L., De Grassi, A., Nunes-Nesi, A., and Fernie, A. R. (2011) Evolution, structure and function of mitochondrial carriers: a review with new insights, *Plant J 66*, 161-181.

110. Robinson, A. J., Overy, C., and Kunji, E. R. S. (2008) The mechanism of transport by mitochondrial carriers based on analysis of symmetry, *P Natl Acad Sci USA 105*, 17766-17771.

111. Yang, M., Cobine, P. A., Molik, S., Naranuntarat, A., Lill, R., Winge, D. R., and Culotta, V. C. (2006) The effects of mitochondrial iron homeostasis on cofactor specificity of superoxide dismutase 2, *Embo J 25*, 1775-1783.

112. Beyer, W. F., and Fridovich, I. (1991) In Vivo Competition between Iron and Manganese for Occupincy of the Active Site Region of the Manganese Superoxide Dismutase of Escherichia Coli, *J Biol Chem 266*, 303-308.

113. Muhlenhoff, U., Gerber, J., Richhardt, N., and Lill, R. (2003) Components involved in assembly and dislocation of iron-sulfur clusters on the scaffold protein Isu1p, *Embo J 22*, 4815-4825.

114. Kispal, G., Csere, P., Prohl, C., and Lill, R. (1999) The mitochondrial proteins Atm1p and Nfs1p are essential for biogenesis of cytosolic Fe/S proteins, *Embo J 18*, 3981-3989.

115. Kim, K.-D., Chung, W.-H., Kim, H.-J., Lee, K.-C., and Roe, J.-H. (2010) Monothiol glutaredoxin Grx5 interacts with Fe-S scaffold proteins Isa1 and Isa2 and supports Fe-S assembly and DNA integrity in mitochondria of fission yeast, *Biochem Bioph Res Co 392*, 467-472.

116. Babcock, M., deSilva, D., Oaks, R., DavisKaplan, S., Jiralerspong, S., Montermini, L., Pandolfo, M., and Kaplan, J. (1997) Regulation of mitochondrial iron accumulation by Yfh1p, a putative homolog of frataxin, *Science 276*, 1709-1712.

117. Nilsson, R., Schultz, I. J., Pierce, E. L., Soltis, K. A., Naranuntarat, A., Ward, D. M., Baughman, J. M., Paradkar, P. N., Kingsley, P. D., Culotta, V. C., Kaplan, J., Palis, J., Paw, B. H., and Mootha, V. K. (2009) Discovery of Genes Essential for Heme Biosynthesis through Large-Scale Gene Expression Analysis, *Cell Metabolism 10*, 119-130.

118. Lesuisse, E., Santos, R., Matzanke, B. F., Knight, S. A. B., Camadro, J. M., and Dancis, A. (2003) Iron use for haeme synthesis is under control of the yeast frataxin homologue (Yfh1), *Hum Mol Genet 12*, 879-889.

119. Miao, R., Kim, H., Koppolu, U. M. K., Ellis, E. A., Scott, R. A., and Lindahl, P. A. (2009) Biophysical Characterization of the Iron in Mitochondria from Atm1p-Depleted Saccharomyces cerevisiae, *Biochemistry-Us 48*, 9556-9568.

120. Miao, R., Martinho, M., Morales, J. G., Kim, H., Ellis, E. A., Lill, R., Hendrich, M. P., Muenck, E., and Lindahl, P. A. (2008) EPR and Mossbauer spectroscopy of intact mitochondria isolated from Yah1p-depleted Saccharomyces cerevisiae, *Biochemistry-Us 47*, 9888-9899.

121. Holmes-Hampton, G. P., Miao, R., Morales, J. G., Guo, Y., Muenck, E., and Lindahl, P. A. (2010) A Nonheme High-Spin Ferrous Pool in Mitochondria Isolated from Fermenting Saccharomyces cerevisiae, *Biochemistry-Us 49*, 4227-4234.

122. Akhmedov, D., De Marchi, U., Wollheim, C. B., and Wiederkehr, A. (2012) Pyruvate dehydrogenase E1 alpha phosphorylation is induced by glucose but does not control metabolism-secretion coupling in INS-1E clonal beta-cells, *Bba-Mol Cell Res 1823*, 1815-1824.

123. Zhao, X. L., Leon, I. R., Bak, S., Mogensen, M., Wrzesinski, K., Hojlund, K., and Jensen, O. N. (2011) Phosphoproteome Analysis of Functional Mitochondria Isolated from Resting Human Muscle Reveals Extensive Phosphorylation of Inner Membrane Protein Complexes and Enzymes, *Molecular & Cellular Proteomics 10*.

124. Herrero, E., Ros, J., Belli, G., and Cabiscol, E. (2008) Redox control and oxidative stress in yeast cells, *Biochimica Et Biophysica Acta-General Subjects 1780*, 1217-1235.

125. Ravindranath, S. D., and Fridovich, I. (1975) Isolation and Characterization of a Manganese Containing Superoxide Dismutase from Yeast, *J Biol Chem 250*, 6107-6112.

126. Whittaker, M. M., and Whittaker, J. W. (2012) Metallation state of human manganese superoxide dismutase expressed in Saccharomyces cerevisiae, *Arch Biochem Biophys 523*, 191-197.

127. Jeong, J. H., Kwon, E. S., and Roe, J. H. (2001) Characterization of the manganese-containing superoxide dismutase and its gene regulation in stress response of Schizosaccharomyces pombe, *Biochem Bioph Res Co 283*, 908-914.

128. Kang, Y., He, Y.-X., Zhao, M.-X., and Li, W.-F. (2011) Structures of native and Fe-substituted SOD2 from Saccharomyces cerevisiae, *Acta Crystallographica Section F-Structural Biology and Crystallization Communications 67*, 1173-1178.

129. Fleischhacker, A. S., Stubna, A., Hsueh, K.-L., Guo, Y., Teter, S. J., Rose, J. C., Brunold, T. C., Markley, J. L., Muenck, E., and Kiley, P. J. (2012) Characterization of the 2Fe-2S Cluster of Escherichia coli Transcription Factor IscR, *Biochemistry-Us 51*, 4453-4462.

130. Rae, T. D., Schmidt, P. J., Pufahl, R. A., Culotta, V. C., and O'Halloran, T. V. (1999) Undetectable intracellular free copper: The requirement of a copper chaperone for superoxide dismutase, *Science 284*, 805-808.

131. Terziyska, N., Lutz, T., Kozany, C., Mokranjac, D., Mesecke, N., Neupert, W., Herrmann, J. M., and Hell, K. (2005) Mia40, a novel factor for protein import into the intermembrane space of mitochondria is able to bind metal ions, *Febs Lett 579*, 179-184.

132. Park, J., McCormick, S. P., Chakrabarti, M., and Lindahl, P. A. (2013) Insights into the iron-ome and manganese-ome of Delta mtm1 Saccharomyces cerevisiae mitochondria, *Metallomics 5*, 656-672.

133. Lutz, T., Westermann, B., Neupert, W., and Herrmann, J. M. (2001) The mitochondrial proteins Ssq1 and Jac1 are required for the assembly of iron sulfur clusters in mitochondria, *J Mol Biol 307*, 815-825.

134. Amutha, B., Gordon, D. M., Gu, Y., Lyver, E. R., Dancis, A., and Pain, D. (2008) GTP is required for iron-sulfur cluster biogenesis in mitochondria, *J Biol Chem 283*, 1362-1371.

135. Pandey, A., Yoon, H., Lyver, E. R., Dancis, A., and Pain, D. (2012) Identification of a Nfs1p-bound persulfide intermediate in Fe-S cluster synthesis by intact mitochondria, *Mitochondrion 12*, 539-549.

136. Rauen, U., Springer, A., Weisheit, D., Petrat, F., Korth, H.-G., de Groot, H., and Sustmann, R. (2007) Assessment of chelatable mitochondrial iron by using

mitochondrion-selective fluorescent iron indicators with different iron-binding affinities, *Chembiochem 8*, 341-352.

137. Petrat, F., de Groot, H., Sustmann, R., and Rauen, U. (2002) The chelatable iron pool in living cells: A methodically defined quantity, *Biol Chem 383*, 489-502.

138. Sturm, B., Bistrich, U., Schranzhofer, M., Sarsero, J. P., Rauen, U., Scheiber-Mojdehkar, B., de Groot, H., Ioannou, P., and Petrat, F. (2005) Friedreich's ataxia, no changes in mitochondrial labile iron in human lymphoblasts and fibroblasts: a decrease in antioxidative capacity?, *J Biol Chem 280*, 6701-6708.

139. Atkinson, A., Khalimonchuk, O., Smith, P., Sabic, H., Eide, D., and Winge, D. R. (2010) Mzm1 influences a labile pool of mitochondrial zinc important for respiratory function, *J Biol Chem 285*, 19450-19459.

140. Caporale, T., Ciavardelli, D., Di Ilio, C., Lanuti, P., Drago, D., and Sensi, S. L. (2009) Ratiometric-pericam-mt, a novel tool to evaluate intramitochondrial zinc, *Experimental neurology 218*, 228-234.

141. Costello, L. C., Guan, Z., Franklin, R. B., and Feng, P. (2004) Metallothionein can function as a chaperone for zinc uptake transport into prostate and liver mitochondria, *J Inorg Biochem 98*, 664-666.

142. Sensi, S. L., Ton-That, D., Sullivan, P. G., Jonas, E. A., Gee, K. R., Kaczmarek, L. K., and Weiss, J. H. (2003) Modulation of mitochondrial function by endogenous Zn2+ pools, *Proc Natl Acad Sci U S A 100*, 6157-6162.

143. Chyan, W., Zhang, D. Y., Lippard, S. J., and Radford, R. J. (2014) Reaction-based fluorescent sensor for investigating mobile Zn2+ in mitochondria of healthy versus cancerous prostate cells, *Proc Natl Acad Sci U S A 111*, 143-148.

144. Costello, L. C., and Franklin, R. B. (1998) Novel role of zinc in the regulation of prostate citrate metabolism and its implications in prostate cancer, *The Prostate 35*, 285-296.

145. Atkinson, A., Khalimonchuk, O., Smith, P., Sabic, H., Eide, D., and Winge, D. R. (2010) Mzm1 Influences a Labile Pool of Mitochondrial Zinc Important for Respiratory Function, *J Biol Chem 285*, 19450-19459.

146. McCranor, B. J., Bozym, R. A., Vitolo, M. I., Fierke, C. A., Bambrick, L., Polster, B. M., Fiskum, G., and Thompson, R. B. (2012) Quantitative imaging of mitochondrial and cytosolic free zinc levels in an in vitro model of ischemia/reperfusion, *J Bioenerg Biomembr 44*, 253-263.

147. Sensi, S. L., Ton-That, D., and Weiss, J. H. (2002) Mitochondrial sequestration and Ca(2+)-dependent release of cytosolic Zn(2+) loads in cortical neurons, *Neurobiol Dis 10*, 100-108.

148. Costello, L. C., Fenselau, C. C., and Franklin, R. B. (2011) Evidence for operation of the direct zinc ligand exchange mechanism for trafficking, transport, and reactivity of zinc in mammalian cells, *J Inorg Biochem 105*, 589-599.

149. Cobine, P. A., Ojeda, L. D., Rigby, K. M., and Winge, D. R. (2004) Yeast contain a non-proteinaceous pool of copper in the mitochondrial matrix, *J Biol Chem 279*, 14447-14455.

150. Cobine, P. A., Pierrel, F., Bestwick, M. L., and Winge, D. R. (2006) Mitochondrial matrix copper complex used in metallation of cytochrome oxidase and superoxide dismutase, *J Biol Chem 281*, 36552-36559.

151. Cobine, P. A., Pierrel, F., and Winge, D. R. (2006) Copper trafficking to the mitochondrion and assembly of copper metalloenzymes, *Biochim Biophys Acta 1763*, 759-772.

152. Yang, L., McRae, R., Henary, M. M., Patel, R., Lai, B., Vogt, S., and Fahrni, C. J. (2005) Imaging of the intracellular topography of copper with a fluorescent sensor and by synchrotron x-ray fluorescence microscopy, *Proc Natl Acad Sci U S A 102*, 11179-11184.

153. Dodani, S. C., Leary, S. C., Cobine, P. A., Winge, D. R., and Chang, C. J. (2011) A Targetable Fluorescent Sensor Reveals That Copper-Deficient SCO1 and SCO2 Patient Cells Prioritize Mitochondrial Copper Homeostasis, *J Am Chem Soc 133*, 8606-8616.

154. Vest, K. E., Leary, S. C., Winge, D. R., and Cobine, P. A. (2013) Copper import into the mitochondrial matrix in Saccharomyces cerevisiae is mediated by Pic2, a mitochondrial carrier family protein, *J Biol Chem 288*, 23884-23892.

155. Sea, K. W., Sheng, Y., Lelie, H. L., Kane Barnese, L., Durazo, A., Valentine, J. S., and Gralla, E. B. (2013) Yeast copper-zinc superoxide dismutase can be activated in the absence of its copper chaperone, *J Biol Inorg Chem 18*, 985-992.

156. Holmes-Hampton, G. P., Chakrabarti, M., Cockrell, A. L., McCormick, S. P., Abbott, L. C., Lindahl, L. S., and Lindahl, P. A. (2012) Changing iron content of the mouse brain during development, *Metallomics 4*, 761-770.

157. Eide, D. J. (2006) Zinc transporters and the cellular trafficking of zinc, *Bba-Mol Cell Res 1763*, 711-722.

158. Theobald, U., Mailinger, W., Baltes, M., Rizzi, M., and Reuss, M. (1997) In vivo analysis of metabolic dynamics in Saccharomyces cerevisiae .1. Experimental observations, *Biotechnol. Bioeng. 55*, 305-316.

159. Wahlländer, A., Soboll, S., Sies, H., Ingrid, L., and Monika, M. (1979) Hepatic mitochondrial and cytosolic glutathione content and the subcellular distribution of GSH-S-transferases, *Febs Lett 97*, 138-140.

160. Klein, J. M., Busch, J. D., Potting, C., Baker, M. J., Langer, T., and Schwarz, G. (2012) The mitochondrial amidoxime-reducing component (mARC1) is a novel signal-anchored protein of the outer mitochondrial membrane, *J Biol Chem 287*, 42795-42803.

161. Crichton, R. R., Wilmet, S., Legssyer, R., and Ward, R. J. (2002) Molecular and cellular mechanisms of iron homeostasis and toxicity in mammalian cells, *J Inorg Biochem 91*, 9-18.

162. Moos, T., and Morgan, E. H. (2004) The metabolism of neuronal iron and its pathogenic role in neurological disease - Review, *Ann Ny Acad Sci 1012*, 14-26.

163. Muhlenhoff, U., Stadler, J. A., Richhardt, N., Seubert, A., Eickhorst, T., Schweyen, R. J., Lill, R., and Wiesenberger, G. (2003) A specific role of the

yeast mitochondrial carriers Mrs3/4p in mitochondrial iron acquisition under iron-limiting conditions, *J Biol Chem 278*, 40612-40620.

164. Pamp, K., Kerkweg, U., Korth, H. G., Homann, F., Rauen, U., Sustmann, R., de Groot, H., and Petrat, F. (2008) Enzymatic reduction of labile iron by organelles of the rat liver. Superior role of an NADH-dependent activity in the outer mitochondrial membrane, *Biochimie 90*, 1591-1601.

165. Petrat, F., de Groot, H., and Rauen, U. (2001) Subcellular distribution of chelatable iron: a laser scanning microscopic study in isolated hepatocytes and liver endothelial cells, *Biochem J 356*, 61-69.

166. Kaur, D., Rajagopalan, S., and Andersen, J. K. (2009) Chronic expression of H-ferritin in dopaminergic midbrain neurons results in an age-related expansion of the labile iron pool and subsequent neurodegeneration: implications for Parkinson's disease, *Brain Res 1297*, 17-22.

167. Sohal, R. S., Wennberg-Kirch, E., Jaiswal, K., Kwong, L. K., and Forster, M. J. (1999) Effect of age and caloric restriction on bleomycin-chelatable and nonheme iron in different tissues of C57BL/6 mice, *Free Radical Bio Med 27*, 287-293.

168. Magaki, S., Mueller, C., Yellon, S. M., Fox, J., Kim, J., Snissarenko, E., Chin, V., Ghosh, M. C., and Kirsch, W. M. (2007) Regional dissection and determination of loosely bound and non-heme iron in the developing mouse brain, *Brain Res 1158*, 144-150.

169. Meguro, R., Asano, Y., Odagiri, S., Li, C., and Shoumura, K. (2008) Cellular and subcellular localizations of nonheme ferric and ferrous iron in the rat brain: a light and electron microscopic study by the perfusion-Perls and -Turnbull methods, *Arch Histol Cytol 71*, 205-222.

170. Palumaa, P., Eriste, E., Njunkova, O., Pokras, L., Jornvall, H., and Sillard, R. (2002) Brain-specific metallothionein-3 has higher metal-binding capacity than ubiquitous metallothioneins and binds metals noncooperatively, *Biochemistry-Us 41*, 6158-6163.

171. Viles, J. H. (2012) Metal ions and amyloid fiber formation in neurodegenerative diseases. Copper, zinc and iron in Alzheimer's, Parkinson's and prion diseases, *Coordin Chem Rev 256*, 2271-2284.

172. Dean, K. M., Qin, Y., and Palmer, A. E. (2012) Visualizing metal ions in cells: An overview of analytical techniques, approaches, and probes, *Bba-Mol Cell Res 1823*, 1406-1415.

173. Tomat, E., and Lippard, S. J. (2010) Imaging mobile zinc in biology, *Curr Opin Chem Biol 14*, 225-230.

174. Levenson, C. W. (2005) Zinc supplementation: Neuroprotective or neurotoxic?, *Nutr Rev 63*, 122-125.

175. Lee, J.-Y., Kim, J. S., Byun, H.-R., Palmiter, R. D., and Koh, J.-Y. (2011) Dependence of the histofluorescently reactive zinc pool on zinc transporter-3 in the normal brain, *Brain Res 1418*, 12-22.

176. Gaetke, L. M., and Chow, C. K. (2003) Copper toxicity, oxidative stress, and antioxidant nutrients, *Toxicology 189*, 147-163.

177. Zheng, W., and Monnot, A. D. (2012) Regulation of brain iron and copper homeostasis by brain barrier systems: Implication in neurodegenerative diseases, *Pharmacol Therapeut 133*, 177-188.

178. Zhou, B., and Gitschier, J. (1997) hCTR1: A human gene for copper uptake identified by complementation in yeast, *P Natl Acad Sci USA 94*, 7481-7486.

179. Kono, S. (2012) Aceruloplasminemia, *Curr Drug Targets 13*, 1190-1199.

180. Carr, H. S., and Winge, D. R. (2003) Assembly of cytochrome c oxidase within the mitochondrion, *Accounts Chem Res 36*, 309-316.

181. Culotta, V. C., Yang, M., and O'Halloran, T. V. (2006) Activation of superoxide dismutases: Putting the metal to the pedal, *Bba-Mol Cell Res 1763*, 747-758.

182. Stasser, J. P., Siluvai, G. S., Barry, A. N., and Blackburn, N. J. (2007) A multinuclear copper(I) cluster forms the dimerization interface in copper-loaded human copper chaperone for superoxide dismutase, *Biochemistry-Us 46*, 11845-11856.

183. Hirayama, T., Van de Bittner, G. C., Gray, L. W., Lutsenko, S., and Chang, C. J. (2012) Near-infrared fluorescent sensor for in vivo copper imaging in a murine Wilson disease model, *P Natl Acad Sci USA 109*, 2228-2233.

184. Brown, D. R. (2010) Metalloproteins and neuronal death, *Metallomics 2*, 186-194.

185. Matthews, R. G., Koutmos, M., and Datta, S. (2008) Cobalamin-dependent and cobamide-dependent methyltransferases, *Curr Opin Struc Biol 18*, 658-666.

186. Cvetkovic, A., Menon, A. L., Thorgersen, M. P., Scott, J. W., Poole, F. L., II, Jenney, F. E., Jr., Lancaster, W. A., Praissman, J. L., Shanmukh, S., Vaccaro, B. J., Trauger, S. A., Kalisiak, E., Apon, J. V., Siuzdak, G., Yannone, S. M., Tainer, J. A., and Adams, M. W. W. (2010) Microbial metalloproteomes are largely uncharacterized, *Nature 466*, 779-U718.

187. Bronowicka-Adamska, P., Zagajewski, J., Czubak, J., and Wrobel, M. (2011) RP-HPLC method for quantitative determination of cystathionine, cysteine and glutathione: An application for the study of the metabolism of cysteine in human brain, *J Chromatogr B 879*, 2005-2009.

188. Zhuang, Y. L., Ma, F., Li-Ling, J., Xu, X. F., and Li, Y. D. (2003) Comparative analysis of amino acid usage and protein length distribution between alternatively and non-alternatively spliced genes across six eukaryotic genomes, *Mol Biol Evol 20*, 1978-1985.

189. Wilson, M., Hogstrand, C., and Maret, W. (2012) Picomolar Concentrations of Free Zinc(II) Ions Regulate Receptor Protein-tyrosine Phosphatase beta Activity, *J Biol Chem 287*, 9322-9326.

190. Lincoln, S. F. (2005) Mechanistic studies of metal aqua ions: A semi-historical perspective, *Helv Chim Acta 88*, 523-545.

191. Nunez, M. T., Gaete, V., Watkins, J. A., and Glass, J. (1990) Mobilization of Iron from Endocytic Vesicles - the Effects of Acidification and Reduction, *J Biol Chem 265*, 6688-6692.

192. Sargent, P. J., Farnaud, S., and Evans, R. W. (2005) Structure/function overview of proteins involved in iron storage and transport, *Curr Med Chem 12*, 2683-2693.

193. Ganz, T. (2013) Systemic iron homeostasis, *Physiological reviews 93*, 1721-1741.

194. Stankiewicz, J., Panter, S. S., Neema, M., Arora, A., Batt, C. E., and Bakshi, R. (2007) Iron in chronic brain disorders: imaging and neurotherapeutic implications, *Neurotherapeutics : the journal of the American Society for Experimental NeuroTherapeutics 4*, 371-386.

195. Erikson, K. M., Pinero, D. J., Connor, J. R., and Beard, J. L. (1997) Regional brain iron, ferritin and transferrin concentrations during iron deficiency and iron repletion in developing rats, *The Journal of nutrition 127*, 2030-2038.

196. Siimes, M. A., Refino, C., and Dallman, P. R. (1980) Physiological anemia of early development in the rat: characterization of the iron-responsive component, *American Journal of Clinical Nutrition 33*, 2601-2608.

197. Meynard, D., Babitt, J. L., and Lin, H. Y. (2014) The liver: conductor of systemic iron balance, *Blood 123*, 168-176.

198. D´Anna, M. C., Giorgi, G., and Roque, M. E. (2011) Immunohistochemical Studies on Duodenum, Spleen and Liver in Mice: Distribution of Ferroportin and

Prohepcidin in an Inflammation Model, *International Journal of Morphology 29*, 747-753.

199. Ganz, T. (2012) Macrophages and systemic iron homeostasis, *J. innate immun. 4*, 446-453.

200. Taylor, E. M., and Morgan, E. H. (1990) Developmental changes in transferrin and iron uptake by the brain in the rat, *Brain Res Dev Brain Res 55*, 35-42.

201. Brissot, P., Ropert, M., Le Lan, C., and Loreal, O. (2012) Non-transferrin bound iron: a key role in iron overload and iron toxicity, *Biochimica et Biophysica Acta 1820*, 403-410.

202. Wright, T. L., Brissot, P., Ma, W. L., and Weisiger, R. A. (1986) Characterization of non-transferrin-bound iron clearance by rat liver, *J Biol Chem 261*, 10909-10914.

203. Ueda, F., Raja, K. B., Simpson, R. J., Trowbridge, I. S., and Bradbury, M. W. (1993) Rate of 59Fe uptake into brain and cerebrospinal fluid and the influence thereon of antibodies against the transferrin receptor, *Journal of Neurochemistry 60*, 106-113.

204. Grebe, M., Profrock, D., Kakuschke, A., Broekaert, J. A., and Prange, A. (2011) Absolute quantification of transferrin in blood samples of harbour seals using HPLC-ICP-MS, *Metallomics : Integrated Biometal Science 3*, 176-185.

205. Craven, C. M., Alexander, J., Eldridge, M., Kushner, J. P., Bernstein, S., and Kaplan, J. (1987) Tissue distribution and clearance kinetics of non-transferrin-

bound iron in the hypotransferrinemic mouse: a rodent model for hemochromatosis, *P Natl Acad Sci USA 84*, 3457-3461.

206. Cavill, I. (1971) The preparation of 59 Fe-labelled transferrin for ferrokinetic studies, *J Clin Pathol 24*, 472-474.

207. Parkes, J. G., Randell, E. W., Olivieri, N. F., and Templeton, D. M. (1995) Modulation by iron loading and chelation of the uptake of non-transferrin-bound iron by human liver cells, *Biochimica et Biophysica Acta 1243*, 373-380.

208. Hider, R. C. (2002) Nature of nontransferrin-bound iron, *Eur J Clin Invest 32 Suppl 1*, 50-54.

209. Evans, R. W., Rafique, R., Zarea, A., Rapisarda, C., Cammack, R., Evans, P. J., Porter, J. B., and Hider, R. C. (2008) Nature of non-transferrin-bound iron: studies on iron citrate complexes and thalassemic sera, *J Biol Inorg Chem 13*, 57-74.

210. Jacobs, E. M., Hendriks, J. C., van Tits, B. L., Evans, P. J., Breuer, W., Liu, D. Y., Jansen, E. H., Jauhiainen, K., Sturm, B., Porter, J. B., Scheiber-Mojdehkar, B., von Bonsdorff, L., Cabantchik, Z. I., Hider, R. C., and Swinkels, D. W. (2005) Results of an international round robin for the quantification of serum non-transferrin-bound iron: Need for defining standardization and a clinically relevant isoform, *Analytical Biochemistry 341*, 241-250.

211. Simpson, R. J., Raja, K. B., Halliwell, B., Evans, P. J., Aruoma, O. I., Konijn, A. M., and Peters, T. J. (1991) Iron speciation in hypotransferrinaemic mouse serum, *Biochem Soc T 19*, 317S.

212. May, P. M., Linder, P. W., and Williams, D. R. (1977) Computer-Simulation of Metal-Ion Equilibria in Biofluids - Models for Low-Molecular-Weight Complex Distribution of Calcium(Ii), Magnesium(Ii), Manganese(Ii), Iron(Iii), Copper(Ii), Zinc(Ii), and Lead(Ii) Ions in Human-Blood Plasma, *J Chem Soc Dalton*, 588-595.

213. Grootveld, M., Bell, J. D., Halliwell, B., Aruoma, O. I., Bomford, A., and Sadler, P. J. (1989) Non-transferrin-bound iron in plasma or serum from patients with idiopathic hemochromatosis. Characterization by high performance liquid chromatography and nuclear magnetic resonance spectroscopy, *J Biol Chem 264*, 4417-4422.

214. Link, G., Pinson, A., and Hershko, C. (1985) Heart-Cells in Culture - a Model of Myocardial Iron Overload and Chelation, *J Lab Clin Med 106*, 147-153.

215. Liuzzi, J. P., Aydemir, F., Nam, H., Knutson, M. D., and Cousins, R. J. (2006) Zip14 (Slc39a14) mediates non-transferrin-bound iron uptake into cells, *P Natl Acad Sci USA 103*, 13612-13617.

216. Chen, T. T., Li, L., Chung, D. H., Allen, C. D., Torti, S. V., Torti, F. M., Cyster, J. G., Chen, C. Y., Brodsky, F. M., Niemi, E. C., Nakamura, M. C., Seaman, W. E., and Daws, M. R. (2005) TIM-2 is expressed on B cells and in liver and kidney and is a receptor for H-ferritin endocytosis, *The Journal of experimental medicine 202*, 955-965.

217. Li, J. Y., Paragas, N., Ned, R. M., Qiu, A., Viltard, M., Leete, T., Drexler, I. R., Chen, X., Sanna-Cherchi, S., Mohammed, F., Williams, D., Lin, C. S., Schmidt-

Ott, K. M., Andrews, N. C., and Barasch, J. (2009) Scara5 is a ferritin receptor mediating non-transferrin iron delivery, *Developmental cell 16*, 35-46.

218. Barisani, D., Berg, C. L., Wessling-Resnick, M., and Gollan, J. L. (1995) Evidence for a low Km transporter for non-transferrin-bound iron in isolated rat hepatocytes, *Am J Physiol 269*, G570-576.

219. Dallman, P. R., and Spirito, R. A. (1977) Brain iron in the rat: extremely slow turnover in normal rats may explain long-lasting effects of early iron deficiency, *The Journal of nutrition 107*, 1075-1081.

220. Malecki, E. A., Cook, B. M., Devenyi, A. G., Beard, J. L., and Connor, J. R. (1999) Transferrin is required for normal distribution of ^{59}Fe and ^{54}Mn in mouse brain, *J Neurol Sci 170*, 112-118.

221. Pinilla-Tenas, J. J., Sparkman, B. K., Shawki, A., Illing, A. C., Mitchell, C. J., Zhao, N., Liuzzi, J. P., Cousins, R. J., Knutson, M. D., and Mackenzie, B. (2011) Zip14 is a complex broad-scope metal-ion transporter whose functional properties support roles in the cellular uptake of zinc and nontransferrin-bound iron, *American journal of physiology. Cell physiology 301*, C862-871.

222. Beard, J. L., Wiesinger, J. A., Li, N., and Connor, J. R. (2005) Brain iron uptake in hypotransferrinemic mice: influence of systemic iron status, *J Neurosci Res 79*, 254-261.